Searching for Supersymmetry in the three- and four lepton final states with the CMS-Detector at the LHC

Stefan Wayand

Zur Erlangung des akademischen Grades eines

DOKTORS DER NATURWISSENSCHAFTEN

an der Fakultät für Physik des Karlsruhe Instituts für Technologie (KIT)

genehmigte

DISSERTATION

von

Dipl.-Phys. Stefan Wayand
aus Hagenbach

Tag der mündlichen Prüfung: 13.02.2015

Referent: Prof. Dr. Wim de Boer
Institut für Experimentelle Kernphysik (EKP)

Korreferent: Prof. Dr. Günter Quast
Institut für Experimentelle Kernphysik (EKP)

I declare that I have developed and written the enclosed thesis completely by myself, and have not used sources or means without declaration in the text.

Karlsruhe, 27. 01. 2015

. . . .

(**Stefan Wayand**)

Contents

1. Introduction

We want to know the fundamental laws of nature since the dawn of humanity. In the year 2012 a new level of success has been achieved by the discovery of the Higgs boson by the ATLAS and CMS experiments at the LHC in 2012 [1; 2], which is essential for the Standard Model (SM) of particle physics. With the Higgs boson, the Standard Model of particle physics is complete. Nevertheless, the Standard Model cannot be the fundamental theory describing everything, e.g. it does not describe the dark matter, which makes up more than 80% of the matter in the universe [3]. A popular extension of the Standard Model is supersymmetry (SUSY), see [4–6] for a review. SUSY is a symmetry between fermions and bosons, which can only be realized in nature if one doubles the particle spectrum of the SM. i.e. one introduces a boson (fermion) for each fermion (boson). SUSY provides with the lightest supersymmetric particle a perfect candidate for the dark matter (DM) in the universe and makes clear predictions for the production of supersymmetric particles. The supersymmetric partners of the W and Z bosons with spin 1/2 are the so-called charginos ($\tilde{\chi}_1^{\pm}$) and neutralinos ($\tilde{\chi}_2^0$), which can be produced in pairs, just like the WZ production. The SUSY particles decay into the SM particles plus the weakly interacting DM candidate, which is the lightest supersymmetric particle. Since these weakly interacting DM particles behave like neutrinos, they produce missing energy and momentum in the events. This leads to multilepton events with missing transverse energy E_{T}^{miss} if the charginos and neutralinos decay leptonically. Such signatures have been searched for at lower energies [7–9] and no SUSY signatures were found, possibly because the centre-of-mass (CM) energy was not high enough. In this thesis the SUSY searches in multi-lepton signatures have been optimized for the high energies and backgrounds of the LHC. With the present luminosity of 19.7 fb^{-1} at a CM energy of 8 TeV one could explore a large region of the hitherto unexplored region of the SUSY parameter space, published in [10]. No signal has been found so far, but an outlook for the expected 150-fold increase in the luminosity after an almost doubling of the CM energy will be given.

The thesis is organized as following: After introducing the theoretical basis in Chapter 2, the LHC program with a focus on the CMS detector will be presented in Chapter 4. The observables needed to perform this analysis will be introduced in Chapter 5. Chapter 6 discusses the signal signatures and Chapter 7 the Standard Model backgrounds. The search strategy and the result are presented in Chapter 8. The interpretation of the results into SUSY signatures is given in Chapter 9. Chapter 10 summarizes this thesis and gives an outlook. Natural units are used in this thesis ($\hbar = c = 1$).

2. Theory

In this chapter, the theoretical basis of this thesis will be introduced. First the ideas and concepts of the Standard Model of particle physics will be presented. Afterward, several problems of the Standard Model will be discussed. Then the idea behind supersymmetry will be explained, and some aspects of the Minimal Supersymmetric Standard Model (MSSM) will be discussed. Some features about colliding protons will be presented at the end of this chapter

2.1. Standard Model

The particle physics of the late 20th and the beginning of the 21st century is a great success story of the Standard Model (SM) of particle physics. A few selected topics are presented in this section. An extensive introduction can be found in [11; 12]. In the Standard Model, all fundamental particles are fermions (spin=1/2), with a wavefunction denoted by a spinor $|\Psi\rangle$. The spinors are solutions of the Dirac equation:

$$(\gamma^i \partial_i - m) |\Psi\rangle = (\not{\partial} - m) |\Psi\rangle = 0, \tag{2.1}$$

with γ the so-called gamma or Dirac matrices and m the mass of the particle. The four-dimensional space-time index i runs from 0 to 3. This equation also allows solutions that travel back in time. It was Paul Dirac who identified these solutions as particles with opposite quantum numbers, which are called antiparticles denoted as $|\bar{\Psi}\rangle$. The spinors are wavefunctions with a complex phase. The detection of a particle compromises the measurement of the real amplitude of its wavefunction $\langle\Psi|\Psi\rangle$. Therefore, the spinor $|\Psi\rangle$ is invariant under an $e^{-i\phi}$ transformation. This invariance leads to a conserved quantity that is called chirality and has two eigenvalues [13]. All spinors can be written as a linear combination of the two corresponding eigenstates:

$$|\Psi\rangle = \sin\alpha |\Psi_L\rangle + \cos\alpha |\Psi_R\rangle, \tag{2.2}$$

with $\sin\alpha^2 + \cos\alpha^2 = 1$. The component $|\Psi_L\rangle$ is called left-handed and Ψ_R right-handed, respectively.

The interaction between these particles is mediated by three forces:[1]: the electromagnetic force, the strong force, and the weak force. A forces couples to the charge of a particle and this charge is a conserved quantity arising from a symmetry [13]. The three basic symmetries and the resulting fundamental forces will be introduced in the next three subsections 2.1.1-2.1.3.

2.1.1. Quantum Electrodynamics (QED)

The Quantum ElectroDynamics (QED) is the theory that describes the electromagnetic force. Every particle with an electromagnetic charge does interact with this force. The Lagrangian $\mathcal{L}_{QED}$ of the QED is defined as:

$$\mathcal{L}_{QED} = -\frac{1}{4}F_{\mu\nu}F^{\mu\nu} + \bar{\Psi}(i\slashed{\partial})\Psi - m\bar{\Psi}\Psi + e\bar{\Psi}\slashed{A}\Psi, \qquad (2.3)$$

with Ψ the particle (electron), A the photon field, $F_{\mu\nu}=\partial_\mu A_\nu - \partial_\nu A_\mu$ the (electromagnetic) field strength tensor, m the mass of the fermion (=electron) and e the electromagnetic coupling constant (=elementary charge). Applying the Euler-Lagrange equation to $\mathcal{L}_{QED}$ results in the Dirac and Maxwell equation. The source of the charge is a local $U_A(1)$ symmetry, meaning that the Lagrangian $\mathcal{L}$ of the QED is invariant under a local gauge transformation generated by $\Lambda(x)$. The fields transform like: $\Psi(x) \to e^{ie\Lambda(x)}\Psi(x)$, $\bar{\Psi}(x) \to e^{-ie\Lambda(x)}\bar{\Psi}(x)$ and $A_\mu(x) \to A_\mu(x) + \partial_\mu\Lambda(x)$. The $\mathcal{L}_{QED}$ can be rewritten with the so-called covariant derivative $D_\mu = \partial_\mu - ieA_\mu$:

$$\mathcal{L}_{QED} = -\frac{1}{4}F_{\mu\nu}F^{\mu\nu} + \bar{\Psi}(i\slashed{D} - m)\Psi \qquad (2.4)$$
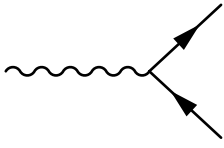
This notation is elegant since it shows that the requirement of local gauge invariance generates the interaction term ($e\bar{\Psi}\slashed{A}\Psi$). The quantization of the fields leads to the fermion (electron) propagator, photon propagator, and photon vertex, which are presented in table 2.1.

2.1.1.1. Running of the coupling constant

The term "constant" usually implies that a variable is constant. In quantum field theory, this is not true. In leading order, the coupling constant e is given by the photon fermion vertex. The corrections to this vertex also couples with the constant e. These corrections depend on the energy (so-called virtuality Q^2) mediated by this vertex. The measured value of e includes all orders of corrections simultaneously, and so e can be written as a series depending on the energy scale. The definition of e as the elementary charge is given in the Thomson limit ($Q^2 \to 0$). With this input, we can calculate e at every energy scale.

---

[1]Gravitation is not included in the SM.

Table 2.1.: Feynman diagrams of the QED.

Name	Diagram	Description
Fermion propagator:		The fermion propagator results from the Dirac part $(\bar{\Psi}(i\slashed{\partial} - m)\Psi)$ of the Lagrangian. Meaning a fermion with momentum p travels from the left to the right or the antifermion travels from the right to left.
Photon propagator:		The photon propagator results from the photon potential part $(-\frac{1}{4}F_{\mu\nu}F^{\mu\nu})$ of the Lagrangian, meaning that a photon with momentum p travels from the left to the right.
Photon vertex:		The photon vertex results from the interaction part $(e\bar{\Psi}\slashed{A}\Psi)$ of the Lagrangian, meaning that incoming photon decays into a fermion anti-fermion pair in this representation. The vertex can also be rotated by 180 degrees, meaning that a fermion anti-fermion pair annihilate into a photon or rotated in such way that a fermion radiate a photon.
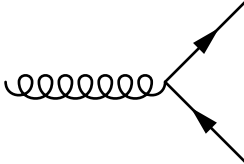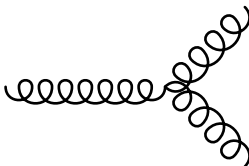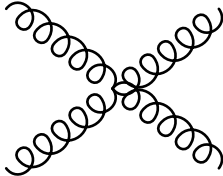
2.1.2. Quantum Chromodynamics (QCD)

The basic symmetry behind the Quantum Chromodynamics (QCD) is the SU(3) group. It has eight generators (T_a with a=1,..,8) which are the so-called Gell-Mann matrices. The charge of the QCD is the so-called color charge and is represented by three different colors. The sum of all colored eigenstates results in a color neutral state. The SU(3) group is non-abelian. For this reason, the force carriers mediating this force, which are called gluons (G_μ^a), are charged. Only a subset of the fermions interacts with the strong force, which are called quarks and are written as q. The Lagrangian of the QCD can be written as:

$$\mathcal{L}_{QCD} = -\frac{1}{4}F_{\mu\nu}^a F^{a\mu\nu} + \bar{q}(i\slashed{D} - m)q, \tag{2.5}$$

with the covariant derivative $D_\mu = \partial_\mu - ig_s T_a G_\mu^a$ and the field strength tensor $F_{\mu\nu}^a = \partial_\mu G_\nu^a - \partial_\nu G_\mu^a + g_s f^{abc} G_\mu^b G_\nu^c$. The f^{abc} are called structure constants. The quantization of this Lagrangian leads to a new Feynman propagator and new vertices listed in table 2.2.

Table 2.2.: Feynman diagrams of the QCD.

Name	Diagram	Description
Gluon propagator:		The gluon propagator results from the potential part $(-\frac{1}{4}F_{\mu\nu}^a F^{a\mu\nu})$ of the Lagrangian, meaning that a gluon with momentum p and color travels from the left to the right.
Quark-gluon vertex:		The quark-gluon vertex results from the interaction part $(g_s\bar{q}\gamma^\mu T^a G_\mu^a q)$ of the Lagrangian, meaning that incoming gluon decays into a fermion anti-fermion pair in this representation. The vertex can also be rotated by 180 degrees, meaning that a quark anti-quark pair annihilates into a gluon or rotated in such way that a quark radiates a gluon.
Three-gluon vertex:		Three-gluon vertex results from the potential part $(-\frac{1}{4}F_{\mu\nu}^a F^{a\mu\nu})$ of the Lagrangian, meaning that incoming gluon split into two gluons. The vertex can also be rotated by 180 degrees, meaning that a gluon pair fuses to one gluon.
Four-gluon vertex:		The four-gluon vertex results from the potential part $(-\frac{1}{4}F_{\mu\nu}^a F^{a\mu\nu})$ of the Lagrangian, meaning that two gluons fuse into two other gluons.

2.1.2.1. Confinement and Asymptotic freedom

The QCD coupling constant g_s is not constant in the same way as it is not constant for QED. For the coupling constant g_s the limit $Q^2 \to 0$ tends to infinity due to the gluon self-interaction. By trying to separate two colored particles, they will start to exchange gluons. The force increases with distance and so the energy density. Above the pair building threshold the gluons will create quark pairs. This phenomenon is known as confinement. For this reason, quarks live only in a small volume bounded by gluons. These bound states are known as mesons or baryons, e.g. the proton is a baryon with a size in the order of fm. In order to investigate theses

small scales, a high energy (Q^2) of the order of a GeV is needed. Below this threshold, the QCD is not valid[2]. Instead, one interacts with the bound states as a whole, which is described by effective theories. If Q increases g_s is getting smaller, which leads to the so-called asymptotic freedom. It explains the fact that the series expansion of g_s converges, and the QCD predictions are meaningful in this regime.

2.1.3. Electroweak unification

The missing force is the weak force, which is responsible for the decay of heavy particles. The basic symmetry describing this force is the SU(2) symmetry. The weak force has some unique properties. It only couples to left-handed particles and to right-handed anti-particles. In addition, the force carriers mediating the weak force are massive. With these requirements, it is not possible to write the Lagrangian, so that is invariant under the SU(2) symmetry. The solution to this problem gives the Higgs mechanism by introducing a new scalar field, the so-called Higgs field. This field has the following potential:

$$V(\Phi) = \mu^2 \Phi^\dagger \Phi + \lambda (\Phi^\dagger \Phi)^2, \tag{2.6}$$

where μ and λ are simple parameters. If μ^2 is smaller than zero, the vacuum expectation value becomes non-zero $|\Phi|^2 = \frac{-\mu}{2\lambda} = v$. The Higgs field can be written as:

$$\Phi(x) = \begin{pmatrix} \Phi^+(x) \\ \Phi^0(x) \end{pmatrix} = \frac{1}{\sqrt{2}} \begin{pmatrix} \phi_1(x) + i\phi_2(x) \\ \phi_3(x) + i\phi_4(x) \end{pmatrix} = \frac{1}{\sqrt{2}} \begin{pmatrix} 0 \\ v + h(x) \end{pmatrix}, \tag{2.7}$$

where the representation of the form ϕ_1, ϕ_2, ϕ_3 and ϕ_4 illustrates that this complex scalar field has four degrees of freedom. In the right-hand side, only one degree of freedom is visible, which is represented by the field $h(x)$ and ends in the Higgs boson. The other three degrees of freedom are carried by so-called Goldstone bosons which give the W^+, W^- and the Z boson mass[3]. This Higgs field breaks the $SU_L(2) \times U_Y(1)$ symmetry into the $U_A(1)$ symmetry (QED). The kinetic term of the Higgs Lagrangian reads as:

$$T(\Phi) = (D_\mu \Phi)^\dagger (D^\mu \Phi), \tag{2.8}$$

with $D_\mu = \partial_\mu - ig\frac{\tau^j}{2}W_\mu - ig'\frac{1}{2}B_\mu$, W are the gauge field of SU(2) with the coupling constant g, B is the gauge field of $U_Y(1)$ with the coupling g'. The Pauli matrices τ^j (j=1,2,3) are the generators of the SU(2) symmetry. The charge of the SU(2) symmetry is called the isospin (I) and the charge of the U(1) is known as the hypercharge (Y). Q=I_3+Y/2 connects the electric charge Q with the hypercharge and isospin. The Higgs Lagrangian and the electroweak Lagrangian leads to many new Feynman propagator and vertices, which are illustrated in table 2.3. The field of the electroweak gauge bosons is a linear combination of these fields:

---

[2]Which means that QCD cannot make predictions for this energy regime.
[3]The Goldstone boson goes into the longitudinal polarization of the W^+, W^- and the Z boson.

- Photon (γ) $A_\mu = \sin(\Theta_W)W^3_\mu + \cos(\Theta_W)B_\mu$

- Z boson $Z_\mu = \cos(\Theta_W)W^3_\mu + \sin(\Theta_W)B_\mu$

- W boson $W^\pm_\mu = \frac{1}{\sqrt{2}}(W^1_\mu \mp iW^2_\mu)$

The angle Θ_W is the Weinberg angle and has a value of $\sin^2(\Theta_W) = 0.231$ at Q=91.2 GeV. The masses of the W and Z boson are determined by the coupling to the Higgs field. The photon field does not couple to the Higgs field and stays massless. The masses of the fermions are also generated by the coupling to the Higgs field. E.g the mass term of the down quark m_d reads:

$$y_d(\bar{u}, \bar{d})_L \begin{pmatrix} 0 \\ \frac{v+h(x)}{\sqrt{2}} \end{pmatrix} d_R + cc \rightarrow m_d = \frac{y_d v}{\sqrt{2}}, \tag{2.9}$$

with y_d the Yukawa coupling of the down quark to the Higgs field $h(x)$. Each massive particle has its own Yukawa coupling, which is a free parameter of the Standard Model.
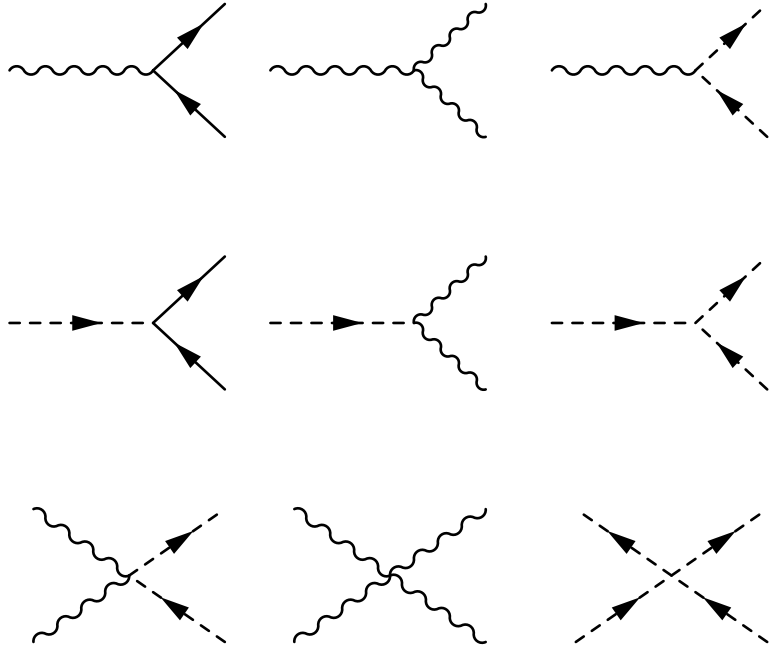
2.1.4. Particle content of the Standard Model

The particles, which are fermions (spin=1/2), and the force carriers, which are mediated by gauge boson (spin=1), were introduced above. In order to give the weak gauge bosons mass via the Higgs mechanism, one Higgs field has to be introduced as weak isospin doublet with 4 degrees of freedom. Three of them are needed to give mass to the W+, W- and Z boson. The remaining degree of freedom results in the Higgs boson, which is essential for the Standard Model. In table 2.1.4 all particles and forces of the Standard Model are listed. The quantum number $SU(2)_L$ gives the representation of the field in the $SU(2)_L$ symmetry, e.g. $(\nu_e, e)^T_L$ is a doublet state, meaning it has eigenvalues of I_3=1/2,-1/2. If it is a singlet (I_3=0) the particle does not interact with this force. The same meaning has the quantum number $SU(3)_C$, but since this symmetry is unbroken we denote only one single particle. E.g. the d-quark is a triplet state (d_{C1},d_{C2},d_{C3}), with C1,C2,C3 as colors index. There are eight different gluons ($g_1..g_8$), which can transfer this triplet state into another triplet state. The $U(1)_Y$ number shows direct the Y quantum number and the electric charge is given by the formula Q=I_3+Y/2. For the fermions, three different generations are known. Each generation is a copy of the first generation, but with different Yukawa couplings leading to different masses. The full particle spectrum also includes the anti-particles, which have opposite charges. The anti-particles are grouped into right-handed doublet states and left-handed singlet states for representation in the SU(2) symmetry.

2.1.5. Measurements of the Standard Model particles

With the data collected in 2011 and 2012, it was possible to measure the production cross section of several Standard Model processes and compare the results with the prediction from theory. Figure 2.1 shows the recent preliminary results published by CMS [14]. The agreement between data and prediction is amazing and confirms the Standard Model one more time.

Table 2.3.: Additional Feynman diagrams from the electroweak and Higgs part of the Lagrangian.

Name	Diagrams	Description
Additional propagators:		The additional propagators result from the individual potential part of the Lagrangian. The first propagator is either a uncharged Z boson or a charged $W^{\pm}$. The second probegater is the Higgs boson propagator, meaning that the particle travels from the left to the right.
Additional vertices:		The additional vertices result from the different kinetic parts of the Lagrangian. It includes Higgs and boson decays into fermion anti-fermion pairs, bosons pairs or Higgs pairs. For the decay of the W boson, it is the decay into left-handed fermion and right-handed anti-fermion of the iso-doublet partner. On all vertices, the quantum numbers have to be conserved.

2.1.6. Problems of the Standard Model

The Standard Model was developed in the 1970's and improved the understanding of particle physics deeply. However, some phenomena are not included in the Standard Model and still leave some questions unanswered:

- Free parameters: It has at least 18 free parameters[4], and these parameters are very different. E.g the electron mass is ~ 0.0005 GeV and the mass of the top is ~ 170 GeV,

---

[4]The parameters of the neutrino masses does not appear in this counting.

Table 2.4.: The particle content of the Standard Model. For further explanation, please note the text above.

Fermions Spin=1/2							
	1. Gen	2. Gen	3. Gen	$SU(3)_C$	$SU(2)_L$	$U(1)_Y$	Q
Quarks	$\begin{pmatrix} u \\ d \end{pmatrix}_L$	$\begin{pmatrix} c \\ s \end{pmatrix}_L$	$\begin{pmatrix} t \\ b \end{pmatrix}_L$	3	2	1/3	2/3 −1/3
	u_R	c_R	t_R	3	1	4/3	2/3
	d_R	s_R	b_R	3	1	-2/3	-1/3
Leptons	$\begin{pmatrix} \nu_e \\ e \end{pmatrix}_L$	$\begin{pmatrix} \nu_\mu \\ \mu \end{pmatrix}_L$	$\begin{pmatrix} \nu_\tau \\ \tau \end{pmatrix}_L$	1	2	-1	0 −1
	e_R	μ_R	τ_R	1	1	-2	-1
Gauge bosons Spin=1							
Interaction	Boson			$SU(3)_C$	$SU(2)_L$	$U(1)_Y$	Q
Electromagnetic	γ			1	1	0	0
Weak	Z^0 $W^\pm$			1	3	0	0 ±1
Strong	$g_1..g_8$			8	1	0	0
Higgs bosons Spin=0							
Field	Boson			$SU(3)_C$	$SU(2)_L$	$U(1)_Y$	Q
Higgs	h			1	2	1	0

which is strange for a fundamental theory.

- Fine tuning problem: The Higgs mass is at the electroweak scale ($\sim$100 GeV). In order to have a valid theory up to the Planck scale ($\sim 10^{19}$ GeV) large fine tuning is necessary due to the radiative loop corrections to the Higgs mass.

- In the SM there are three very different couplings for the three forces, which also do not unify at high energy.

- Dark matter: No particle of the SM can form the so-called dark matter.

- Gravitation: The Standard Model ignores the gravitational force.

Since the Standard Model is validated to a high precision, the most challenging part for new physics is to recap the results from the Standard Model.

2.2. SUSY

Supersymmetry is a possible extension of the Standard Model. The shortcut for supersymmetry is SUSY. This section gives a short overview of what supersymmetry is and discusses some aspects of of supersymmetry. Further information can be found in [5].
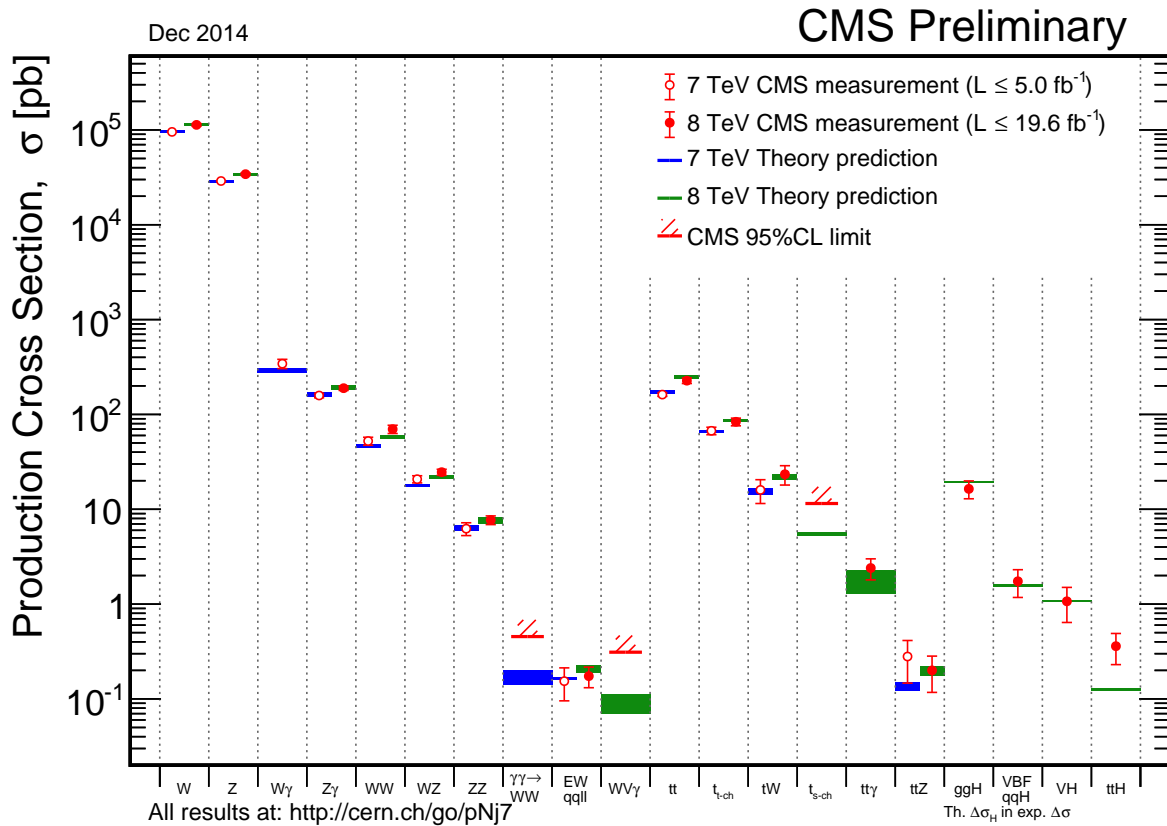
Figure 2.1.: Recent measurements of the production cross section of Standard Model particles with the CMS detector compared to the prediction from theory. The figure is taken from [14].

2.2.1. Motivation

Many problems of the Standard Model (section 2.1.6) can be solved by introducing SUSY. Two topics will be discussed in this subsection.

2.2.1.1. The way to the Grand Unified Theory (GUT)

One of the biggest wishes of particle physics is the unification of the Standard Model into one great symmetry. The group $SU(5)$[5] is the smallest group which allows such an unification. This unification should happen at the so-called GUT scale. The $SU(5)$ symmetry has overall $N^2-1=24$ gauge fields and as a result 12 new force carriers must be introduced. The proton decay $(P \rightarrow e^+ + \pi^0)$ is allowed with one of these new force carrier, which leads to a proton lifetime τ_P of:

$$\tau_P \approx \frac{1}{\alpha_{SU(5)}} \frac{M_X^4}{m_P^5}, \tag{2.10}$$

where m_P is the proton mass, $\alpha_{SU(5)}$ is the unified coupling constant of the force carrier causing the proton decay and M_X is the unified mass of this force carrier. Since no proton decay has been

---

[5]SO(10) is also a possible group.

found so far, these force carriers must be heavy. With a lifetime of the proton $\tau_P > 10^{33}$ follow $M_x > 2.4 \cdot 10^{15}$ GeV [15]. This result needs a knowledge about the unified coupling constant $\alpha_{SU(5)}$. The couplings are computed with the so-called renormalization group equations. Figure 2.2 shows the running of the coupling constants for the Standard Model and SUSY. In the right figure for the SUSY scenario, the running of the coupling constants have some kinks. These kinks represent the energy scale where the SUSY particle starts to exist. It is a general feature of SUSY that it can unify all couplings at a typical GUT scale of 10^{16} GeV, which is sufficient to increase the predicted proton lifetime above its experimental limit.
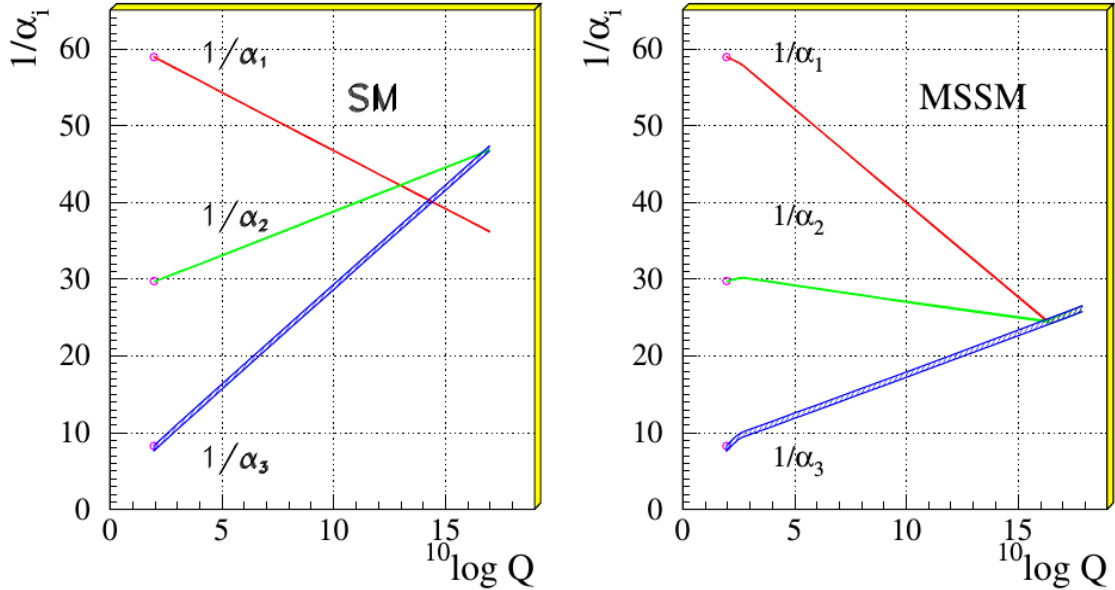
Figure 2.2.: This Figure shows the inverse of the coupling constants vs. the logarithmic energy scale. α_1 is the coupling of the unbroken $U_Y(1)$ symmetry, α_2 of the unbroken $SU_L(2)$ symmetry, and α_3 of the $SU(3)$ symmetry. The evolution of the measured gauge couplings at LEP is shown for the Standard Model on the left and a SUSY model (MSSM) on the right [16].

2.2.1.2. Dark Matter

Ordinary baryonic matter provides about 5% of the energy density of our universe, which is known from satellite experiments [3; 17]. 27% of the energy density is built of so-called cold dark matter. This matter does not interact with photons as the name dark suggests. The characteristic cold means that the particles forming this dark matter are non-relativistic and have a large mass with respect to the temperature of the early universe (at the time of structure formation). For this reason, no Standard Model particle has the right attributes to form dark matter.

One other constrain on dark matter is coming from restrictions of the Big Bang. The universe was hot at the very beginning. Consequently, all particle masses were low compared to the

temperature of the very early universe. As a result, the dark matter particles annihilated and were produced with a the same rate and stayed in thermodynamical equilibrium with each other. With the expansion of the universe, the temperature decreases. As a consequence the amount of dark matter decreased since the production of dark matter particles was impossible but the annihilation process still continued. All dark matter particles would have annihilated in a static universe. However, the universe expands, and if the expansion rate exceeds the annihilation rate, freeze-out occurs. This freeze-out leads to a finite relic density [18]:

$$\Omega_{DM} h^2 = m_{DM} n_{DM} / \rho_C \approx 3 \cdot 10^{-27} / < \sigma_{DM} v >, \tag{2.11}$$

with Ω_{DM} the energy density of the dark matter normalized to the critical density ρ_C, h the Hubble constant, m_{DM} the mass of the dark matter particle, n_{DM} the number density and $< \sigma_{DM} v >$ is the thermally averaged annihilation cross section of the dark matter particle. Since h and Ω_{DM} are known, the cross section for the dark matter particles are also known. This cross section is in the order of the weak force, and those dark matter particles are also known as Weakly Interacting Massive Particles (WIMPS). SUSY predicts with the lightest neutralino ($\tilde{\chi}_1^0$) a particle with the right attributes to be a WIMP.

2.2.2. Some aspects of Supersymmetry

Supersymmetry introduces a new symmetry between bosons spin 0,1,2 and fermions spin $\frac{1}{2}, \frac{3}{2}$. At least one new operator Q is needed which transforms a fermion state into a boson state:

$$Q \left| fermion \right\rangle \propto \left| boson \right\rangle \text{ and } Q \left| boson \right\rangle \propto \left| fermion \right\rangle \tag{2.12}$$

The simplest SUSY model consists of doublets given in table 2.5. In SUSY models the num-

Table 2.5.: This table shows the possible doublets in this simple SUSY model

$\begin{pmatrix} \varphi & \Psi \end{pmatrix}$		$\begin{pmatrix} \lambda & A_\mu \end{pmatrix}$		$\begin{pmatrix} \tilde{g} & g \end{pmatrix}$	
Spin 0	Spin $\frac{1}{2}$	Spin $\frac{1}{2}$	Spin 1	Spin $\frac{3}{2}$	Spin 2
scalar	chiral fermion	majorana fermion	vector	gravitino	graviton

ber of fermions must be equal to the number of bosons. Since the Standard Model has 28 bosonic degrees of freedom and 90 fermionic degrees of freedom, the SM bosons cannot be the superpartners of the SM fermions. Therefore, SUSY requires the introduction of new particles.

2.2.3. The Minimal Supersymmetric Standard Model

The Minimal Supersymmetric Standard Model (MSSM) is one well-studied realization of supersymmetry. It introduces the minimal number of new particles. The particles are given in

table 2.6. Half of the particles are known from the Standard Model, the new supersymmetric particles are all marked with a ˜. For the naming, the following convention is chosen. The supersymmetric fermions get an -ino added, e.g. The wino is the superpartner of the SM W-boson. The supersymmetric bosons get and s as prefix, e.g. slepton is the superpartner of the lepton.

Table 2.6.: Particle content of MSSM. For further explanation, please note the text above.

Superfield	Bosons	Fermions	$SU_C(3)$	$SU_L(2)$	$U_Y(1)$
Gauge					
G^a	g^a	$\tilde{g}^a$	8	1	0
V^k	W^k ($W^\pm$,Z)	$\tilde{W}^k(\tilde{W}^\pm, \tilde{Z})$	1	3	0
B	$B(\gamma)$	$\tilde{B}(\tilde{\gamma})$	1	1	0
Matter					
L_i	$\tilde{L}_i = (\tilde{\nu}, \tilde{e})_L$	$L_i = (\nu, e)_L$	1	2	-1
E_i	$\tilde{E}_i = \tilde{e}_r$	$E_i = e_R$	1	1	-2
Q_i	$\tilde{Q}_i = (\tilde{u}, \tilde{d})_L$	$Q_i = (u, d)_L$	3	2	1/3
U_i	$\tilde{U}_i = \tilde{u}_R$	$U_I = u_R$	3*	1	4/3
D_i	$\tilde{D}_i = \tilde{d}_R$	$D_i = d_R$	3*	1	-2/3
Higgs					
H_u	H_u	$\tilde{H}_u$	1	2	-1
H_d	H_d	$\tilde{H}_d$	1	2	1

The supersymmetric Lagrangian[6] can be written as:

$$\mathcal{L} = \mathcal{L}_{gauge} + \mathcal{L}_{Yukawa} + \mathcal{L}_{SoftBreaking} \tag{2.13}$$

The $\mathcal{L}_{SoftBreaking}$ is new and responsible for the breaking of SUSY. It has many free parameters ($\mathcal{O}(100)$). Usually terms that would allow proton decays are forbidden in the Lagrangian. This leads to the conservation of the R-parity:

$$R = (-1)^{3(B-L)+2S}, \tag{2.14}$$

with B the number of baryons, L the number of leptons and S the spin. The R-parity for Standard Model particles is +1 and for SUSY particles is -1. The conservation of the R-parity forbids the decay of the lightest supersymmetric (LSP) particle into Standard Model particles. Since LSP is heavy, it is a perfect candidate for a cold dark matter particle. Another consequence of conserved R-parity is that SUSY particles are always produced in pairs.

---

[6]This lagrangian is supersymmetric since it consists of superfields.

2.2.3.1. Charginos, Neutralinos and Sleptons

The superpotential for the Yukawa part of the Lagrangian can be written as:

$$W_R = \epsilon_{ij}(y_{ab}^U Q_q^j U_b^c H_2^i + y_{ab}^D Q_a^j D_b^c H_1^i + y_{ab}^L L_a^j E_b^c H_1^i + \mu H_1 H_2), \qquad (2.15)$$

with i,j=1,2 the indices of the SU(2) symmetry and the a,b=1,2,3 are the indices for the three different generations. In SUSY two Higgs fields must be introduced. One Higgs field couples to the up-type fermions (H_u) and the other couples to the down-type fermions (H_d). The supersymmetric partners of the left-handed particles can have different masses as the supersymmetric partners of the right-handed particles. It is possible that the left-handed and right-handed particles mix, which is enhanced for the third generation particles.

The supersymmetric transformation of the two Higgs fields leads to the higgsinos. They have the same quantum numbers as the wino and bino and, for this reason, all these fields will blend into a mixed state. Therefore, a distinction is drawn between neutralinos ($\tilde{\chi}_n^0$) and charginos($\tilde{\chi}_m^\pm$). The four neutralinos (n=1,2,3,4) can be written as:

$$\tilde{\chi}_n^0 = N_{1n}\tilde{B} + N_{2n}\tilde{W}^3 + N_{3n}\tilde{H}_u^0 + N_{4n}\tilde{H}_d^0, \qquad (2.16)$$

where N is a 4×4 unitary matrix. The four states are classified by their masses: $m_{\tilde{\chi}_1^0} < m_{\tilde{\chi}_2^0} < m_{\tilde{\chi}_3^0} < m_{\tilde{\chi}_4^0}$. In usual SUSY scenarios, the $\tilde{\chi}_1^0$ dominantly consists of bino, $\tilde{\chi}_2^0$ dominantly consists of wino and $\tilde{\chi}_3^0/\tilde{\chi}_4^0$ dominantly consists of higgsinos. The two charginos (m=1,2) are:

$$\tilde{\chi}_m^\pm = M_{1m}\tilde{W}^\pm + M_{2m}H_{u/d}^{\tilde{\pm}}, \qquad (2.17)$$

where M is a 2×2 unitary matrix. The two states are classified by their masses: $m_{\tilde{\chi}_1^\pm} < m_{\tilde{\chi}_2^\pm}$. In the usual SUSY scenario, the $\tilde{\chi}_1^\pm$ dominantly consists of wino and $\tilde{\chi}_2^\pm$ dominantly consists of higgsino.

2.3. Colliding Particles

The Large Hadron Collider (LHC) collides protons with an center of mass energy of 8 TeV in 2012. The proton is not a fundamental particle since it is build of three so-called valence quarks (two up-quarks and one down-quark). The valence quarks frequently exchange gluons with each other. These gluons can split into virtual quark anti-quark pairs, which are the so-called sea quarks. All of these constituents carry a fraction x of the momentum of the proton. This information is summarized in the so-called parton distribution function (pdf). The pdf is a function of f(x,Q^2), since the strong coupling depends on the virtuality Q^2. The pdf for Q^2 =100 GeV is shown in figure 2.3. The gluons have a high density and, for this reason, the LHC is sometimes called gluon collider. However, at high x values the valence quarks are still important. These high x values are needed to produce heavy particles, e.g. SUSY particles.
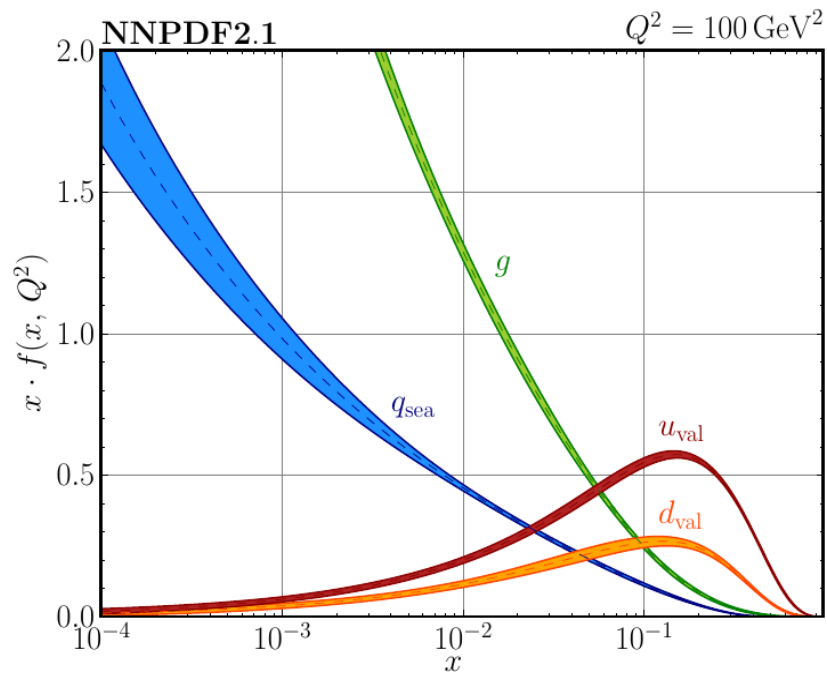
Figure 2.3.: Parton distribution function (pdf) of a proton. The x-axis represents the energy fraction x and the y-axis represents the probability scaled with x. The values are from the NNPDF collaboration and the figure is taken from [19; 20]

3. Statistical Model

In order to make a statistical interpretation, a confidence level (CL) has to be defined. For this reason, we use the so-called CL_{s} method, which is based on the likelihood formalism [21–23]. The likelihood function consists of two different ingredients. First the statistical component, which follows a Poisson function:

$$Poisson(n|\mu) = e^{-\mu}\frac{\mu^n}{n!}, \tag{3.1}$$

with n the number of measured events and μ the number of excepted events. Second are the systematic uncertainties, which are called nuisance parameters, and can follow different probability density function (pdf)[1]. In this analysis, all systematic δ uncertainties follow the log-normal distribution [24]:

$$Lognormal(\delta|\mu,\sigma) = \frac{1}{\delta\sigma\sqrt{2\pi}}e^{-\frac{(ln\delta-\mu)^2}{2\sigma^2}}, \tag{3.2}$$

where μ is the so-called location parameter and σ is the shape parameter. The likelihood function for the combination on N_{bins} search bins can be written as:

$$L(n|H) = \prod_k^{N_{bins}} Poisson(n_k|r \cdot s_k + b_k) \prod_i^{N_{nuis}} Lognormal(f_k^i \cdot \delta_i|ln(b_k),\sigma_i), \tag{3.3}$$

where n_k denotes the number of observed events per bins, b_k the number of events predicted by backgrounds and s_k the number of events predicted by signal. The variable r is the so-called signal strength parameter. The scale factor f_k^i gives the contribution of each nuisance parameter (δ_i) into this search bin. N_{nuis} is the number of nuisance parameters. In this analysis, we have uncertainties which are commonly shared by each bin. However, there are also so-called bin-by-bin uncertainties, which are only valid for one individual bin, e.g the uncertainties on

---

[1]Attention, it is different to the parton density function, which also is called pdf!

the statistics of the background sample. In order to get rid of the nuisance parameters, they get profiled out under the requirement to maximize the likelihood function. The profiled test statistic calculated as:

$$Q = \frac{max(L(n|r \cdot s, b, \hat{\delta}^b))}{max(L(n|\hat{r} \cdot s, b, \hat{\delta}^b))}, \tag{3.4}$$

where the hat $\hat{}$ indicates that this variable is profiled out. This test statistic Q is converted into q=-2ln(Q). The result for some possible test statistics q's are shown in figure 3.1, where q_{obs} is the observed value and $p_{s+b} = P(q \geq q_{obs}|s+b)$ is the probability to measure this signal + background hypothesis with a signal strength of r=1 (illustrated as f(q|1) on the left plot and as f(q|s+b) on the right plot). The probability for the background only hypothesis is $1 - p_b = 1 - P(q \leq q_{obs}|b)$ (illustrated as f(q|0) on the left plot and as f(q|b) on the right plot). Now the 95% CL_s limit is defined as following:

$$CL_s(r) = \frac{p_{r \cdot s+b}}{1 - p_b} < 0.05 \tag{3.5}$$

The advantage is visible on the right plot of figure 3.1. Here both hypothesis are very similar and does not match data (q_{obs}) due to a statical downward fluctuation. The use of the 1-p_b as denominator prevents from making exclusion on signal models, where we are not sensitive to.
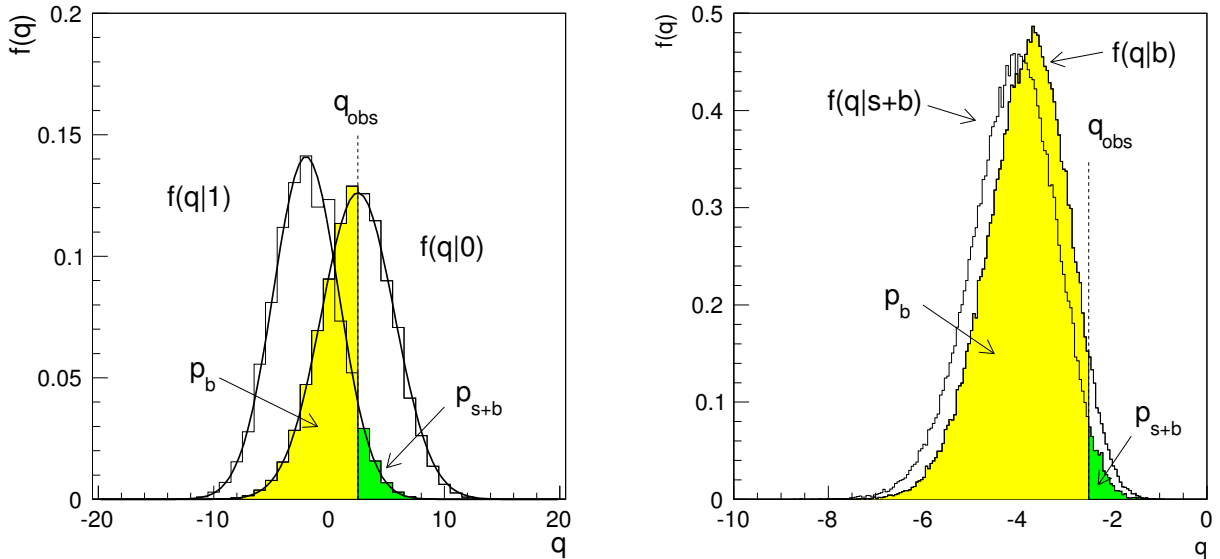
Figure 3.1.: Test statistic q distribution for the two example analysis. These figures are taken from [25].

The expected limit is calculated from pseudo-data using the likelihood function $L(n|0, b, \hat{\delta}^b)$.

4. The CMS-Experiment at the LHC

The CMS-experiment is a general-purpose detector built on the the Large Hadron Collider (LHC), which is hosted by the European Organization for Nuclear Research (CERN) near Geneva. Without the enormous effort of thousands of people working for CERN it would be impossible to build and run the accelerators, maintenance of the computing facilities, development of the software tools and contributions to the experiments, which are largely built by the external users. Therefore, it is important to keep in mind that the analysis of the data is only the last step. In this chapter, the important facilities as well as the important tools used in this thesis are presented.

4.1. The Large Hadron Collider (LHC)

The LHC is the largest particle collider built by CERN. It has a circumference of 27 km and is up to 175 m deep in the underground of the Franco-Swiss border near Geneva. It accelerates protons up to an energy of 7 TeV in both directions. The ring consists of two vacuum pipes inside superconducting magnets with a field strength of up to 8.33 Tesla. The magnet field is continually adapted to hold the protons on a circuit. The beamlines intersect at four different positions, where the four main experiments are located. The name of these detectors are: ATLAS (A Toroidal LHC ApparatuS, CMS (Compact Muon Solenoid), LHCb (Large Hadron Collider beauty) and ALICE (A Large Ion Collider Experiment) [26–29]. The LHCb experiment is designed to study physics with b-quarks. The physics of the strong force and, in particular, the search for the quark-gluon plasma is investigated with the ALICE detector. CMS and ATLAS are general purpose detectors sharing the same physics program with a focus on the discovery of the Higgs boson and the search for new physics.

The protons are pre-accelerated before they get injected into the LHC. An overview of the different accelerators is given in figure 4.1. First the protons are accelerated to 50 MeV by a linear accelerator (LINAC2). They obtain an energy of 1.4 GeV after the Proton Synchrotron

Booster (PSB). Then they get injected into the Proton Synchrotron (PS) which accelerates the protons to 26 GeV. The last accelerator before the LHC is the Super Proton Synchrotron (SPS) which gives the protons an energy of 450 GeV. The LHC is designed to accelerate ∼2800 bunches of protons to an energy of 7 TeV. A bunch consist of to 1.15×10^{11} protons and the spacing between the bunches is 25 ns. The event rate is given by:

$$\frac{dN}{dt} = \sigma_{prod}\mathcal{L},\qquad(4.1)$$

where σ_{prod} is the production cross section and $\mathcal{L}$ is the luminosity. The design luminosity is $\mathcal{L} = 10^{34}$ cm^{-2}s^{-1}. In 2012 LHC ran with a center-of-mass energy of 8 TeV (=4 TeV per beam) and reached a peak luminosity of $\mathcal{L} = 0.76 \times 10^{34}$ cm^{-2}s^{-1}. The LHC can also accelerate and
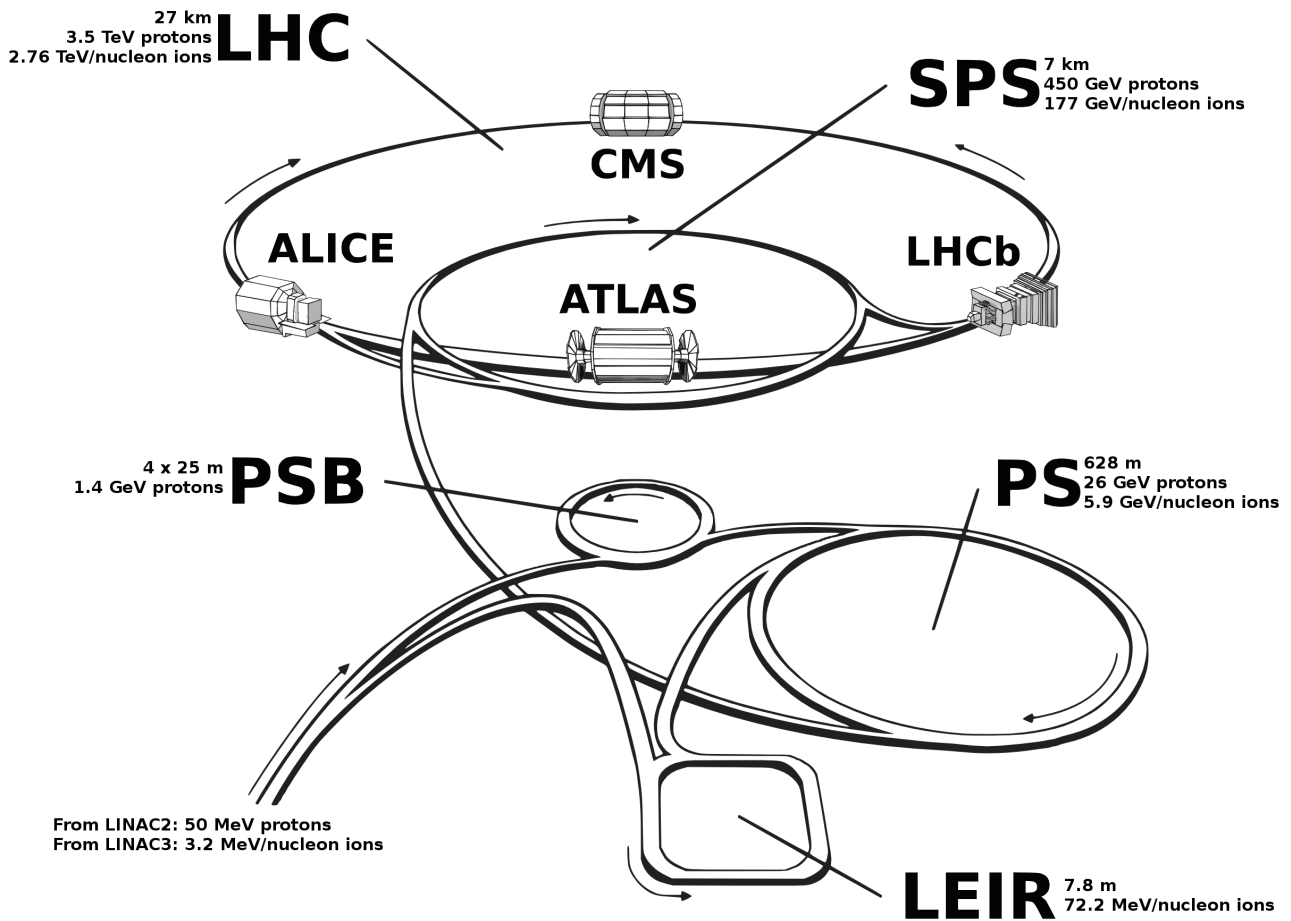
Figure 4.1.: Overview of the LHC ring and the preaccelerators. The picture is taken from [30].

collide ions instead of protons, which is of special interest for the ALICE detector.

4.2. The CMS Detector

The Compact Muon Solenoid (CMS) detector is a general purpose detector at the LHC [31]. It is located near Cessy (France) close to the Franco-Swiss border. It has a length of 21.6 m, a diameter of 14.6 m and weight of about 14500 tons. With these sizes, the name "compact" sounds ironic but is explained by the design of the detector. A silicon tracker, a crystal calorimeter, and a hadron calorimeter are placed inside of a large solenoid magnet as shown schematically in figure 4.2. Only the muon chambers are placed in between the iron yoke of the magnet. The solenoid magnet is 13m long, has an inner diameter of 5.9m and reaches a field strength of 3.8T, which allows good momentum resolution for the charged particles. The coordinate system is
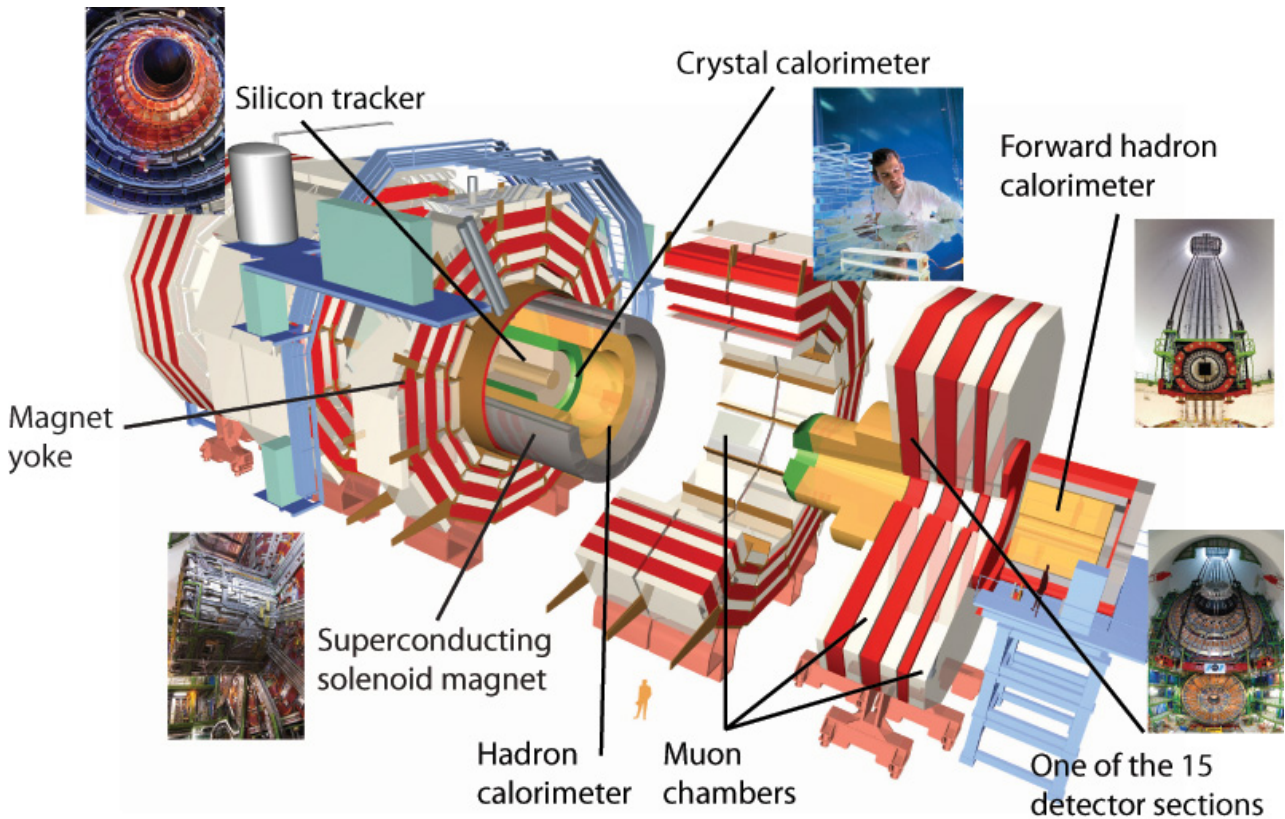
Figure 4.2.: Overview of the CMS detector. The picture is taken from [32].

defined as follows:

- The origin is in the center of the CMS detector.

- The z-axis is along the beam pipe.

- The x-axis is the horizontal axis, The y-axis is the vertical axis.

- The ϕ angle lies in the x-y plane and is zero along the x-axis.

- The θ angle is defined between the x-y plane and the z-axis. It is zero along in the z-axis.

- The pseudorapidity η is defined as η=-ln(tan(θ/2)).

CMS has an onion-like structure of the sub-detectors, which are presented in the following subsections. More extensive information about the detector can be found in [28]. Figure 4.3 shows the arrangement of the sub-detector parts.

4.2.1. Tracker

The tracker system is the heart of the CMS and built of silicon. It consists of pixel and strip detectors. The pixel detectors are placed next to the beam pipe. The over 66 million pixels have a resolution of 10 μm in the r-ϕ plane and 20 μm in the z direction. The strip detectors surround the pixel detectors. They consists of 9.6 million stripes. The resolution is between 23-52 μm in the r-ϕ plane and 230-530 μm in the z direction. The tracker system covers the pseudorapidity $|\eta| < 2.5$. The software of the tracker system is responsible for the track reconstruction and the vertex reconstruction. It is possible to reconstruct thousands of tracks and up to 100 vertices in one single event.

4.2.2. Calorimeter

CMS has two calorimeters, an electromagnetic calorimeter, and a hadron calorimeter. The readout of the calorimeter system is very fast and is used as a seed for the trigger.

4.2.2.1. Electromagnetic Calorimeter

The Electromagnetic Calorimeter (ECAL) consists of lead tungstate crystals, with a radiation length of X_0=0.89cm. It is separated in the barrel region $|\eta| < 1.479$ and the endcaps region 1.479 $|\eta| < 3.0$. The 75848 crystals measure 2.2 $\times$ 2.2 $\times$ 23cm ($\sim$26X_0) in the barrel and 3 $\times$ 3 $\times$ 22cm ($\sim$24.7X_0) in the endcaps. All electrons and photons are stopped in the ECAL. The read out of the crystals is done via avalanche photodiodes (vacuum phototriodes) in the barrel (endcaps) region. The ECAL is responsible for the energy measurement of the electrons and photons. It cannot distinguish between them, but due to the fine granularity the energy deposit can be matched to the information obtained by the tracker.

4.2.2.2. Hadron Calorimeter

In order to stop hadrons material with a high density is needed. For this reason, brass is used in the magnet, and stainless steel is used elsewhere. Fluorescent scintillators are located between the absorbers to extract a light signal. This signal is sent via optic fiber to the photodetectors, which amplify the signal. The amount of photons is proportional to the energy of the particle. The HCAL stops and measures all hadronic particles. Therefore, it is built not to miss any particle in the range of 0 $|\eta| < 3.0$. Moreover, together with the hadron forward calorimeter, $|\eta| < 5.0$ are covered. This great coverage is necessary for observables including multiple particles, e.g the missing transverse energy which will be defined later.

4.2.3. Muon Chambers

The muon chambers lie outside of the solenoid. They are implemented in between the iron layer of the yoke and consists of three different types. Drift tubes (DT) and cathode strip chambers (CSC) are used for a good resolution. Additional resistive plate chambers (RPC) are used for a good time resolution and a fast response. All three components use the fact that muons ionize gas, which is measurable with the help of electric fields. The RPC uses the avalanche effect to be very fast and, for this reason, it is used as input for the trigger system. The muon system covers $|\eta| < 2.4$
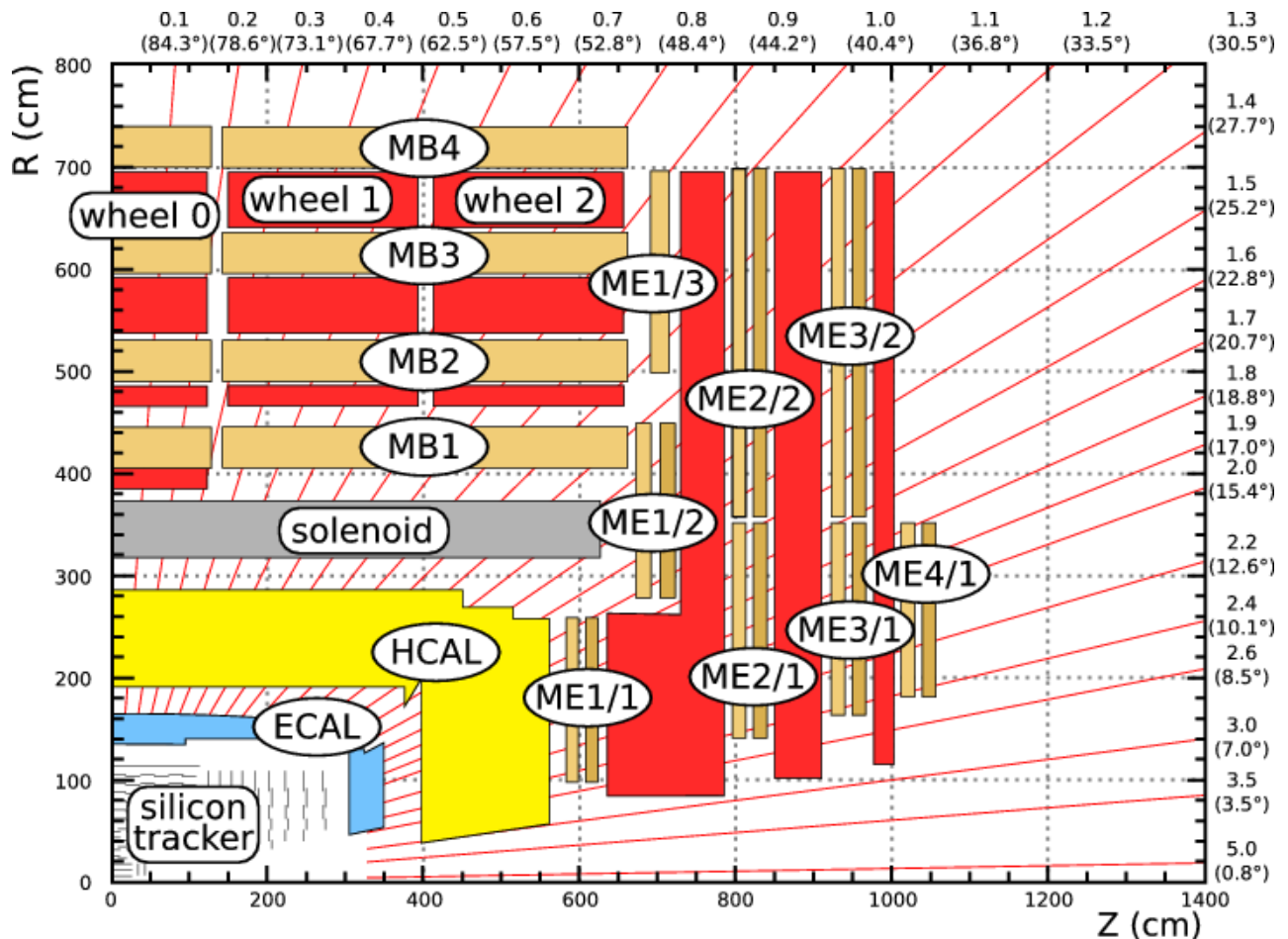
Figure 4.3.: Longitudinal view of one-quarter of the CMS detector. One can see the onion-like structure of the CMS detector. The tracker system is placed in the center surrounded by the electromagnetic calorimeter. The next layer is the hadron calorimeter that is still inside of the solenoid. The muon chambers (MB and ME) are placed in between the yoke. The picture is taken from [33].

4.2.4. Trigger

The trigger system selects those events that will be worthwhile to be transferred to the next selection stage [34; 35]. It is impossible to store all events, E.g. with an event rate of 20 MHz

(50 ns bunch spacing) and an average event size of ~ 1.5 MB would lead to 30 TB per second. For this reason, the trigger system must decide which events contain interesting physics. In order to satisfy all these requirements the triggering is split into two parts: the L1 hardware triggers and the HLT (L3) software triggers. The L1 trigger system reduces the event rate to 100 kHz by using raw objects. E.g. large energy deposits in some ECAL crystals, which can be either from a photon or an electron. The HLT trigger system is realized by a large computing farm, which uses information from all sub-detectors. The HLT object reconstruction is very similar to the offline reconstruction. An event will be transmitted to the offline computing if it fulfills certain requirements, e.g. the event consists of two isolated electrons with momenta above a certain threshold. The HLT output rate is 150 Hz leading to 225 MB/s which will be stored offline.

4.3. Computing

The computing is the third important part of the CMS experiment. Without the powerful Grid, it would be impossible to analyze the large amount of data. This section introduces the resources and tools that are used for this thesis.

4.3.1. The Grid

In order to handle the large amount of data, the grid has been constructed [36]. The grid is a network of computer centers distributed all over the world. It consists of three layers. There is one tier 0 center which is located at CERN and is connected to nine tier 1 centers. They are located in: KIT (Germany), PIC (Spain), IN2P3 (France), IFN-CNAF (Italy), JINR (Russian Federation), ASGC (Taipei), GridPP (United Kingdom), Fermilab-CMS (US), and CERN (Switzerland). The tier 0 and tier 1 centers are responsible for the reconstruction of the raw CMS data. In order to prevent data loss, the data is stored twice. One copy is saved at the tier 0 center and one copy is saved at one of the tier 1 centers. Each tier 1 center is connected to several tier 2 centers. The tier 2 centers are designated for the data analyzers. The tier 2 centers can get a local copy of the reconstructed data from a tier 1 center, and analyzers can run jobs that need these data on the batch system of the tier 2. In order to use the computing resources in a more efficient way, it is also possible for analyzers to run their jobs on available recourses of tier 1 centers.

4.3.2. Software

Several software package are used in this thesis. This subsection gives an overview of the most important of them.

4.3.2.1. ROOT

ROOT is a data analysis framework [37]. It is written in cpp, with a strict class hierarchy. It is open source and can be included in other frameworks. ROOT comes with its data files, which are the so-called root files. These root files are used to store the data. ROOT also provides functions to make 1D,2D or 3D histograms out of the data, which allows a nice representation of the experimental results.

4.3.2.2. ROOFIT and ROOSTAT

The ROOFIT and ROOSTAT are two important cpp classes embedded in the ROOT framework. They include many statistic and fitting tools, which can be used to analyze and understand the data.

4.3.2.3. TMVA

The Toolkit for MultiVariate data Analysis (TMVA) contains many multivariate tools for analyzing the data [38]. It is embedded in the ROOT framework and helps to distinguish signal and background on an event by event basis. The inputs are several observables that can help to discriminate signal from background. One popular tool is the Boosted Decision Tree (BDT). In order to distinguish between signal and background, a BDT gets trained on a training sample. After this training it can be applied to data. The output for each event of the BDT is a discriminator value between -1 and 1. The larger the discriminator value, the more likely is the signal hypothesis for this event. The BDT shows very good discrimination power also with correlated input variables.

4.3.2.4. CMSSW

The CMSSW framework was developed to analyze events that are recorded with the CMS detector. It is highly modular and can be complemented with different software packages. E.g. with the MC interfaces it is possible to produce simulated events by only using this framework. The CMSSW package uses the cpp and the python language. It combines the two main features of them, the flexibility of python and the fast calculation of cpp. The file format used to store the data bases on the root file format and filled with classes containing physics objects and their properties. The typical CMSSW workflow is to load an event, compute and add new properties to the event and then make decisions based on the related information.

4.3.2.5. Tag and Probe

In order to determine the reconstruction efficiencies for leptons, one has to ensure that the test object is a real lepton. This is provided by the so called tag-and-probe package. It uses resonances decaying into lepton pairs. For our purpose, Z bosons are sufficient. It works in two steps. At first one has to collect the tag-and-probe pairs. A tag lepton fulfills all identification

criteria, whereas the probe lepton has not to fulfill all of them. The invariant mass of the tag
and probe pair is calculated and stored and so the information if the probe passes or fails the
identification. The second step is applying fits on the invariant mass distributions of passing and
failing sample. The fit includes a signal and a background hypothesis. It is done separately for
all pairs where the probe passes the identification and where the probe fails the identification.
An example fit is shown in figure 4.4. The advantage of this method is that all leptons of the
signal hypothesis are real lepton. The efficiency of lepton identification calculate as:

$$\epsilon = \frac{N_{sig}^{pass}}{N_{sig}^{pass} + N_{sig}^{fail}} \tag{4.2}$$

with N_{sig}^{pass} all signal events where the probe passes the identification and N_{sig}^{fail} all signal events
where the probe fails the identification. The determination of differential efficiencies is possible
because the LHC produced many Z events.
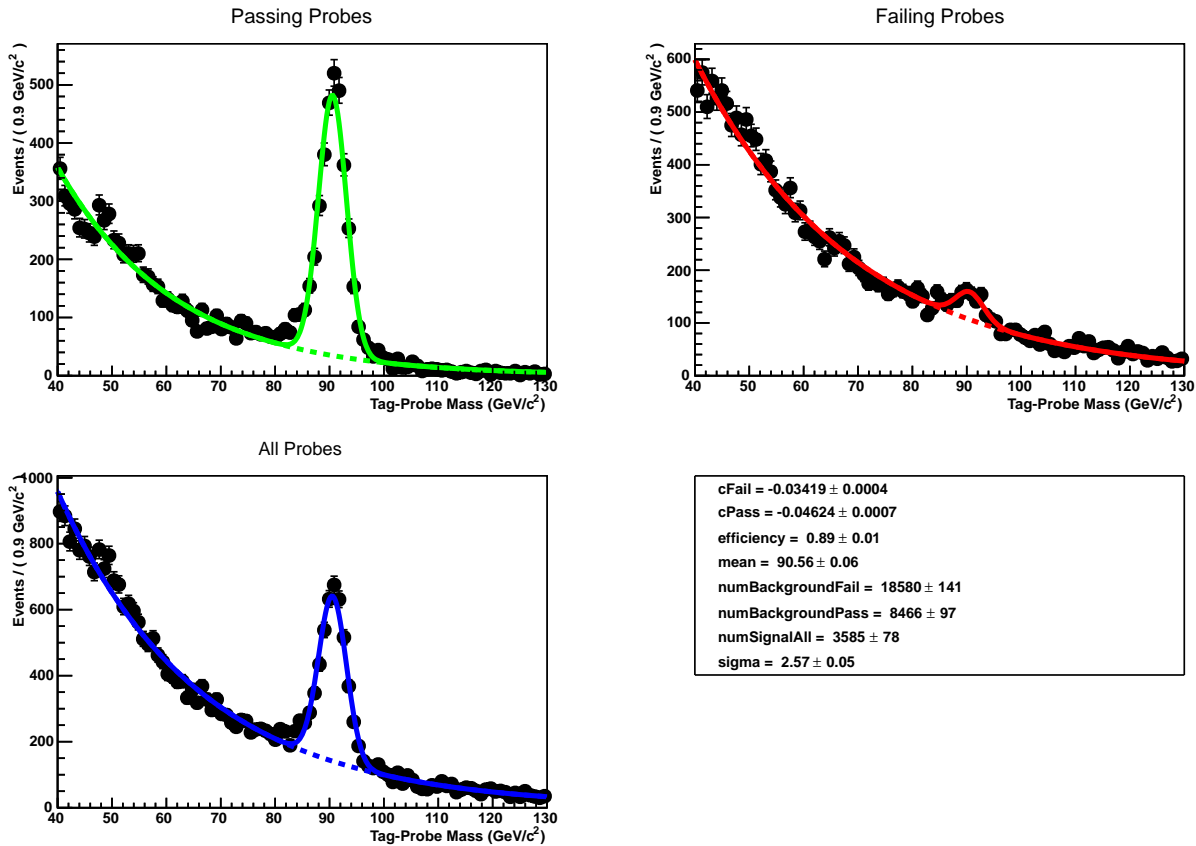
Figure 4.4.: This figure shows one fit from the tag and probe package. The fit is done on events
where the probe passes (top left), where the probe fails (top right), and on all
pairs (bottom left). The info box (bottom right) shows the combined result of the
fit. The dashed lines are the background hypothesis, and the solid lines are the
background plus signal hypothesis described in the text.

This software package is written in $C++$, uses the ROOT and ROOFIT libraries and has an
interface to CMSSW.

4.3.2.6. Combine tool

The Combine tool is a software package which includes the statistical model presented in section 3 [21; 22; 39]. It is built as a CMSSW module that provides an interface to the Roostats package. It is highly modular, and different test statistics can be used. The user only has to provide standardized data cards as input. The outcome are confidence intervals obtained with the CL_s method. This method does not always provide the best limit, but it is robust against statistical downward fluctuation. For this reason, ATLAS and CMS agreed to publish their results with these CL_s intervals.

4.3.2.7. Monte-Carlo event generation

The generation of simulated events is a multi-step procedure. The so-called Monte-Carlo (MC) generators are used for calculating the hard process of an event. In this thesis following MC generators are used: MadGraph 5, POWHEG BOX and PYTHIA 6 [40–42]. After the hard process has been computed it must be matched with the fragmentation, which is done with the PYTHIA package. The fragmentation step builds the hadrons and decays unstable particles. In the next step, the events are passed trough the detector simulation, which is done with GEANT 4 [43]. Now the simulated events have the same quality like "real" events and are passed through the same reconstruction algorithm.

4.3.2.8. DELPHES

DELPHES is designed to simulate different detectors [44]. For this reason, it uses efficiency as input and avoids the simulation of a detector and the reconstruction. E.g. the lepton efficiency, which will be presented in chapter 5, can be used as input. All efficiencies were validated with a full CMS detector simulation. DELPHES is used if extensive statistics is needed, e.g. for the projection to high luminosity.

5. Objects

With the measurements of all sub-detectors, the physics objects can be reconstructed. All particles leave their individual signature in the detector. A charged particle leaves a track in the tracker system. Photons and electrons lose their whole energy in the electromagnetic calorimeter and hadrons in the hadron calorimeter. Muons escape the yoke and leave hits in the muon chambers. In this analysis electrons, muons, tau leptons, missing transverse energy (E_{T}^{miss}) and b-jets are used and will be introduced below.

5.1. Leptons

The most important objects for a search in the three and four lepton final state are leptons. The CMS-Detector can detect all three charged lepton flavors, electrons, muons, and taus. Tau leptons have a short life-time since they are heavy. As a result, all produced taus decay within the tracker system. In order to detect a tau, one has to search for its decay products. Taus can either decay into lighter leptons (electrons and muons) or hadrons, e.g. pions or kaons. For the latter, a particular reconstruction algorithm is necessary.

5.1.1. Electron and Muons

Electrons and muons carry electric charge, and as a result they leave a single track in the tracker system (section 4.2.1). An electron deposits its whole energy in the ECAL (section 4.2.2), while on the contrary the muon can escape the calorimeter system with almost no energy loss and leaves a track in the muon chambers (section 4.2.3). The measurements of these sub-detectors result in several variables helping to identify electrons and muons. These identification variables are commonly used within the CMS collaboration for many analyses [45; 46]. For the electron identification we use a BDT (section 4.3.2.3), because it has good efficiency at low electron momenta. More information about the electron identification can be found in [45]. For muons,

the identification is based on simple cuts since they already have a good efficiency, even at small energies. Further information for the muon identification are given in [46]. The isolation variable is treated separately, because this is the critical variable to distinguish prompt leptons from objects that fake leptons, in the following just called fakes. Non-prompt leptons produced in jets are also called fakes in the context of this thesis. The source of fakes are jets, which are often produced in addition to the main process. A more detailed discussion of faked leptons will follow in section 7.1.1. The leptons from our signal process are prompt leptons with a similar kinematic signature as leptons from a Z boson. As a result, the Z boson is the perfect object for calibrating the lepton performance. With the help of the tag-and-probe method (section 4.3.2.5) it is possible to test the identification and isolation efficiency. The comparison of the efficiencies obtained by data and simulation is shown in figure 5.1 for electrons and figure 5.2 for muons. Only leptons with a transverse momentum $p_\mathrm{T} > 10$ GeV and a pseudorapidity $|\eta| < 2.4$ are considered. For electrons, a veto in the transition region ($1.4442 < |\eta| < 1.566$) is applied, because this region has a high fake rate. The isolation must be corrected with the so-called pileup correction to remove the influence of additional interactions per bunch crossing [47; 48]. For this reason, the computed isolation efficiency is almost constant with respect to the number of vertices[1], which is illustrated in the plot showing the isolation efficiency versus the number of vertices. The plots at the bottom of figure 5.1 and 5.2 prove that the efficiency was stable during the data taking period in 2012. Here the horizontal axis shows the run number that represents the time, e.g. run number 190645 was the first run in April 2012 and run number 208686 corresponds to the last run in December 2012.

Correction factors are applied for the remaining differences between data and simulation. The factors are given in table 5.1. The correction factors for muons are close to one, and the corrections for electrons are below one.

The chosen fit function has an influence on the determined efficiency, which is explained by the example below. Considering a lepton, which fails the final state radiation requirement. The failing probes lost energy, and the invariant mass is shifted to lower values. This shift leads to a different invariant mass shape compared to the passing probes which have no energy lost. Of course, the variables also have some correlations between each other. E.g. it is more likely for a lepton making final state radiation also to fail the isolation requirement. In order to determine the systematic uncertainty for the reconstruction of a prompt lepton, different fit functions have been used. The scale factors obtained with this other fit functions are all between 3% ($p_\mathrm{T} >$ 20 GeV) and 5% ($p_\mathrm{T} < 20$ GeV) of the values given in the table. An uncertainty of 3% (5%) for prompt leptons with $p_\mathrm{T} > 20$ GeV ($p_\mathrm{T} < 20$ GeV) has been assigned.

5.1.1.1. Lepton Trigger

In this analysis, we trigger on events containing either two electrons, two muons or one electron and one muon. These are the so-called double lepton triggers. Electrons and muons are

---

[1]Because the number of reconstructed vertices is proportional to the number of interactions per bunch crossing.
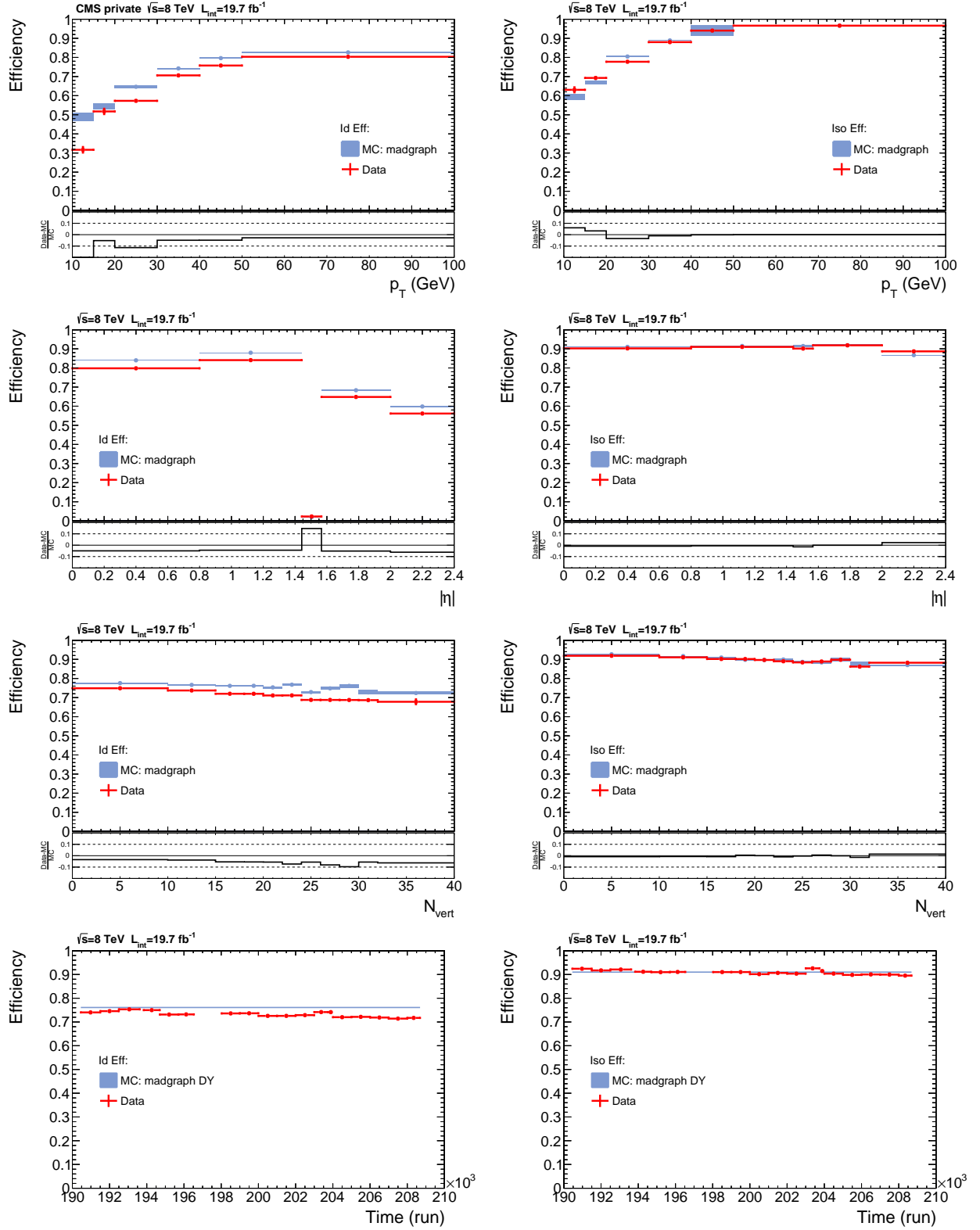
Figure 5.1.: Efficiency for an electron to pass the identification (left) and isolation (right) criteria. The first row shows the efficiency over the transverse momentum p_T. The second row shows the efficiency over the pseudorapidity η. The third row shows the efficiency over the number of vertices, and the fourth row shows the efficiency over the run number. The plots include only statistical uncertainties.
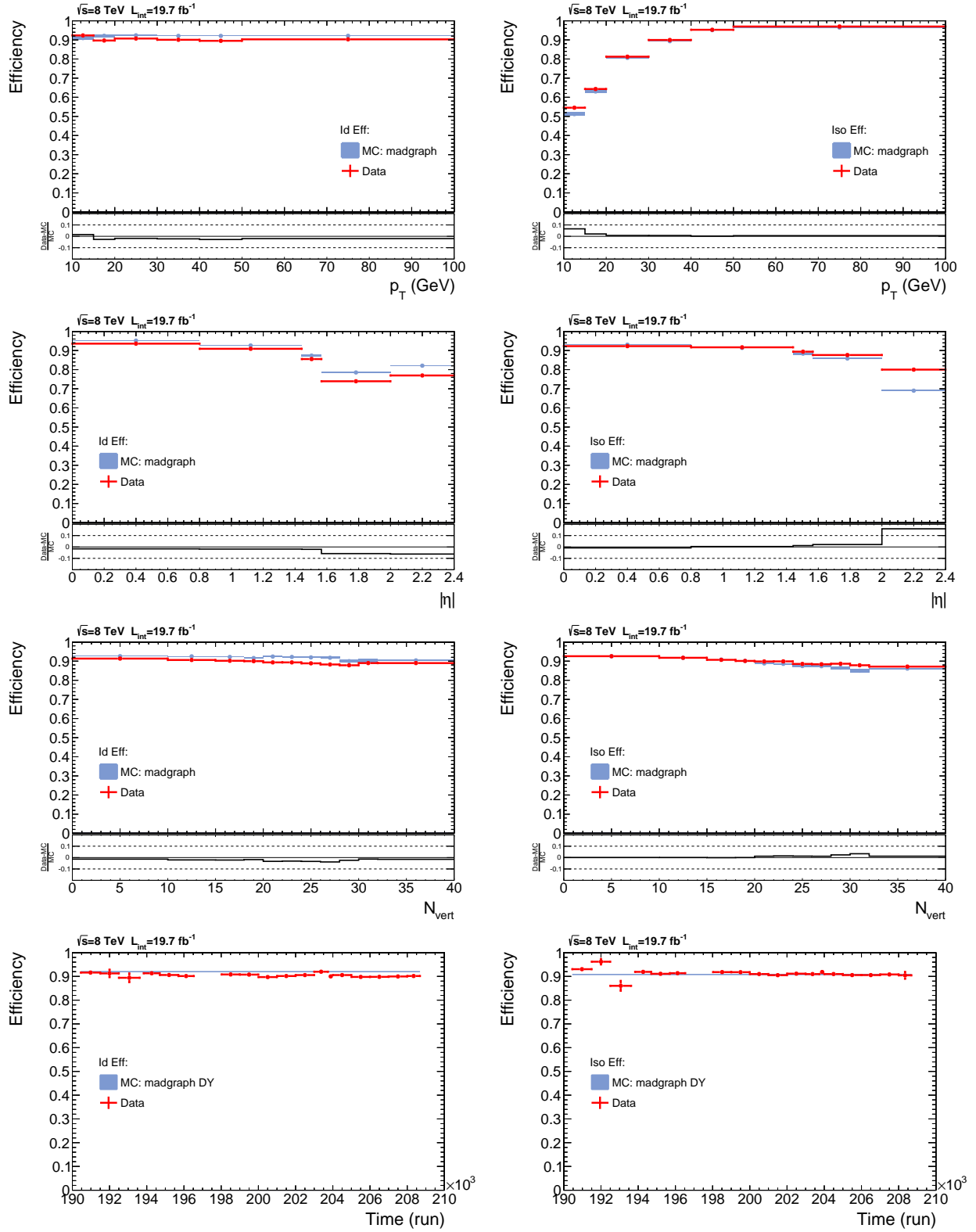
Figure 5.2.: Efficiency for a muon to pass the identification (left) and isolation (right) criteria.
The first row shows the efficiency over the transverse momentum p_T. The second
row displays the efficiency over the pseudorapidity η. The third row shows the
efficiency over the run number, and the fourth row shows the efficiency over the
run number. The plots include only statistical uncertainties.

Table 5.1.: Muon and electron MC scale factors

pseudorapidity $|\eta|$	0 - 0.8	0.8 - 1.442	1.442 - 1.556	1.556 - 2.0	2.0 - 2.4
	Muon mc scale factors				
p_T: 10 - 15 GeV	0.917	1.161	0.826	1.323	1.207
p_T: 15 - 20 GeV	0.957	0.917	1.023	1.162	1.536
p_T: 20 - 30 GeV	0.963	0.981	1.073	0.913	1.356
p_T: 30 - 40 GeV	0.975	0.984	1.050	1.010	1.138
p_T: 40 - 50 GeV	0.970	0.979	0.969	0.948	1.046
p_T: $\geq$ 50 GeV	0.982	0.983	0.993	0.976	1.011
	Electron mc scale factors				
p_T: 10 - 15 GeV	0.853	0.947	-	0.775	0.313
p_T: 15 - 20 GeV	0.947	0.867	-	0.848	0.652
p_T: 20 - 30 GeV	0.868	0.913	-	0.898	0.918
p_T: 30 - 40 GeV	0.921	0.939	-	0.930	0.975
p_T: 40 - 50 GeV	0.942	0.943	-	0.958	0.967
p_T: $\geq$ 50 GeV	0.951	0.967	-	0.990	0.983

reconstructed online for each event. If this event contains the constituents as given above with a transverse momentum greater than 17 GeV and 8 GeV, it will be recorded and sent to the offline reconstruction. The four triggers used for this analysis are:

Trigger	leading lepton	trailing lepton
Double muon	muon $p_T > 13$ GeV	muon $p_T > 8$ GeV
Double electron	electron $p_T > 17$ GeV	electron $p_T > 8$ GeV
Muon electron	muon $p_T > 17$ GeV	electron $p_T > 8$ GeV
Electron muon	electron $p_T > 17$ GeV	muon $p_T > 8$ GeV

All leptons passing our offline selection can fire the trigger. Therefore the trigger efficiency is calculated as:

$$\epsilon_{Trigger} = \frac{\text{Events pass trigger requirements and trigger fired}}{\text{Events pass trigger requirements}} \tag{5.1}$$

In order to have an unbiased data sample[2], we take data which was recorded with hadronic triggers. From this sample, we can obtain the trigger efficiency from data and compare it with simulation. In figures 5.3,5.4,5.5 and 5.6 the efficiencies depending on the leading and trailing lepton kinematics are shown. The trigger efficiency is constant if the leading (trailing) lepton has a transverse momentum greater than 20 (10) GeV. Hence, each event has to have at least one lepton with $p_T > 20$ GeV, and all other leptons must satisfy $p_T > 10$ GeV. The trigger efficiency of the double muon trigger considering simulation is about 5%-10% to high and depends on the muon kinematics. Besides this, small discrepancies for the muon object in the electron

---

[2]A data sample recorded without leptonic requirements.

muon trigger shows up. For all this differences, corrections are applied. Data and simulation agree within 5% for all other trigger objects. However, it is redundant to trigger with double lepton triggers when taking events with three or four leptons. As a result, the combination of all four triggers gives a trigger efficiency close to one and a reduced uncertainty. If there are only two leptons to fire the trigger an uncertainty of 5% is applied. If the event consist of three or more leptons with only one lepton having a transverse momentum greater than 20 GeV, an uncertainty of 3% is applied. An uncertainty of 1% is applied if an event contains three or more leptons, and two of them have at lest a transverse momentum greater than 20 GeV.
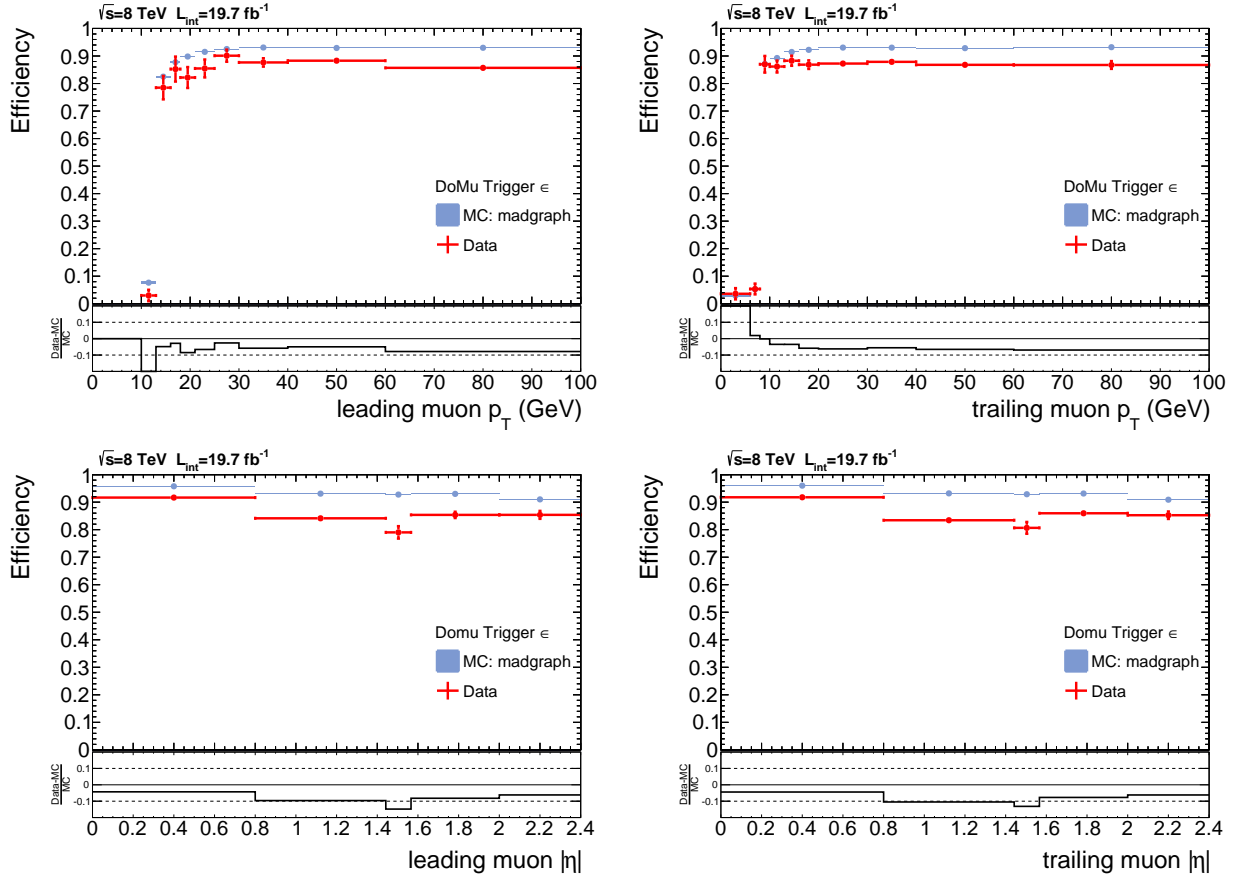
Figure 5.3.: Efficiency of the double muon (DoMu) trigger for data and MC simulation. On the left (right) the efficiency for the leading (trailing) muon. The top row shows the efficiency versus the transverse momentum. The bottom row shows the efficiency over the pseudorapidity.

All four triggers were fully functional during the 2012 data taking period, which can be seen in figure 5.7.

5.1.2. Tau leptons

In order to identify tau leptons one has to search for their decay products, since all taus will decay within the CMS detector with a typical decay length of a few millimeters. The tau decay
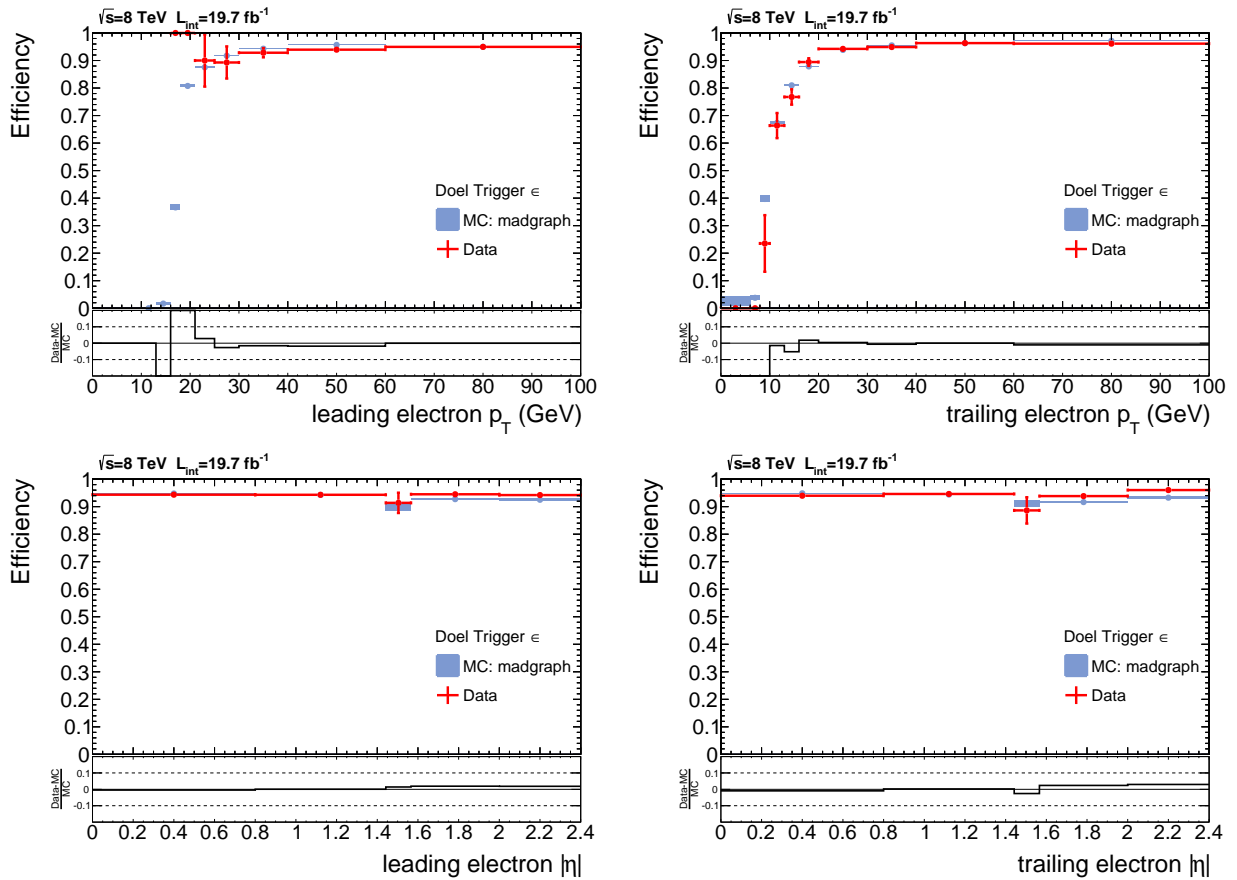
Figure 5.4.: Efficiency of the double electron (DoEl) trigger for data and MC simulation. On the left (right) the efficiency for the leading (trailing) electron. The top row shows the efficiency versus the transverse momentum. The bottom row shows the efficiency over the pseudorapidity.

modes are well-known [15]. In about 35%, the tau decays into one charged lepton(electron and muon) and two neutrinos. This decay mode leads to a final state with one isolated electron or one isolated muon and two neutrinos. The performance of the electron and muon identification has already been discussed in section 5.1.1. The other decay modes involve charged hadrons, mostly $\pi^{\pm}$ (section 2.3), and only one neutrino. One can distinguish between three different final states:

1. Single Prong (about 12% of total decay width)

2. Single Prong + π^0 (about 37% of total decay width)

3. Three Prong (about 15% of total decay width)

In CMS, the so-called Hadron Plus Stripes (HPS) algorithm was developed to account for all three final states [49]. This algorithm is based on a MVA (section 4.3.2.3) method to suppress the background. The isolation variable is crucial to identify taus and separate them from jets. In addition, discriminators are used to filtering out electrons and muons that may be miss-identified as taus. Measuring the tau properties is harder, because there is no clean selection
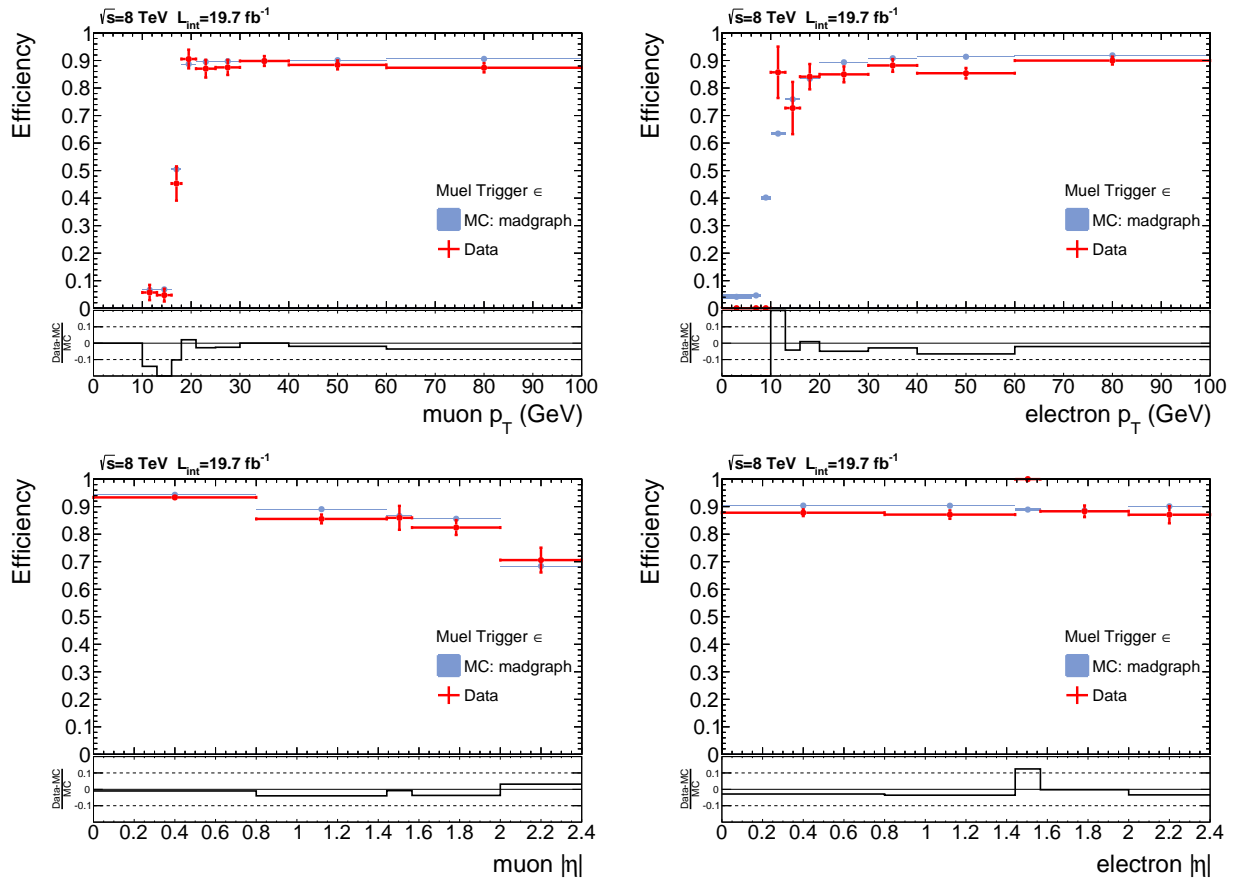
Figure 5.5.: Efficiency of the muon-electron (MuEl) trigger for data and MC simulation. On the left (right) the efficiency for the muon (electron). The top row shows the efficiency versus the transverse momentum. The bottom row shows the efficiency over the pseudorapidity.

that only contains prompt taus. This tau identification is used by many analyses within the CMS collaboration, and the tau properties are well known. For a prompt tau, no correction factor is needed, and the uncertainty is 6%. For electrons faking a tau a correction factor of 1.4 in the barrel region and 0.8 in the endcap region is applied, which was studied in [49]. No correction factor is needed for events containing a muon that fakes a tau. The uncertainty for this process is 30%. The dominant source for fake taus are jets and will be discussed in section 7.2.3.

5.2. Particle Flow Objects

CMS has established the so-called particle flow concept [50]. This is possible due to the fine granularity of the ECAL (section 4.2.2). Each single track can be assigned to an energy deposit in the calorimeter system. The energy deposits that cannot be assigned to a track, seeds the neutral particle flow candidates. It is possible to allocate a particle hypothesis to each energy flow. This knowledge improves the resolution. The particle flow concept has the advantage that all sub-detector parts work like one detector. Therefore, the particle flow objects are more
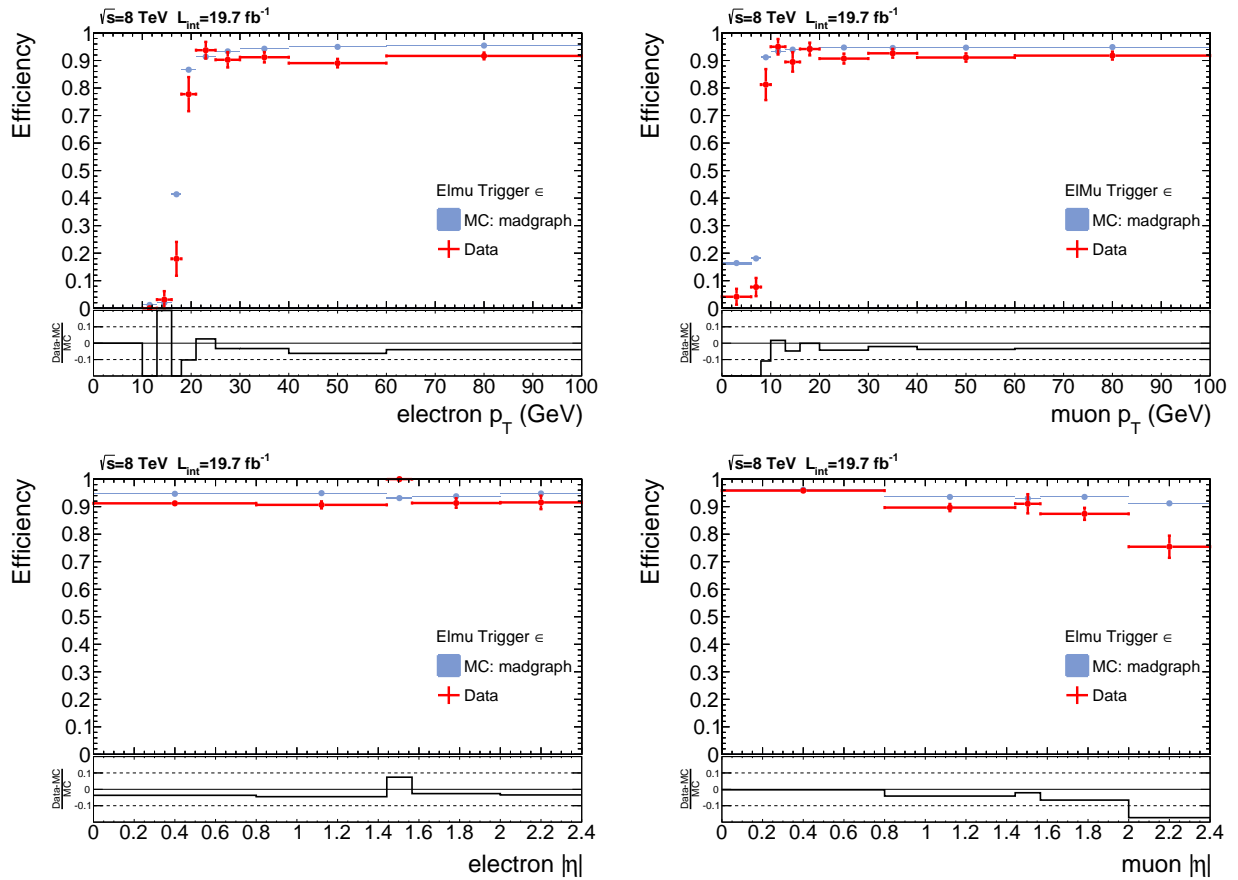
Figure 5.6.: Efficiency of the electron-muon (Elmu) trigger for data and MC simulation. On the left (right) the efficiency for the electron (muon). The top row shows the efficiency versus the transverse momentum. The bottom row shows the efficiency over the pseudorapidity.

accurate than just the addition of all measurements from the sub-detectors.

5.2.1. Jets and b-tagged jets

Because of the confinement a color charged particle (a quark or a gluon) always hadronizes [3] and leads to jets of hadrons, photons and leptons. Jets leave a clear signature in the detector. In the tracker system, they produce collimated tracks, in the electromagnetic calorimeter they deposit electromagnetic energy and in the hadron calorimeter they deposit the remaining energy. The CMS jet reconstruction uses the so-called anti-kt 05 algorithm [51]. The particle flow objects are taken as input. The results are jets, which are cones (diameter R=$\sqrt{\Delta\eta^2 + \Delta\phi^2} < 0.5$) filled with pf objects. At last some minimal requirements are applied on the jets: The jet should contain at least one charged hadron and have some energy deposit in the hadron calorimeter. Jets originating from b-quarks have a slightly different signature than jets form light quarks or gluons. A b-quark hadronizes into B-mesons. The B-mesons have a long lifetime, because of the CKM suppression [15]. So they fly a few millimeters before they decay. The b-meson has a

---

[3] Except for the heavy top quark, which decays before it can hadronizes.
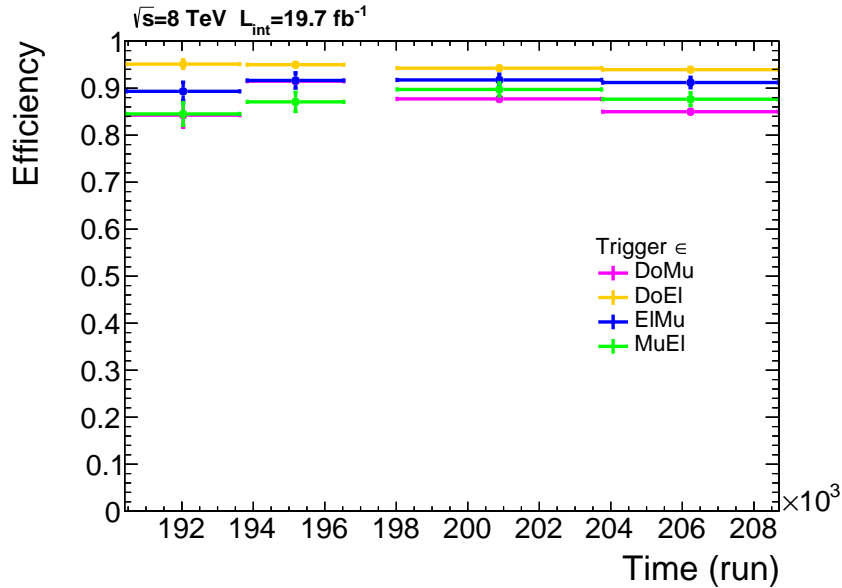
Figure 5.7.: Time evolution of the trigger efficiency for the four triggers used in this analysis.

large mass and for this reason, the decay products are boosted from the initial B-meson flight direction. This boost leads to kinked tracks and produces a secondary vertex. The B-mesons have a long decay chain, and, as a result, the jets consist of many tracks. All this information are put together in the combined secondary algorithm [52; 53]. This algorithm is based on a likelihood function, and the output is a discriminator value. A jet with a discriminator value above a certain threshold is a b-tagged jet (b-jet). In this thesis, the medium working point is used as the threshold. Meaning the b-tagging has an efficiency of about 70% and a miss-tag rate of 1% for light jets and 20% for jets originating from c-quarks.

5.2.2. Missing transverse Energy

Missing transverse energy E_{T}^{miss} is the critical variable for many SUSY searches. The source of this missing energy are particles that do not interact with the detector. In the Standard Model, such particles are neutrinos and in supersymmetric extensions of the Standard Model the lightest supersymmetric particles are additional sources. The reason, why only the transverse component gives a reliable result, is that the beam pipe is located along the z-direction. Therefore, it is possible that particles escape the detector in the longitudinal direction. Since the colliding partons only carry a fraction (see Section 2.3) of the proton momentum, the remaining partons carry much energy and fly close to the beam pipe.

The missing transverse energy E_{T}^{miss} calculated as:

$$E_{\mathrm{T}}^{miss} = \left| \sum_{all\ PF} \vec{p}_T \right| \tag{5.2}$$

so E_T^{miss} is the magnitude of the sum of the transverse components of all particle flow candidates momenta. Even if the calculation looks simple the E_T^{miss} is one of the most complicated quantities, since the measurement of each single particle is included in the calculation. All corrections and uncertainties of the individual particles must be considered for the E_T^{miss} calculation, too. In order to get the best possible E_T^{miss} performance, we use a MVA algorithm for the E_T^{miss} calculation [54]. This methode reduces the dependency on the noise within the detector. Noise smears the true E_T^{miss}. The missing transverse energy obtained with this method has an improved resolution compared to the classical sum. Nevertheless, this method depends on the detector noise and of the correct modeling of this noise in the simulation. So-called recoil corrections are applied [54]. In order to determine the recoil corrections, events with two opposite sign muons that are originating from a Z boson are selected. Their invariant mass has to be between 75 GeV and 105 GeV and we treat the sum of the 4-momenta as Z candidate. Then we split the E_T^{miss} into two components, one perpendicular to the Z boson direction and the other parallel to it. In the Z-direction, we are sensitive to the recoil of the hard scattering and can measure the resolution of it. The perpendicular component is sensitive to all sources of noise that are not affected by the proper event. We correct for the small differences. In figure 5.8 the uncorrected and the corrected E_T^{miss} distributions are shown. After the recoil correction, the E_T^{miss} in data and simulation shows a good agreement. Further information about the E_T^{miss} performance in the CMS detector can be found in [54–56].
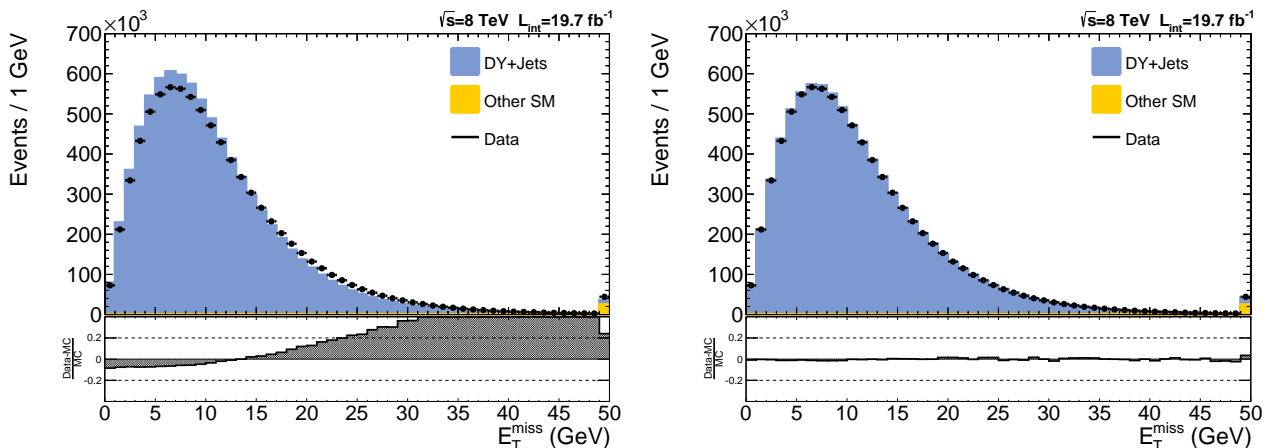
Figure 5.8.: E_T^{miss} distribution for events with two muons is shown. Data is compared to simulation. Most of these events stems from Z$\rightarrow \mu\mu$ decays (blue). On the left the E_T^{miss} distribution before the correction and on the right the E_T^{miss} distribution after applying the corrections are shown.

Many effects contribute to the uncertainty since E_T^{miss} dependence on many input variables. The largest part of the uncertainty stems from the jets (jet energy scale) [57]. By varying all input variables by $\pm 1\sigma$ the uncertainty of the missing transverse energy can be obtained. Later the data is split into different E_T^{miss} regions, and an uncertainty for each region is determined. Typical values for the uncertainty of E_T^{miss} is in order of 2% to 15%.

6. Signal

This analysis is a search for supersymmetry in the 3ℓ and 4ℓ final states. In order to emphasize the strength of this analysis, so-called simplified models are used. A simplified model does not claim to be a model that could be realized in nature. The idea is to test individual signatures, which are subsets of full models. With the combination of different simplified signatures several full models can be recovered. A general analysis of full models (pMSSM) can be found in [58]. This paper takes simplified model results, e.g. this analysis, as input.

The main advantage of a simplified model is that it only depends on two or three parameters. These parameters are:

- The mass of the produced supersymmetric particles

- The mass of the supersymmetric particles in the decay chain.

- The mass of the lightest supersymmetric particle

In this analysis, the involved supersymmetric particles are neutralinos, charginos, and sleptons since they can produce final states with three or four leptons. Since R-parity conservation is assumed, supersymmetric particles are always produced in pairs. An other consequence of the R-parity conservation is that the lightest supersymmetric particle (LSP) is stable. The LSP is assumed to be uncharged and for this reason it does not interact with the detector. This leads to events which have a large amount of E_T^{miss}. The amount of E_T^{miss} depends on the kinematic of the supersymmetric particles. E.g if the two LSP are flying back to back the E_T^{miss} is reduced since they partly chancel each other. Typical values reach from 50 GeV up to several hundred GeV.

6.1. Chargino-Neutralino production

The associated production of a $\tilde{\chi}_1^\pm$ $\tilde{\chi}_2^0$ pair is of special interest for the three lepton final state. Here the lightest supersymmetric particle is the $\tilde{\chi}_1^0$, which is assumed to be bino-like. The $\tilde{\chi}_1^\pm$

and $\tilde{\chi}_2^0$ are both wino-like and are expected to have the same mass, so we assume $m_{\tilde{\chi}_1^\pm} = m_{\tilde{\chi}_1^0}$[1]. The full process is: pp $\to \tilde{\chi}_1^\pm \tilde{\chi}_2^0 \to \tilde{\chi}_1^0 \tilde{\chi}_1^0 \ell^+\ell^-\ell^\pm\nu$. For the production of the $\tilde{\chi}_1^\pm \tilde{\chi}_2^0$ pair the mass $m_{\tilde{\chi}_1^\pm}$ ($= m_{\tilde{\chi}_2^0}$) is the only free parameter. It is possible to calculate a cross section since we have assumed they are wino-like. The program resummino is used, which gives NLO+NLL results [59–61]. The values, as well as the uncertainties, are given in table 6.1. The charge asymmetry meaning that more $\tilde{\chi}_1^+ \tilde{\chi}_2^0$ than $\tilde{\chi}_1^- \tilde{\chi}_2^0$ are produced, increases for heavy particles, as demonstrated in table 6.1.

Table 6.1.: NLO+NLL cross section for the pp $\to \tilde{\chi}_1^\pm \tilde{\chi}_2^0$ production at a center of mass energy of 8 TeV. It includes the assumption that $\tilde{\chi}_1^\pm \tilde{\chi}_2^0$ are Wino like and $m_{\tilde{\chi}_1^\pm} = m_{\tilde{\chi}_1^0}$. The uncertainties include scale uncertainties as well as the uncertainty of the parton density functions

mass (GeV)	100	200	300	400	500	600	700	800
pp $\to \tilde{\chi}_1^+ \tilde{\chi}_2^0$ (fb)	7385.1	530.11	100.79	27.50	9.00	3.26	1.28	0.52
pp $\to \tilde{\chi}_1^- \tilde{\chi}_2^0$ (fb)	4128.1	246.50	40.97	10.08	3.05	1.05	0.40	0.16
pp $\to \tilde{\chi}_1^\pm \tilde{\chi}_2^0$ (fb)	11513.2	776.61	141.76	37.58	12.05	4.31	1.68	0.68
uncertainty $\pm 1\sigma_{theory}$ (fb)	327.5	30.02	7.08	2.29	0.84	0.33	0.15	0.07

For the decay into the three lepton final state ($\tilde{\chi}_1^\pm \tilde{\chi}_2^0 \to \tilde{\chi}_1^0 \tilde{\chi}_1^0 \ell^+\ell^-\ell^\pm\nu$) we have more freedom. The first parameter is the mass of the $\tilde{\chi}_1^0$. The particle which mediates the decay also plays an important role. Two scenarios are distinguished. First the decay via sleptons are considered and then the decay via Standard Model bosons will be presented.

6.1.1. Decays via Sleptons

In this scenario the $\tilde{\chi}_1^\pm$ and the $\tilde{\chi}_2^0$ decay via sleptons into the $\tilde{\chi}_1^0$. Therefore, the slepton mass must be between the mass of $\tilde{\chi}_1^\pm$ and the mass of $\tilde{\chi}_1^0$ ($m_{\tilde{\chi}_1^0} < m_{\tilde{\ell}} < m_{\tilde{\chi}_1^\pm} = m_{\tilde{\chi}_2^0}$). The kinematic of the decay product depends on the mass of the slepton, and this influences the acceptance of our analysis. For this reason, three different slepton mass scenarios are considered:

- Light slepton mass: $m_{\tilde{\ell}} = 0.05 m_{\tilde{\chi}_2^0} + 0.95 m_{\tilde{\chi}_1^0}$

- Moderate slepton mass: $m_{\tilde{\ell}} = 0.5 m_{\tilde{\chi}_2^0} + 0.5 m_{\tilde{\chi}_1^0}$

- Heavy slepton mass: $m_{\tilde{\ell}} = 0.95 m_{\tilde{\chi}_2^0} + 0.05 m_{\tilde{\chi}_1^0}$

The last free parameter is the type of the slepton. They can be the superpartner of a left or a right-handed lepton. Sleptons are also called left and right-handed meaning that they are superpartners of left or right-handed leptons, but they have spin 0 and differ in the weak isospin quantum number. The mass of the left and right-handed sleptons differ in many SUSY

---

[1]In a natural model the differences are in order of few GeV.

scenarios. Their coupling to neutralinos and charginos can be different depending on the lepton flavor. If the neutralino or chargino decay via its higgsino component the decay via staus is enhanced. Three flavor scenarios are considered:

- The flavor democratic scenario: All left-handed sleptons are considered and so the sneutrinos must be considered, too. They lead to a 50% reduction of the branching ratio into the three lepton final state. The $\tilde{\chi}_1^\pm$ and $\tilde{\chi}_2^0$ decay democratically into all lepton flavors.

- The tau enriched scenario: All right-handed sleptons are considered. The $\tilde{\chi}_1^\pm$ decays exclusively via a stau and the $\tilde{\chi}_2^0$ decays equally into all lepton flavors.

- The tau dominated scenario: Only right-handed staus are considered. Therefore, the $\tilde{\chi}_1^\pm$ and $\tilde{\chi}_2^0$ decays into final states with taus.

The different scenarios are illustrated in figure 6.1.

Figure 6.1.: Feynman diagrams for Chargino Neutralino production with slepton mediated decays. On the top left, the flavor democratic scenario is illustrated. On the top right the tau enriched and on the bottom the tau dominated scenario. Explanations can be found in the text.

6.1.2. Decays into WZ $\tilde{\chi}_1^0 \tilde{\chi}_1^0$

In this scenario sleptons are heavy such that they do not influence the chargino and neutralino decay. The charginos and neutralinos must decay via Standard Model bosons. The most natural way is the decay into W and Z bosons, which is illustrated in figure 6.2. In order to get final

states with three leptons, the W boson, and the Z boson must decay into leptons. Therefore, only about 3% of the events can be collected, which reduces the sensitivity of this final state compared to the scenario with light sleptons. Nevertheless, the three lepton search plays the significant role for this final sate, because it has little backgrounds.

Figure 6.2.: Feynman diagrams for Chargino Neutralino production with decay into a W boson and a Z boson.

6.2. Neutralino-Neutralino production with Decays into Z Bosons

In this scenario two neutralinos are produced, which subsequently decay into a Z boson and the LSP. However, the cross section for neutralino pair production is suppressed at the LHC. To avoid this, we use a supersymmetric model with gauge mediated symmetry breaking (GMSB) [62–64]. Although it is a full model, it has similar properties to a simplified model in our realization. The gaugino mass parameters are set to $M_1 = M_2 = 1$ TeV and the ratio of the Higgs bosons vacuum expectation values are set to $\tan\beta = 2$. The $\tilde{\chi}_1^\pm$, $\tilde{\chi}_2^0$ and $\tilde{\chi}_1^0$ are higgsino-like and are almost mass degenerated. Their masses are approximately the same as the value of the higgsino mass scale parameter μ ($m_{\tilde{\chi}_1^\pm} \approx m_{\tilde{\chi}_2^0} \approx m_{\tilde{\chi}_1^0} \approx \mu$). This is the parameter that determines the production cross section. The cross section itself is the addition of all possible combinations of charginos neutralino pairs since all of them will decay into the $\tilde{\chi}_1^0$. This decays are very soft and leave no measurable signature in the detector because they are all mass degenerated. In this scenario, the almost massless gravitino is the LSP, and the $\tilde{\chi}_1^0$ must decay via a Standard Model boson into the gravitino. The Feynman diagram of this process is shown in figure 6.3.

For low μ values, the decay into Z bosons is almost 100%. For higher μ values, the decay via a Higgs boson is possible. The branching ratio for GMSB $\to$ ZZ+E_T^{miss} at $\mu = 420$ GeV goes down to about 85%. The cross section for this model can be found in table 6.2. The uncertainty on this cross section is set to 5% that covers scale uncertainties as well the uncertainty of the parton density functions.

Figure 6.3.: Feynman diagrams for the GMSB model. Details can be found in the text.

Table 6.2.: NLO+NLL cross section for pp $\to \tilde{\chi}_i\,\tilde{\chi}_j \to \tilde{\chi}_1^0\,\tilde{\chi}_1^0$ production in a GMSB model at
a center of mass energy of 8 TeV.

μ (GeV)	110	150	200	250	300	350	400	420
full σ (fb)	7288	2141	682.8	271.0	122.4	60.80	32.44	25.37
BR (Z Z $\tilde{G}$ $\tilde{G}$)	1	0.997	0.945	0.905	0.88	0.865	0.855	0.854

7. Backgrounds

Searching for SUSY is always searching for the unknown. An exact knowledge about the backgrounds producing 3ℓ and 4ℓ events is essential for this analysis. These backgrounds are well-known SM-processes, for example, double boson production or $t\bar{t}$ production. First the objects and variables needed for this thesis are recapped. Then the individual backgrounds will be discussed until the end of this chapter.

7.1. Summary of Objects and Variables

This section summarizes the objects and variables used in this analysis. More information can be found in chapter 5.

7.1.1. Leptons

Leptons are the key part of this analysis. If we measure a lepton, it can originate from three different sources. The so-called prompt leptons originate from decays of heavy objects such as SUSY particles, vector bosons or Higgs bosons. They are all produced at the primary vertex because heavy objects have a short lifetime. Figure 7.1 shows the invariant mass distribution for events with two opposite sign leptons $\mu^+\mu^-$, e^+e^- and $\mu^\pm\tau^\mp$. The blue region contains simulated $Z \to \ell^+\ell^-$ events consisting of prompt leptons. For $\mu^+\mu^-$ and e^+e^- small differences around the Z resonance shows up. These differences originate from soft photon radiation of the charged leptons, which is not correctly modeled in the simulation. Leading to a shift of the Z peak of $\sim$1 GeV for electrons and $\sim$0.5 GeV for muons. Later on, we define the onZ region for two opposite-sign same-flavor leptons between 75 GeV and 105 GeV. Within this interval, these effect is negligible and covered by the uncertainty. The $\mu^\pm\tau^\mp$ plot shows that the tau identification works as discussed in section 5.1.2. Here the Z-peak, from prompt $Z \to \tau^+\tau^- \to \mu^\pm\tau^\mp_{had} + 3\nu$ events, is shifted to values around 60 GeV because the neutrinos are not

considered in the invariant mass calculation. In this plot, the amount of other Standard Model backgrounds is large. The major part of this background stems from events with a fake tau, which will be discussed later in this chapter. The visible Z-peak around 90 GeV originates from $Z \to \mu^+\mu^-$ events, where one muon fails the muon identification, but fakes a tau.

Figure 7.1.: Invariant mass distribution for events with two opposite sign leptons. On the top left (right) the invariant mass distribution for tow opposite sign muons (electrons) are shown. On the bottom, the invariant mass distribution of a tau and a muon is shown.

Then there are so-called non-prompt leptons. Such leptons are produced in jets and can escape them so that they can fulfill the isolation criteria. Additionally there are hadrons, mostly $\pi^\pm$'s and $K^\pm$'s, which are wrongly reconstructed as leptons. We do not distinguish between them and summarizes both as fakes. The fake rate depends on the jet characteristics. For this reason, the fake rate will be controlled separately in the DY and the $t\bar{t}$ sample. More information will follow in section 7.2.3.

The third source are leptons from photon conversion. There are again two processes, real and virtual photons. Both processes are similar and will be studied in section 7.2.1.2

7.1.2. Missing transverse Energy and transverse Mass

Large missing transverse Energy (E_T^{miss}) is a typical signature of events including supersymmetric particles, but Standard Model processes can also produce a visible amount of missing transverse energy. For the three lepton final state, these are WZ events, where the Z decays into lepton pairs and the W into one lepton and one neutrino. The neutrino is the source of the missing transverse energy. In order to suppress this kind of background, we introduce the transverse mass variable. It is similar to the invariant mass, but only the transverse components are used, since E_T^{miss} is only defined in the x-y plane. It is calculated as:

$$M_{\mathrm{T}} = \sqrt{2 \cdot E_{\mathrm{T}}^{miss} \cdot p_T^{Wlep}(1 - \cos \Delta \phi)}, \tag{7.1}$$

where $\Delta \phi$ is the angle between the lepton and the E_{T}^{miss} in the x-y plane and p_T^{Wlep} is the transverse momentum of the lepton originate from the W boson. For events where the whole E_{T}^{miss} originates from one neutrino coming from a W-decay, this variable is lower than the W mass. For events including other E_{T}^{miss} sources like SUSY, this relation does not hold.

7.2. Validation of Backgrounds

Dedicated MC samples for each background with 3ℓ and 4ℓ events are used. Most of these samples are produced with the Madgraph framework [40]. Some rare backgrounds are produced with the Powheg package and Pythia package [41; 42]. These events are passed through a detector simulation and have the same observables as real data. Correction factors are applied for the differences between the simulation and real data. The corrections for the prompt lepton efficiency and the E_{T}^{miss} resolution have been explained in chapter 5. In order to match the correct number of interactions per bunch crossings, the simulated events are re-weighted.

For the cross section NLO predictions are used [65–80]. All samples get scaled to an integrated luminosity of $\mathcal{L}_{int}$ = 19.7 fb^{-1}, which corresponds to the full 2012 dataset. The used MC samples are listed in table 7.1. All but one sample have been produced centrally and validated by the CMS collaboration. The ZZ $\to 4\,\ell$ was produced privately, without applying the invariant mass cut used in the centrally produced sample. The cross section of this private sample is obtained due to normalization to the centrally produced sample. Control plots are shown in Appendix B.

The samples are subdivided into four different groups: double boson, fake, photon conversion and rare. The double boson group includes the WZ and ZZ production. They are the most important backgrounds for the 3ℓ and 4ℓ final states. The WW counts into the fake group since it only produces two prompt leptons. The fake group covers all relevant contribution to the 3ℓ and 4ℓ final state including fakes, e.g. $t\bar{t}$ and DY. The photon conversion group includes all backgrounds with a photon in the final state. Additionally, the Z$\gamma^* \to 3\,\ell$ is listed there, which is the same sample as the ZZ $\to 4\,\ell$. But which covers the case if the γ^* undergoes an

asymmetric conversion and one lepton gets lost. The last group covers the rare backgrounds, which includes processes with a small $\sigma\times$BR into the 3ℓ and the 4ℓ final state.

Table 7.1.: Summary of used MC samples. If not quoted otherwise they are computed with the madgraph package. The first column shows the group the of produced sample. The second column gives the production process. The third column shows the cross section for this process that is multiplied by the branching ratio if it is included in the process. The last column gives comments for some processes.

Group	Process pp $\rightarrow$	$\sigma\times$BR (pb)	Comment
Double Boson	WZ $\rightarrow 3\ell$	1.06	
	ZZ $\rightarrow 4\,\ell$	1.0	private MC[1]
Photon conversion	Z$\gamma^* \rightarrow 3\,\ell$	1.0	private MC[1]
	Zγ	159	
	$t\bar{t}\,\gamma$	1.444	
	WWγ	0.528	
Fake	Z $\rightarrow 2\ell$	3532.8	m$_Z$ >50 GeV
	Z $\rightarrow 2\ell$	907.3	10 GeV<m$_Z$ < 50 GeV
	$t\bar{t} \rightarrow 2\ell$	25.1	
	$t\bar{t} \rightarrow 1\ell$	107.7	
	tW	11.0	produced with powheg
	$\bar{t}$W	11.0	produced with powheg
	WW $\rightarrow 2\ell$	5.995	
	W $\rightarrow 1\,\ell$	37509	
Rare	VBF H	1.578	produced with pythia
	ggF H	19.27	produced with pythia
	ZH; WH; $t\bar{t}$ H	1.17	inclusive; produced with pythia
	$t\bar{t}$ W	0.232	
	$t\bar{t}$ Z	0.208	
	$t\bar{t}$ WW	0.00204	LO cross section
	WWW	0.08217	
	WWZ	0.0633	
	WZZ	0.01922	
	ZZZ	0.00459	
	tbZ	0.217	

[1] private MC, more information about this sample can be found in [81]

In this section the MC prediction gets tested, the uncertainty determined and if necessary corrections to this MC samples are applied. In order to do this, we look at a selection which is close to the final selection but does not contain signal events. The following definitions are valid for all selections:

- Lepton means an electron or a muon with $p_{\mathrm{T}} > 10$ GeV and $|\eta| < 2.4$.

- Veto on events containing opposite-sign same-flavor lepton pairs ($\mu^+\mu^-$ or e^+e^-) with an invariant mass < 12 GeV. This rejects events originating from decays of low mass

resonances (for example J/Ψ Meson [15]).

- Tau means a reconstructed hadronic tau lepton with $p_\mathrm{T} > 20$ GeV and $|\eta| < 2.1$.

- E_T^{miss} is the missing transverse energy calculated with a MVA method.

- M_T is the transverse mass of E_T^{miss} and one lepton or one tau.

- b-jet is a jet with $p_\mathrm{T} > 30$ GeV and $|\eta| < 2.1$, where the b-tagging algorithm fulfills the medium requirements.

7.2.1. Double Boson

Double boson backgrounds are the full-leptonic WZ and ZZ decays. They have 3ℓ and 4ℓ events containing exclusively prompt leptons.

7.2.1.1. WZ

WZ is the most essential background for the 3ℓ final state. It has three prompt leptons, like our signal, and with the neutrino also a source of E_T^{miss}. The M_T variable is used to suppress this kind of background. In order to validate the MC prediction events with three leptons (μ,e) are selected. These leptons should have at least one opposite-sign same-flavor pair onZ, meaning that the invariant mass of the pair is between 75 GeV and 105 GeV. The remaining lepton and the E_T^{miss} are used to calculate the transverse mass M_T. In figure 7.2 the result of the selection is shown. The shape is well described, but more data is observed. This is consistent with the outcome of the cross section measurement, which is based on the same events. The problem is that these overshot or a fraction of it could also originate from events with supersymmetric particles. We could oversee the possible SUSY contribtuon by just scaling to the MC prediction. The pure MC-prediction is taken but with an uncertainty of 20% which covers the differences between data and measurement.

7.2.1.2. ZZ and Zγ^*

ZZ is the most essential background for the 4ℓ final state. This background includes also the case where one of the Z bosons is off-shell, so-called γ^*. A madgraph MC sample that includes Zγ^* production has been produced. A detailed description of this sample can be found in [81]. This kind of background has no intrinsic E_T^{miss}. In order to validate this sample events with 4ℓ, two opposite-sign same-flavor pairs and $E_\mathrm{T}^{miss} < 30$ GeV are selected. The result is presented in figure 7.3. It shows that two on-shell Z boson are produced in the most cases. However, also the Z$\gamma^{(*)}$, where the second opposite-sign same-flavor pair is off-shell, has a visible yield. These events are visible in the invariant mass plot for 4 leptons. The threshold, for producing two on-shell Z bosons, is $2\times \mathrm{m}_Z \approx 180$ GeV. Below this threshold one Z has to be off shell and the cross section is small. With a closer look at 125 GeV one can see a small resonance from the other SM-background. This resonance originates from H$\rightarrow$ZZ$\rightarrow 4\ell$ decays. In contrast to
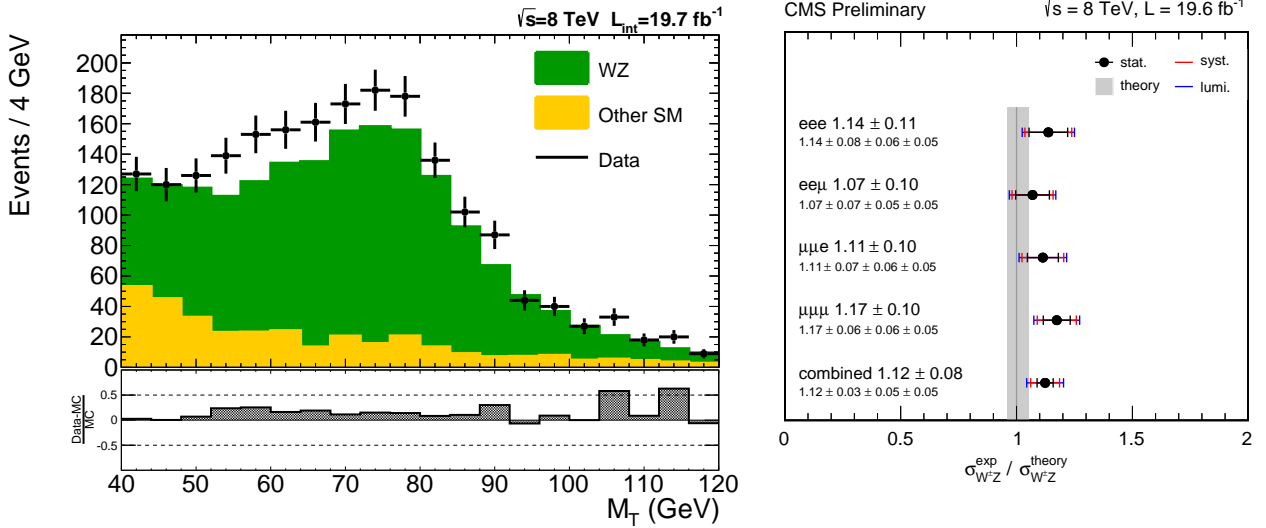
Figure 7.2.: In the left plot the M_T distribution for events with three leptons(μ,e), and at least one opposite-sign same-flavor lepton pair onZ is shown. On the right plot the preliminary result on the cross section measurement is shown. The right plot is taken from [65].

the official measurement, only three H$\rightarrow$ZZ$\rightarrow$4ℓ events are observed [82]. The main difference between the H$\rightarrow$ZZ$\rightarrow$4ℓ measurement is the cut on the invariant mass of opposite-sign same-flavor lepton pairs smaller than 12 GeV and a lepton identification which is optimized also for p_T thresholds smaller than 10 GeV.

The uncertainty for on-shell ZZ production is 2% and for off-shell it is 6%. This covers differences of the LO to NLO calculation as well as scale and pdf uncertainties [70–73].

7.2.2. Photon conversion ($Z\gamma^{(*)}$)

Real photons only convert into electrons. Virtual photons carry some virtual mass and if this mass is more than two times the leptons mass they can decay into this lepton flavor. The production mode for Zγ and Zγ^* is illustrated in figure 7.4. On the right plot, we can see two bands. The first band originates from events with initial state radiation since the invariant mass of the two leptons still lies on the Z mass. The second band shows final state radiation, here the invariant mass of all the two leptons and the photon lies on the Z mass.

All gammas can decay into lepton pairs. The invariant mass <12 GeV cut will reject such events if both leptons are successfully reconstructed. However, this cut does not work if one lepton takes the majority of the photon momentum. For this reason, the other lepton is to soft and fails our acceptance. This phenomena is the so-called asymmetric conversion.

In order to validate the background prediction events with three leptons and at least one opposite-sign same-flavor pair are selected. We apply a $E_T^{miss} < 30$ GeV cut to avoid signal
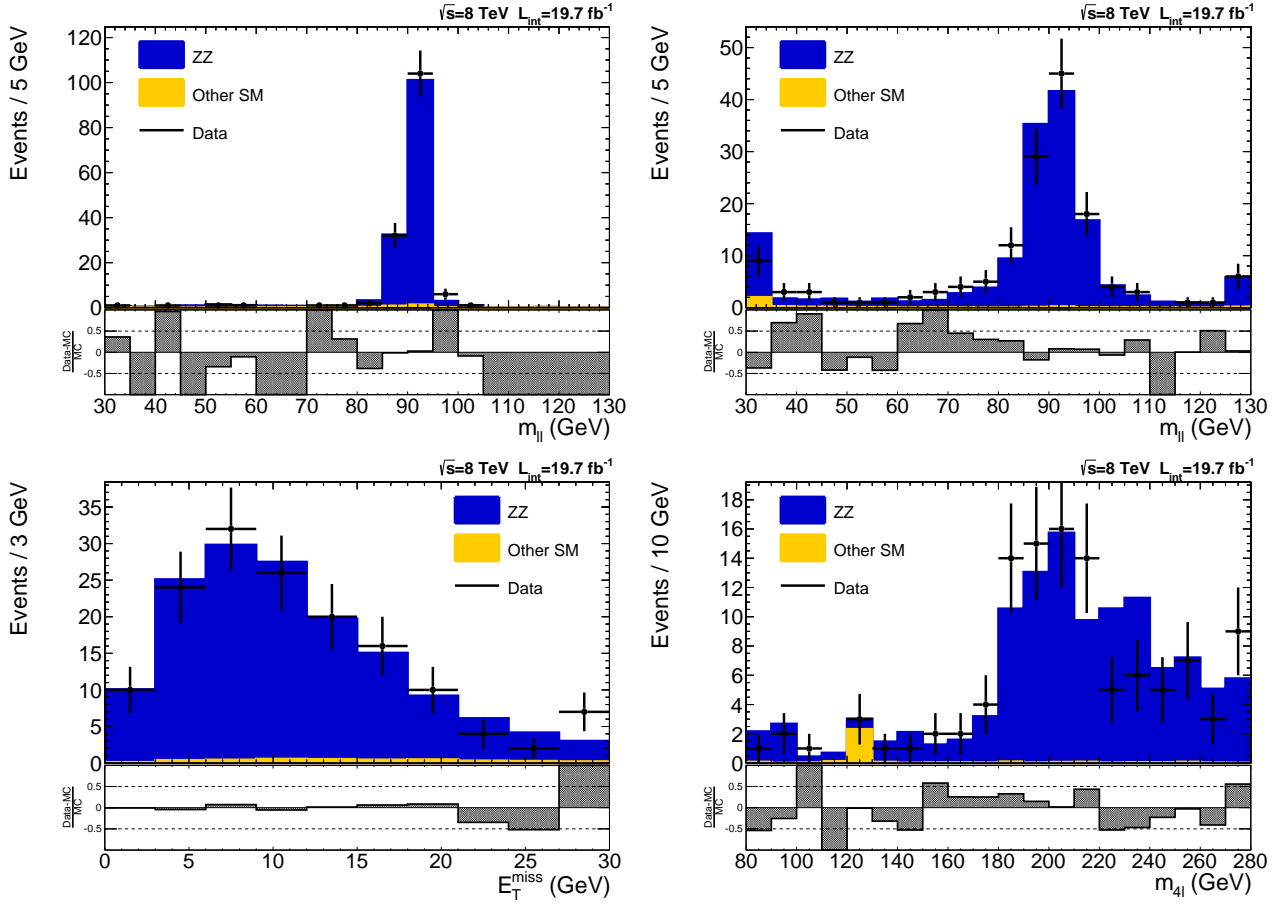
Figure 7.3.: Invariant mass distribution for events with 4ℓ and two opposite-sign same-flavor pairs and $E_{\mathrm{T}}^{miss} < 30$ GeV. On the top left the invariant mass of the pair closest to the Z mass is plotted and on the top right the invariant mass of the other pair. On the bottom left the E_{T}^{miss} distribution and on the bottom right the invariant mass of all 4 leptons is shown.

contribution. The result is shown in figure 7.5. In the plots on the left, the invariant mass of an opposite-sign same-flavor lepton pair plus an additional electron is shown. This electron originates from real photons (light blue) or virtual photons (dark blue). In the plots on the right the invariant mass of an opposite-sign same-flavor lepton pair plus an additional muon is shown. This muon can only come from virtual photons (dark blue). The difference between data and MC prediction is about 50%. For this reason, the uncertainties of this kind of background is 50%. This also applies for the WW plus photon and the $t\bar{t}$ plus photon production.

7.2.3. Fake backgrounds

In order to quantize the fake leptons, we distinguish between tight and loose leptons in this subsection. Tight leptons are leptons that fulfill all ID and isolation requirements. Whereas loose leptons only fulfill the ID requirements but fails the isolation criteria. The loose leptons are dominated by fake leptons. For tau leptons, it is not possible to separate the isolation and identification. So, taus that fulfill the medium working point are tight taus and those which
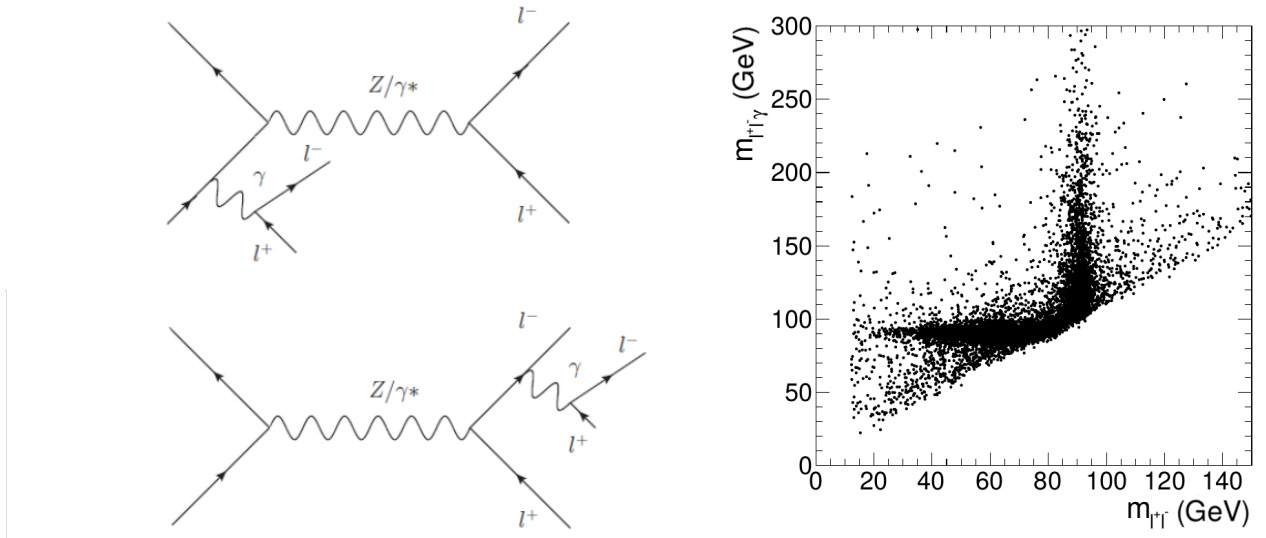
Figure 7.4.: On the left two Feynman diagrams which show initial (top) and final state radiation
(bottom). On the right events with two opposite-sign same-flavor leptons and one
additional photon are plotted. The x-axis is the invariant mass of the lepton pair,
and the y-axis is the invariant mass of the two leptons plus the photon. The right
plot is taken from [81](figure 8.18).

fulfill the loose working point but fail the medium working point are loose tau. Again these
loose taus are dominated by objects faking taus. For electrons, muons and taus the source of
fakes are jets. The probability for a jet to produces a fake lepton depends on the jet flavor and
the jet kinematics. DY and $t\bar{t}$ are the processes that yield to the 3ℓ and 4ℓ finale state with
fake leptons. These processes have a different jet composition. E.g. the jet has to be produced
by initial state radiation or higher order diagrams for DY processes. In contrast to that the
leading order $t\bar{t}$ production always leads to final states with jets, because the top quark decays
into a b-quark and a W boson. The b-quark always hadronizes into a jet, which is the reason
for the jet characteristics being different to DY. Since these characteristics have an influence
on the fake rate, the Drell-Yan, and $t\bar{t}$ background have to be controlled separately.

7.2.3.1. $t\bar{t}$

For the purpose of this thesis we add the single top production (mainly tW) to the usual $t\bar{t}$
production. The single top component is similar to $t\bar{t}$ and sums up to about 5% of the usual
$t\bar{t}$ selection. As $t\bar{t}$ control selection, we use events with exactly one tight muon and one tight
electron with opposite-sign ($\mu^{\pm}e^{\mp}$). The invariant mass of those lepton pairs is shown in figure
7.6. At 50 GeV a peak from $Z \to \tau^{+}\tau^{-} \to \mu^{\pm}e^{\mp} + 4\nu$ shows up. The Z peak is shifted because
the neutrinos are not considered in the invariant mass. To get rid of these events, an invariant
mass greater than 80 GeV is required in the $t\bar{t}$ selection.

In order to test the fake rate we require events with an $\mu^{\pm}e^{\mp}$ pair and an additional loose
muon, electron or tau. The majority of these loose leptons originate from b-quarks within this
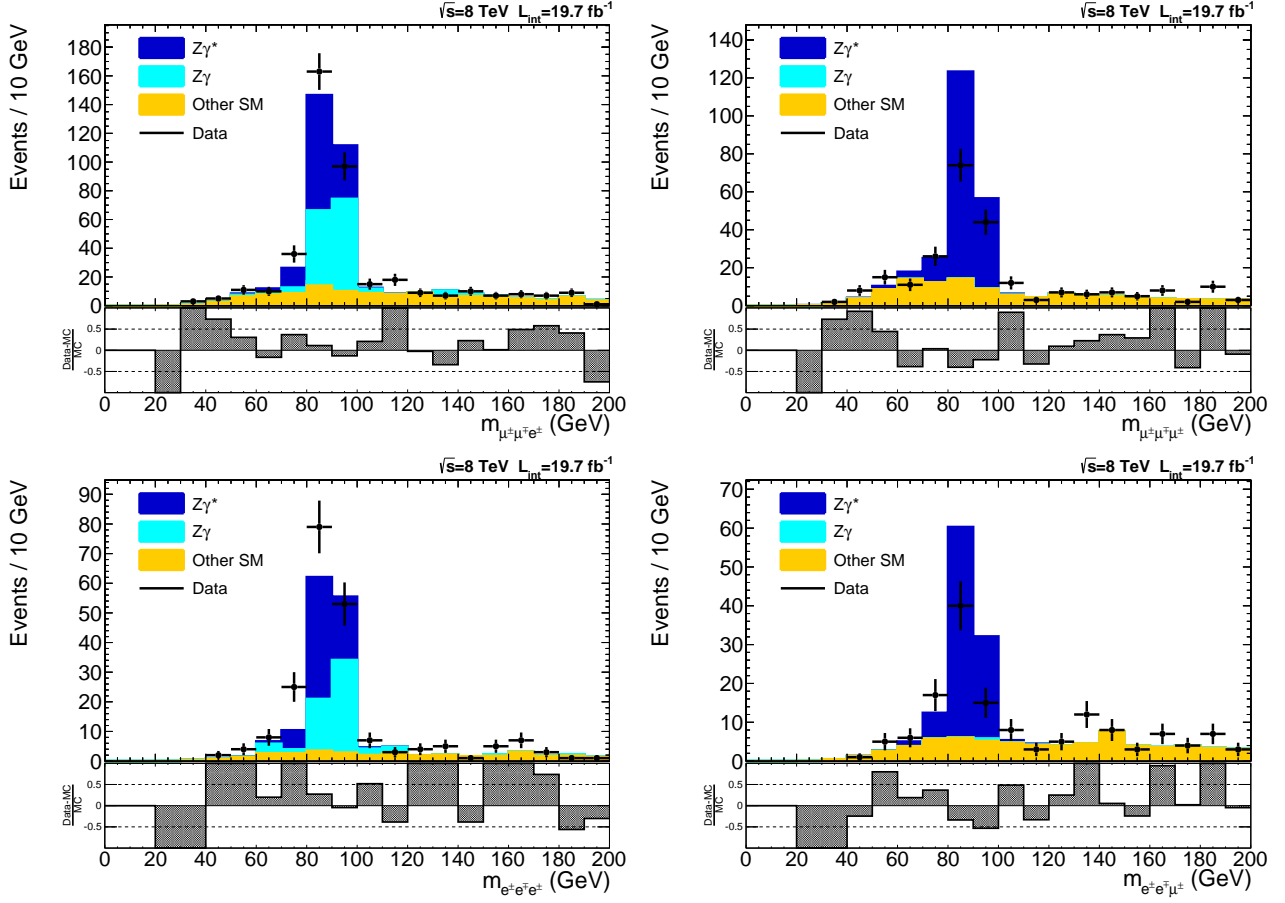
Figure 7.5.: The invariant mass of three leptons with at least one opposite-sign same-flavor pair. On the top left the invariant mass of two muons and one electron, on the top right of three muons, on the bottom right of three electrons and on the bottom left of two electrons and one muon is shown.
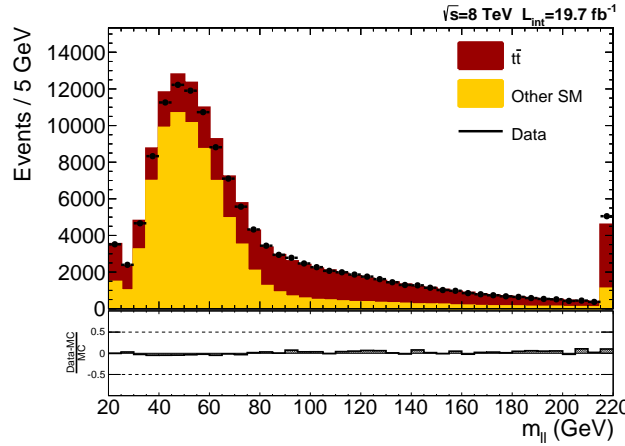
Figure 7.6.: The invariant mass of an electron and a muon with opposite-sign ($\mu^{\pm} e^{\mp}$) is shown. The peak at ∼50 GeV in the other SM sample originates from $Z \rightarrow \tau^{+} \tau^{-} \rightarrow \mu^{\pm} e^{\mp} + 4\nu$ events.

selection. The relative isolation variable for loose muons and electrons are shown in figure 7.7. The fake rate for b-jets is about 20% lower in MC simulation compared to data. A scale factor

is applied to the simulations to correct for the differences.
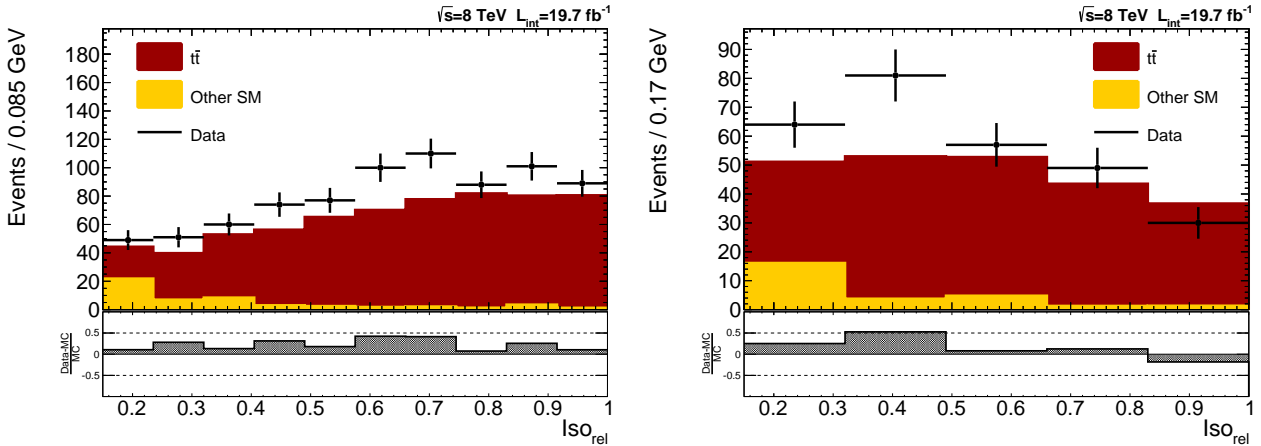
Figure 7.7.: Relative isolation of a loose muon (electron) for events with a muon and electron
with opposite-sign and an additional loose lepton are shown on the left (right). The
invariant mass of the muon and electron has to be larger than 80 GeV.

Figure 7.8 shows the transverse momentum and pseudorapidity distribution for events with an
additional loose tau. The amount of such events are small, hence the fake rate for b-quarks
to fake a tau is much lower than for a light jet. Only about 50% of this loose taus originate
from a b-quarks and the rest from light jets. The fake rate for taus coming from light jets will
be validated in the next section 7.2.3.2. The fake rate for taus originate from b-jets has to be
corrected by a factor of 1.5, by considering the light jet tau fake rate.
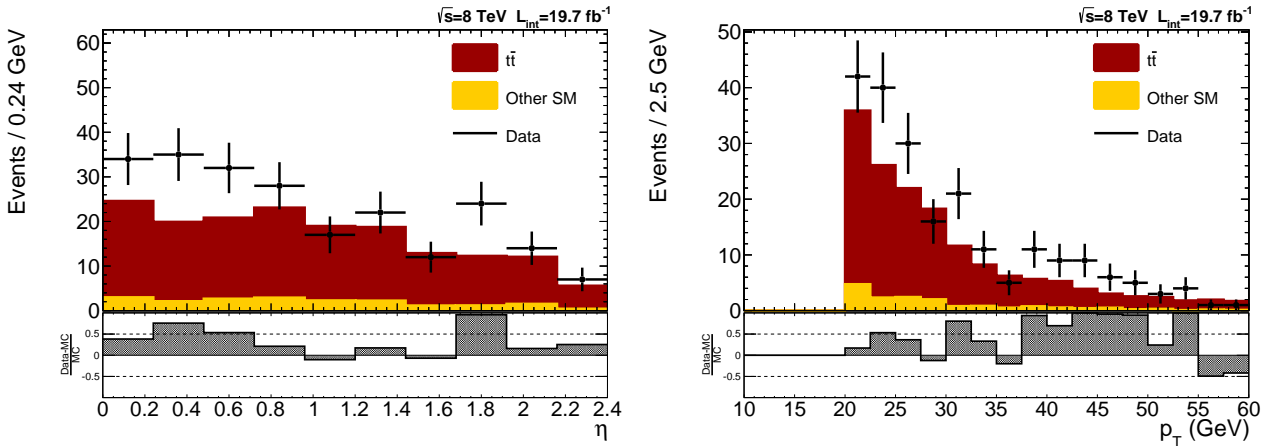
Figure 7.8.: Kinematics of a loose tau for events with a muon and electron with opposite-sign
and an additional loose tau. The invariant mass of the muon and electron has to
be larger than 80 GeV. On the left the transverse momentum is shown and on the
right the pseudo rapidity.

The $t\bar{t}$ contribution can be validated in data. After applying all correction factors the search
variables used for the final selection are presented in figure 7.9 (fake muons), 7.10 (fake electrons)
and 7.11 (fake taus) for the $t\bar{t}$ control selection. These variables are the number of b-jets the

invariant mass of the lepton pair, E_T^{miss} and the M_T calculated with E_T^{miss} and the additional loose lepton. A good agreement between data and simulation within an uncertainty of 20% is observed.
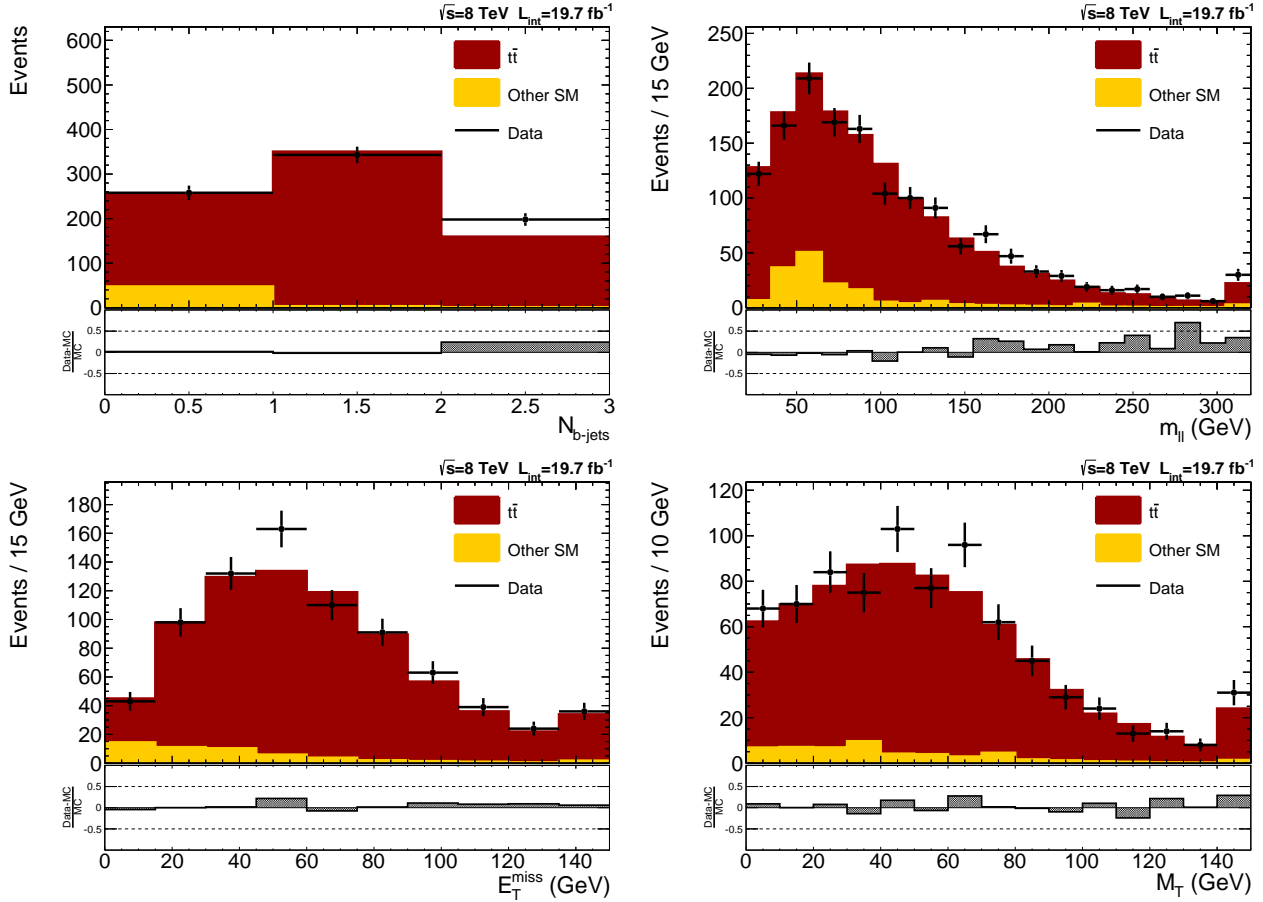
Figure 7.9.: Control plots for $t\bar{t}$ events with an additional loose muon. On the top left the number of b-jets is shown. On the top right the invariant mass distribution for the opposite-sign same-flavor lepton pair is shown. On the bottom right E_T^{miss} distribution is shown and on the bottom left the M_T distribution for E_T^{miss} and the loose muon is shown.

7.2.3.2. Drell Yan (DY)

A DY control selection is build by taking events with two prompt opposite-sign same-flavor leptons ($\mu^+\mu^-$ or e^+e^-) and an additional loose muon, electron or tau. The invariant mass of the opposite-sign same-flavor lepton pair has to be onZ (75 GeV < $m_{\ell\ell}$ < 105 GeV). Figure 7.12 shows that the relative isolation of the additional loose muon or electron. For muons and electrons, the fake rate is described well by simulation.

Events with and additional loose tau originating form light jets are shown in figure 7.13. The tau fake rate in simulation is about 20% higher than in data for the barrel region ($|\eta| < 1.44$). There is almost no depends on the transverse momentum of the loose tau. A correction factor is applied to account for this difference.
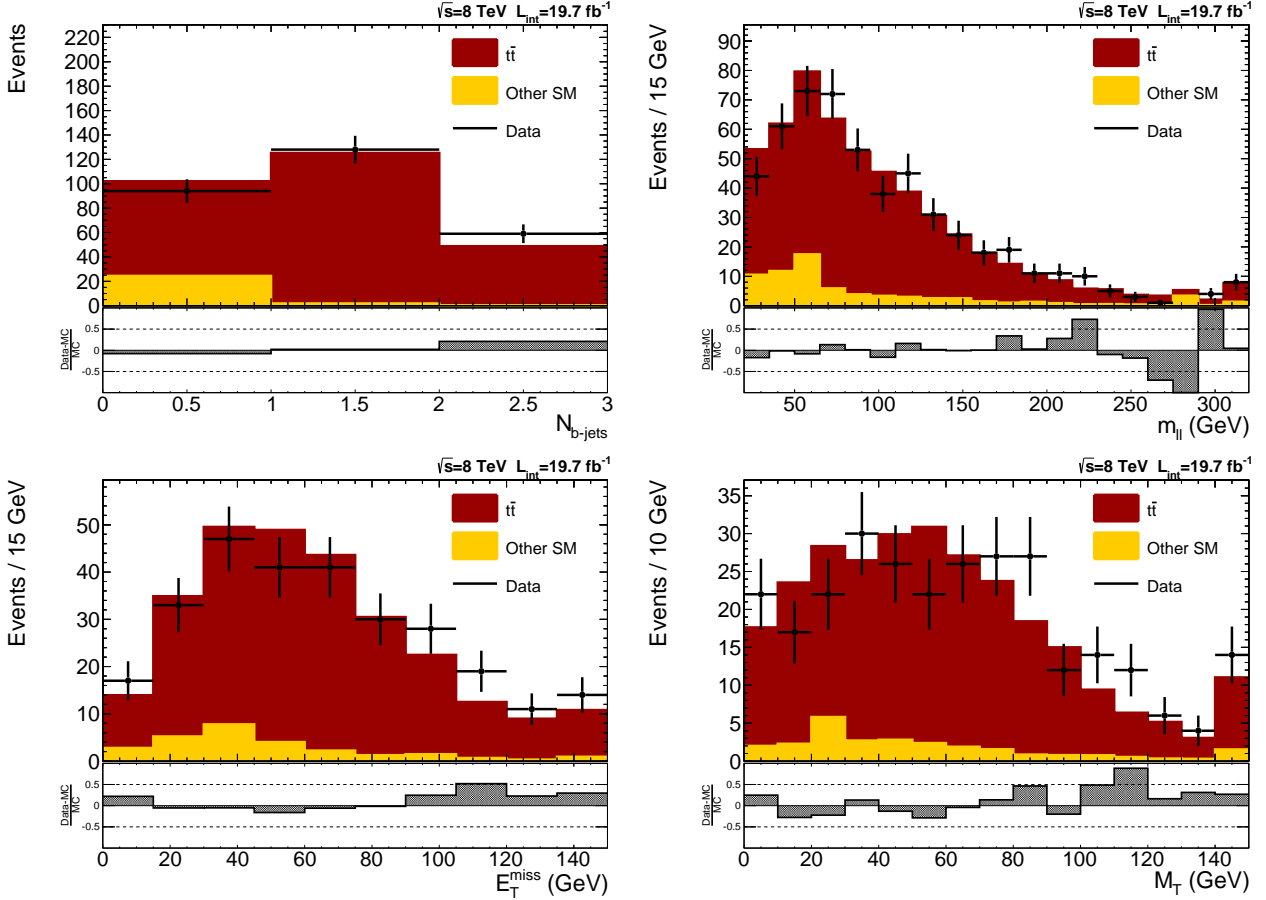
Figure 7.10.: Control plots for $t\bar{t}$ events with an additional loose electron. On the top left the number of b-jets is shown. On the top right the invariant mass distribution for the opposite-sign same-flavor lepton pair is shown. On the bottom right E_T^{miss} distribution is shown and on the bottom left the M_T distribution for E_T^{miss} and the loose muon is shown.

The DY contribution can be validated in data, too. Again correction factors, as described, are applied. The corrected distributions for the important search variables are shown in figure 7.14 (loose muons), 7.15 (loose electrons) and 7.16 (loose taus). A good agreement within 20% uncertainty between data and simulation is observed.

7.2.4. Rare processes

All rare processes have a tiny cross section. This kind of backgrounds includes triple boson production, $t\bar{t}$ plus boson production as well as the Standard Model Higgs production. They can produce 3ℓ or 4ℓ final states with prompt leptons. Because of the tiny cross section no validation is possible, and we relay on pure MC prediction. For this reason, an uncertainty of 50% is applied to this kind of backgrounds. This number is motivated by the uncertainty on the cross section, which are account for the differences between LO and NLO calculations, and on the uncertainties on the couplings of the Higgs boson [76–80].
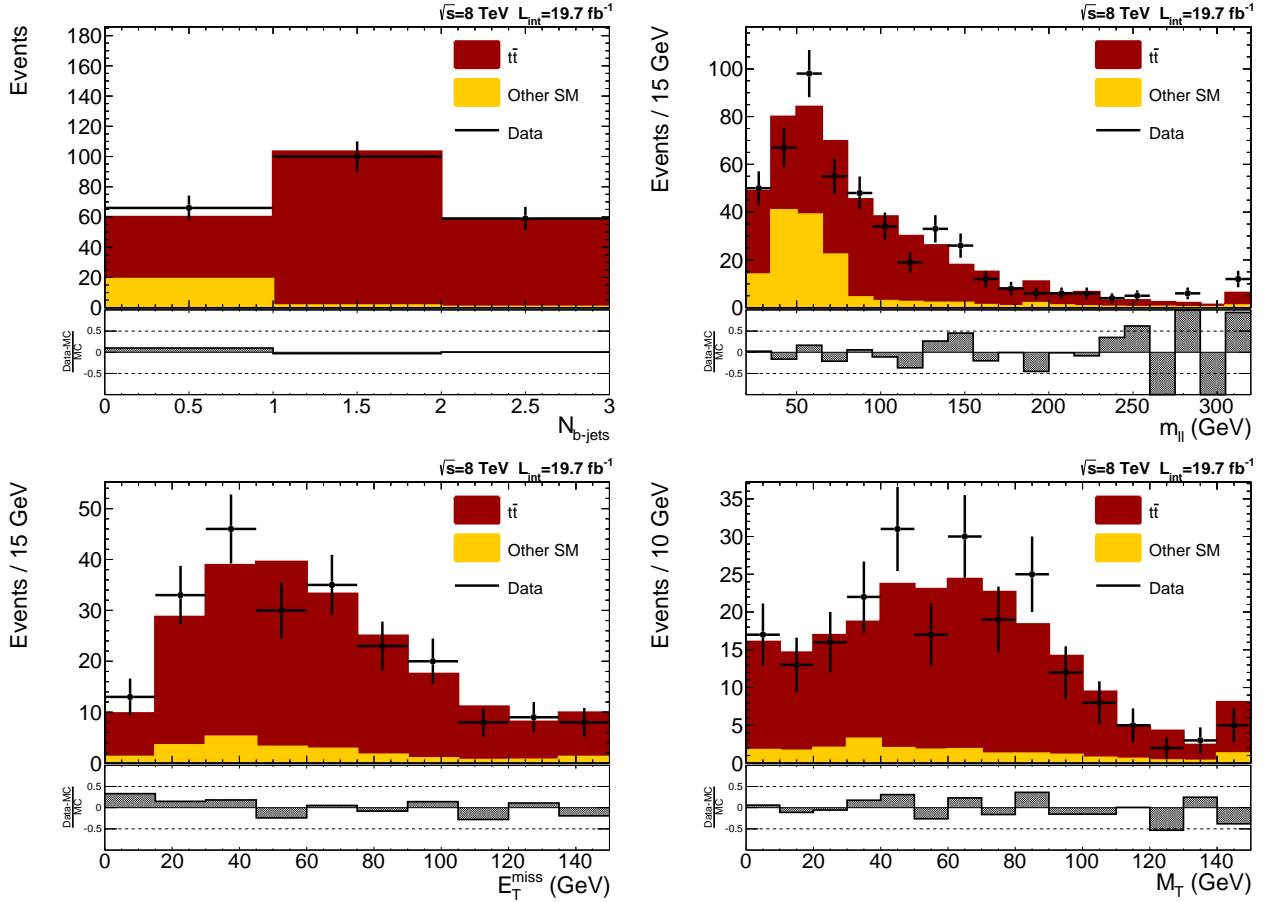
Figure 7.11.: Control plots for $t\bar{t}$ events with an additional loose tau. On the top left the number of b-jets is shown. On the top right the invariant mass distribution for the opposite-sign same-flavor lepton pair is shown. On the bottom right E_T^{miss} distribution is shown and on the bottom left the M_T distribution for E_T^{miss} and the loose muon is shown.
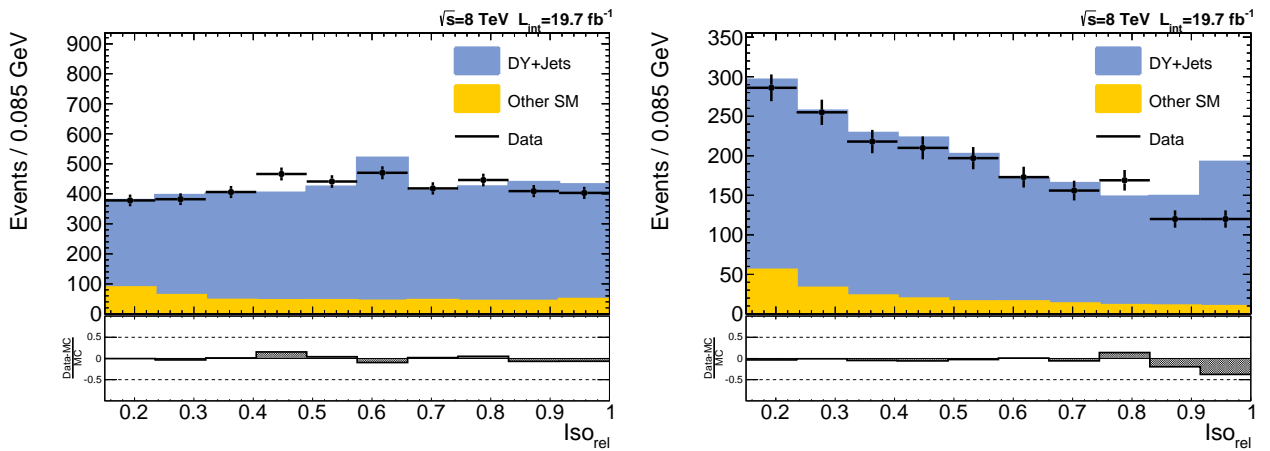
Figure 7.12.: Relative isolation of a loose muon (electron) for events with one opposite-sign same-flavor lepton pair onZ and an additional loose lepton are shown on the left (right).
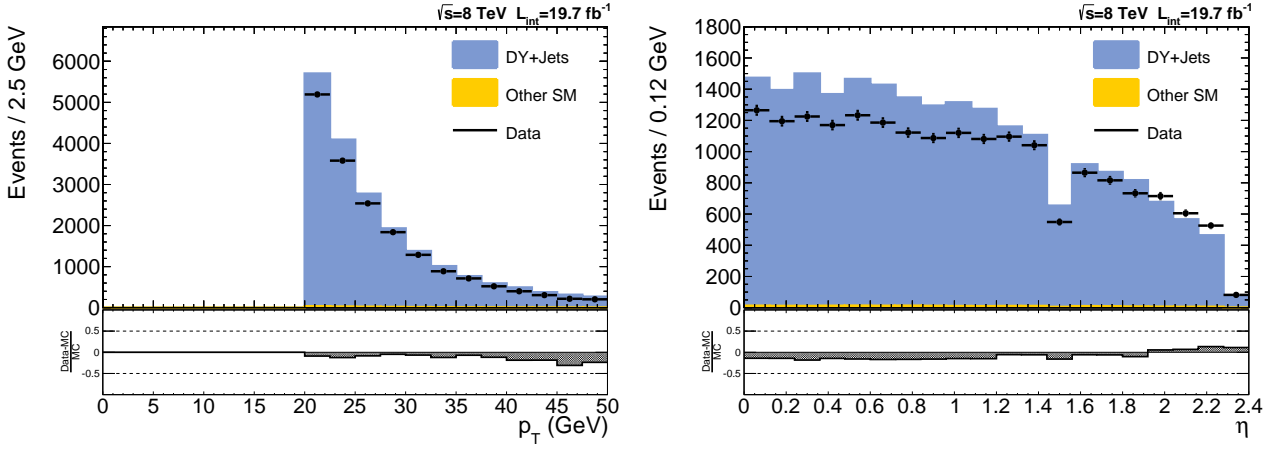
Figure 7.13.: Kinematics of a loose tau for events with one opposite-sign same-flavor lepton pair onZ and an additional loose tau. On the left, the transverse momentum is shown and on the right the pseudorapidity.
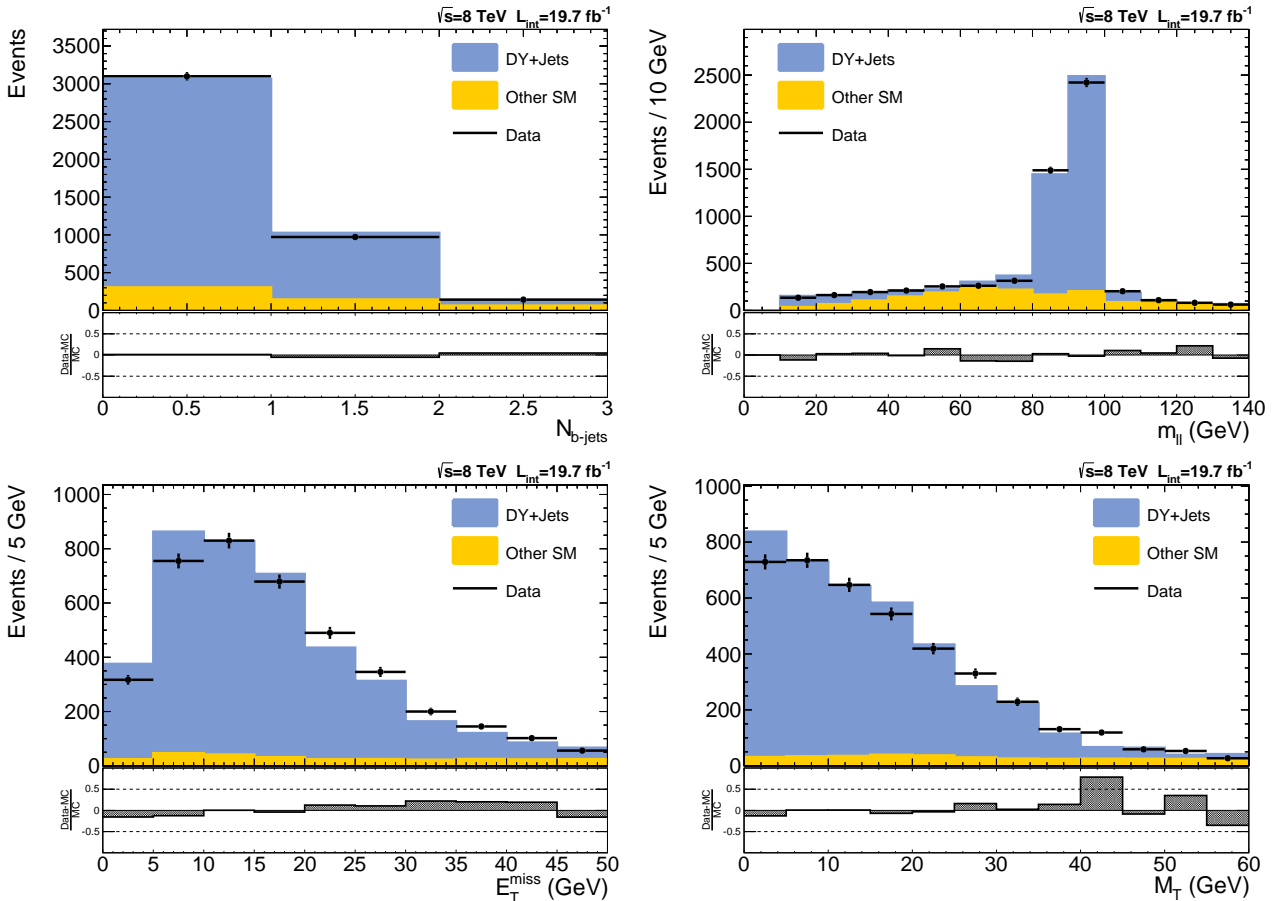
Figure 7.14.: Control plots for DY events with an additional loose muon. On the top left the number of b-tags is shown. On the top right, the invariant mass distribution for the opposite-sign same-flavor lepton pair is shown. On the bottom right E_T^{miss} distribution is shown and on the bottom left the M_T distribution for E_T^{miss} and the loose muon is shown.
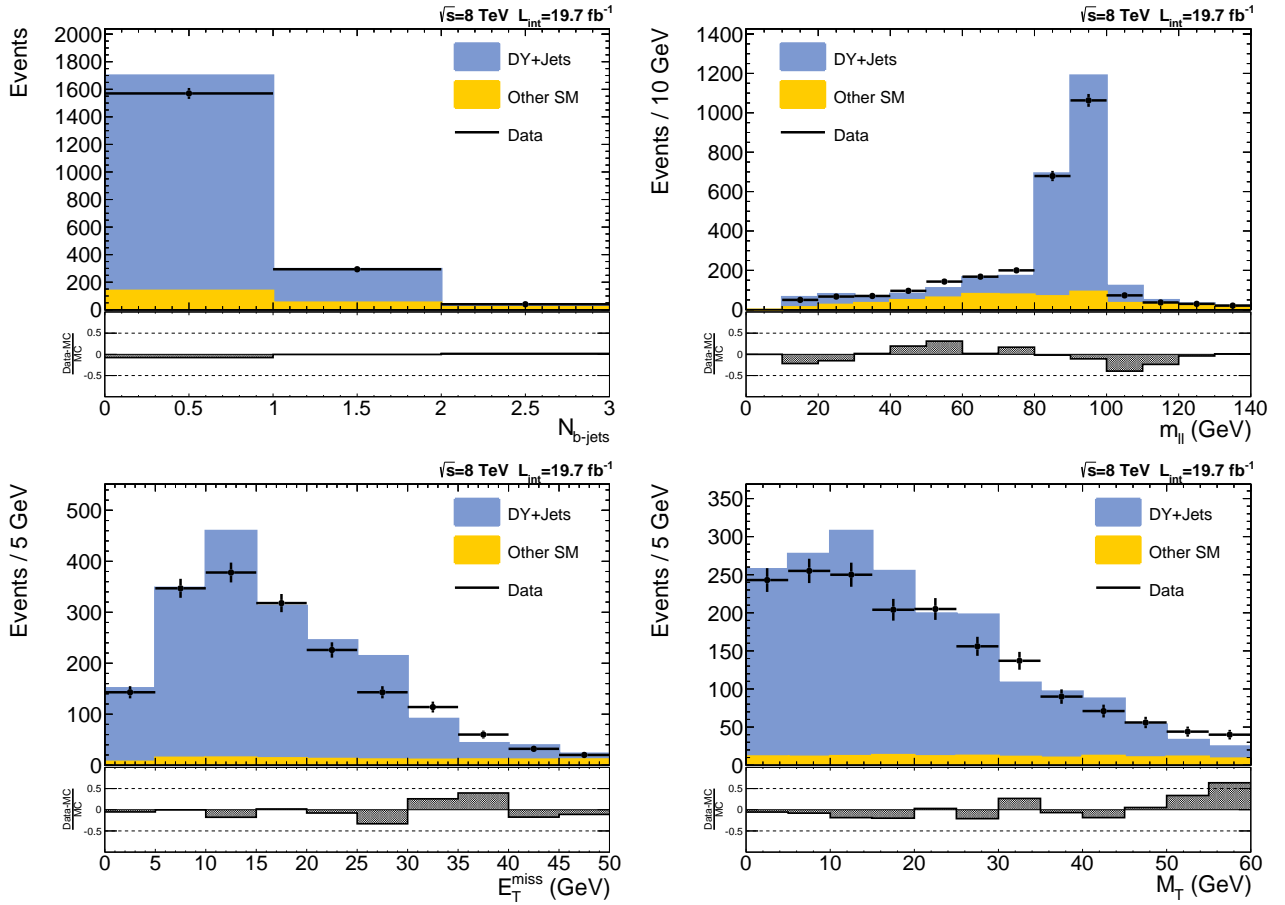
Figure 7.15.: Control plots for DY events with an additional loose electron. On the top left the number of b-tags is shown. On the top right, the invariant mass distribution for the opposite-sign same-flavor lepton pair is shown. On the bottom right E_T^{miss} distribution is shown and on the bottom left the M_T distribution for E_T^{miss} and the loose electron is shown.
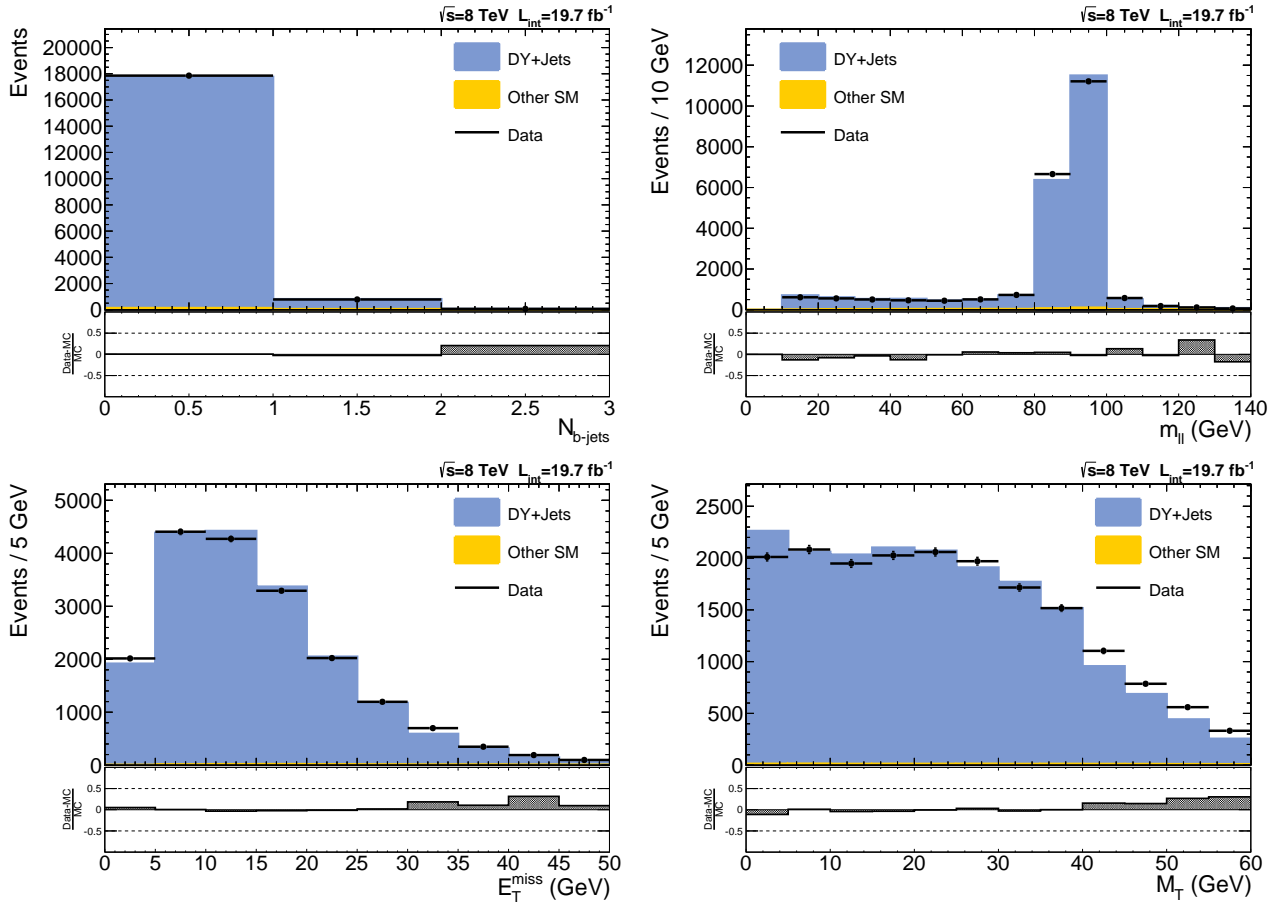
Figure 7.16.: Control plots for DY events with an additional loose tau. On the top left the number of b-tags is shown. On the top right, the invariant mass distribution for the opposite-sign same-flavor lepton pair is shown. On the bottom right E_T^{miss} distribution is shown and on the bottom left the M_T distribution for E_T^{miss} and the loose tau is shown.

8. Result

In this chapter, the result will be presented. First the search strategy will be explained. Then the uncertainties will be summarized. After this, the yields in the 3ℓ and 4ℓ final states will be shown.

8.1. Search Strategy

Our search strategy is to split the signal region into many bins instead of considering only one. This multi-bin approach has the advantage that shape information is considered and that we are sensitive to many supersymmetric scenarios in parallel. The bins are chosen in such a way that the majority of the Standard Model backgrounds are concentrated in a few bins. These bins are also used in the statistical model since they help to constrain the background uncertainties. More information about the statistical model can be found in section 3.

All events have at least three leptons. In order to trigger these events they must have at least either two muons, two electrons or an electron and a muon. Additionally at least one of this electrons or muons must have a transverse momentum greater than 20 GeV.

8.1.1. Three lepton selection

For the three lepton final state events with three leptons, including hadronic taus, are selected. Most of the events in the 3ℓ final states originate from WZ boson production, but also DY $\rightarrow$ $\ell\ell$+fake lepton and $t\bar{t} \rightarrow \ell\ell$+fake are important. The following variables are used to separate signal from background:

- Invariant mass $m_{\ell^+\ell^-}$ of two opposite-sign leptons. ($\mu^+\mu^-$, e^+e^-, $\mu^\pm e^\mp$, $\mu^\pm\tau^\mp$, $e^\pm\tau^\mp$)

- Missing transverse energy E_T^{miss}.

- Transverse mass M_{T} of one lepton and E_{T}^{miss}. (Formula given in section 7.1)

- Veto on events containing a b-jet

The b-jet veto is necessary since it reduces the amount of $t\bar{t}$ background. In order to increase the sensitivity for supersymmetric scenarios with different tau content, the three lepton final states are categorized into five main categories. These categories have the following naming convention:

- OSSF0tau: three μ, e with at least one opposite-sign same-flavor pair: $(\mu^+\mu^-\mu^\pm)$, $(\mu^+\mu^-e^\pm)$, $(e^+e^-\mu^\pm)$ and $(e^+e^-e^\pm)$

- noOSSF0tau: three μ, e with no opposite-sign same-flavor pair: $(\mu^+\mu^+e^-)$, $(e^+e^+\mu^-)$, $(\mu^-\mu^-e^+)$and $(e^-e^-\mu^+)$

- OSSF1tau: two μ, e with opposite-sign same-flavor and one τ: $(\mu^+\mu^-\tau^\pm)$ and $(e^+e^-\tau^\pm)$

- SS1tau: two μ, e with same-sign and one τ: $(\mu^\pm\mu^\pm\tau^\mp)$, $(\mu^\pm e^\pm\tau^\mp)$ and $(e^\pm e^\pm\tau^\mp)$

- OSOF1tau: two μ, e with opposite-sign opposite flavor and one τ: $(\mu^\pm e^\mp\tau^\pm)$ and $(\mu^\pm e^\mp\tau^\mp)$

The next step is to search for the lepton pair, which originates most likely from a Z boson. In events with at least one opposite-sign same-flavor electron or muon pair, the pair which is closest to the Z boson mass (91 GeV) is chosen. In a event without any opposite-sign same-flavor electron or muon pair the hypothesis that the event originates from a $Z \rightarrow \tau\tau$ decay is made. All opposite-sign lepton pairs including hadronic taus are tested. For $\mu^\pm e^\mp$ pairs the mass is probed to be as close as possible to 50 GeV (visible in figure 7.6). If one of the pair leptons is a tau, $\mu^\pm\tau^\mp$ or $e^\pm\tau^\mp$, the pair is probed to be as close as possible to 60 GeV (visible in figure 7.1). The pair, which is closest to its mass hypothesis is chosen. The remaining lepton and E_{T}^{miss} are used for the M_{T} calculation. Since this can cause some confusion, one example is given in the following: One event has three leptons $e^+\mu^-\tau^-$. The invariant mass of the $e^+\mu^-$ pair is 59 GeV and the invariant mass of $e^+\tau^-$ pair is 52 GeV. The $e^+\tau^-$ pair is chosen since it is closer to 60 GeV than the $e^+\mu^-$ to 50 GeV. Additionally, the muon and E_{T}^{miss} are used for the M_{T} calculation. As last step the $\mathrm{m}_{\ell^+\ell^-}$, the M_{T} and the E_{T}^{miss} variables are used to bin our result. The following bin definitions are used:

- Three $\mathrm{m}_{\ell^+\ell^-}$ bins for events with an opposite-sign same-flavor lepton pair (OSSF0tau and OSSF1tau):

    - lowZ: $\mathrm{m}_{\ell^+\ell^-} < 75$ GeV

    - onZ: 75 GeV $< \mathrm{m}_{\ell^+\ell^-} < 105$ GeV

    - highZ: $\mathrm{m}_{\ell^+\ell^-} > 105$ GeV

- Two m$_{\ell^+\ell^-}$ bins for events with no opposite-sign same-flavor lepton pair (noOSSF0tau, noOSSF1tau and SSSF1tau):

    - lowZ: m$_{\ell^+\ell^-}$ < 100 GeV

    - highZ: m$_{\ell^+\ell^-}$ > 100 GeV

- Three M_T bins:

    - M_T < 120 GeV

    - 120 GeV < M_T < 160 GeV

    - M_T > 160 GeV

- Five E_T^{miss} bins:

    - E_T^{miss} < 50 GeV

    - 50 GeV < E_T^{miss} < 100 GeV

    - 100 GeV < E_T^{miss} < 150 GeV

    - 150 GeV < E_T^{miss} < 200 GeV

    - E_T^{miss} > 200 GeV

Summarizing we have 12 m$_{\ell^+\ell^-}$ bins, 3 M_T bins, and 5 E_T^{miss} bins, which sums up to 180 search bins for the three lepton final state.

In figure 8.1 the M_T distribution versus the m$_{\ell^+\ell^-}$ distribution for simulated WZ, DY and $t\bar{t}$ events is shown. WZ mostly concentrates in the onZ M_T < 120 GeV region. The contribution from DY clusters in the E_T^{miss} < 50 GeV region because DY has no intrinsic E_T^{miss}. For $t\bar{t}$, the events are spread over a larger area. For this reason, the b-jet veto is needed to reduce the overall amount of events from this kind of background.

8.1.2. Four lepton selection

The main background in this search region stems from ZZ $\rightarrow 4\ell$ events. The strategy is to search for the opposite-sign same-flavor lepton pairs which originate from Z bosons. The events are distinguished by the number of taus. We count the number of the opposite-sign same-flavor lepton pairs onZ (e^+e^- and $\mu^+\mu^-$), meaning that the invariant mass of those pairs lie in between 75 GeV and 105 GeV. We distinguish following three categories:

- N$_\tau$=0 : four e, μ with a maximum of two onZ pairs:
  $(e^+e^-e^+e^-)$ $(\mu^+\mu^-\mu^+\mu^-)(\mu^+\mu^-e^+e^-)$

- N$_\tau$=1 : three e, μ and one τ with a maximum of one onZ pair:
  $(e^+e^-e^{\pm}\tau^{\mp})$ $(\mu^+\mu^-\mu^{\pm}\tau^{\mp})(e^+e^-\mu^{\pm}\tau^{\mp})$ $(\mu^+\mu^-e^{\pm}\tau^{\mp})$
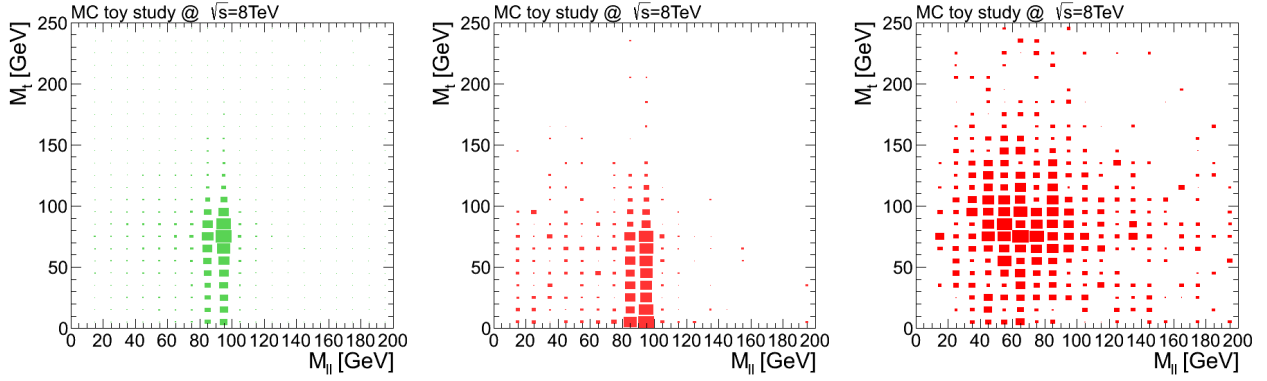
Figure 8.1.: The M_T distribution in respect to the $m_{\ell^+\ell^-}$ distribution for simulated three lepton events is presented. On the left plot, the WZ events are shown. In the middle plot for DY events and on the right plot for $t\bar{t}$ events are shown.

- $N_\tau=2$: two e, μ and two τ with a maximum of one onZ pair:
  $(e^+e^-\tau^+\tau^-)$ $(\mu^+\mu^-\tau^+\tau^-)(\mu^+e^-\tau^+\tau^-)$

Since the ZZ background has no intrinsic missing transverse energy, the following E_T^{miss} binning is chosen:

- $E_\mathrm{T}^{miss} < 30$ GeV

- 30 GeV $< E_\mathrm{T}^{miss} < 50$ GeV

- 50 GeV $< E_\mathrm{T}^{miss} < 100$ GeV

- $E_\mathrm{T}^{miss} > 100$ GeV

In summary we have 12 search bins for the $N_\tau=0$ category, 8 for the $N_\tau=1$ category and 8 for the $N_\tau=2$ category, which sums up into 28 search bins in the 4ℓ final state.

8.2. Uncertainties Summary

Table 8.1 shows a summary fo all uncertainties. The individual uncertainties are treated as statistically uncorrelated. The uncertainty on the signal events stems from the parton density function. The uncertainties on WZ and ZZ are uncertainties of the cross section. The $Z\gamma^{(*)}$ uncertainty of 50% is rather unimportant, because those events are concentrated in the low E_T^{miss} region. For backgrounds from fake sources (mostly DY and $t\bar{t}$) the uncertainty is a mixture of the uncertainty on the cross section and the reconstruction of the fake lepton, at which the second is the dominant source. The uncertainty for the rare backgrounds originates in the uncertainty of their cross section. The uncertainties on the luminosity are taken from [83]. The different binning variables (E_T^{miss}, M_T, $m_{\ell^+\ell^-}$ and b-jet veto) contribute to the uncertainty in the binning. Nevertheless, the dominating part of this kind of uncertainties is the jet energy scale, which directly affect E_T^{miss} and for this reason also M_T. In a few bins, the statistical MC uncertainty are important, but usually it is rather small.

Table 8.1.: Summary of the estimated uncertainties for the background processes

name	uncert. (%)	additional information
Background/Signal only		
Signal	5	(section 6)
WZ	20	(section 7.2.1.1)
ZZ	2-6	on-shell - off-shell (section 7.2.1.2)
$Z\gamma^{(*)}$	50	(section 7.2.2)
Fake	20	(section 7.2.3)
Rare	50	(section 7.2.4)
All events		
Trigger	1-5	depending on triggerable objects (section 5.1.1.1)
Muon	3-5	per muon depending on p_T (section 5.1.1)
Electron	3-5	per electron depending on p_T (section 5.1.1)
Tau	6	per tau (section 5.1.2)
Luminosity	2.6	taken from [83]
Binning	3-15	dominating is JES uncert. for E_T^{miss} (section 5.2.2)
MC statistic	1-100	

8.3. Yields

Finally, the yields can be presented. The 3ℓ and 4ℓ events are separated by the binning scheme described in section 8.1. First the 3ℓ results are shown and then the result of the 4ℓ events. The last word in this section is on a small excess in the 3ℓ final state.

8.3.1. Three lepton yields

The 3ℓ final state covers all events with three leptons including hadronic taus. In order to trigger those events, two leptons have either to be electrons or muons. Events with more than three leptons are not considered in this selection. The events are categorized as described in section 8.1.1.

In figure 8.2 the background predictions and their uncertainties as well as the observed data for the OSSF0tau category is presented. The exact numbers can be found in the table A.1 in the appendix. The WZ background is the dominating background for most of this search bins. Backgrounds with final state γ radiation mostly lead to lowZ and $E_T^{miss} < 50$ GeV events. For the $M_T < 120$ GeV region the background predictions and data agree within their uncertainties. The region $M_T > 120$ GeV, will be discussed in section 8.3.3.

The results of the noOSSF0tau categories can be found in figure 8.3. Numbers can be found in table A.2. Here the yields are rather low. The prompt background from VV comes from events where a Z boson decays into tau pairs, which decay further into two leptons with opposite
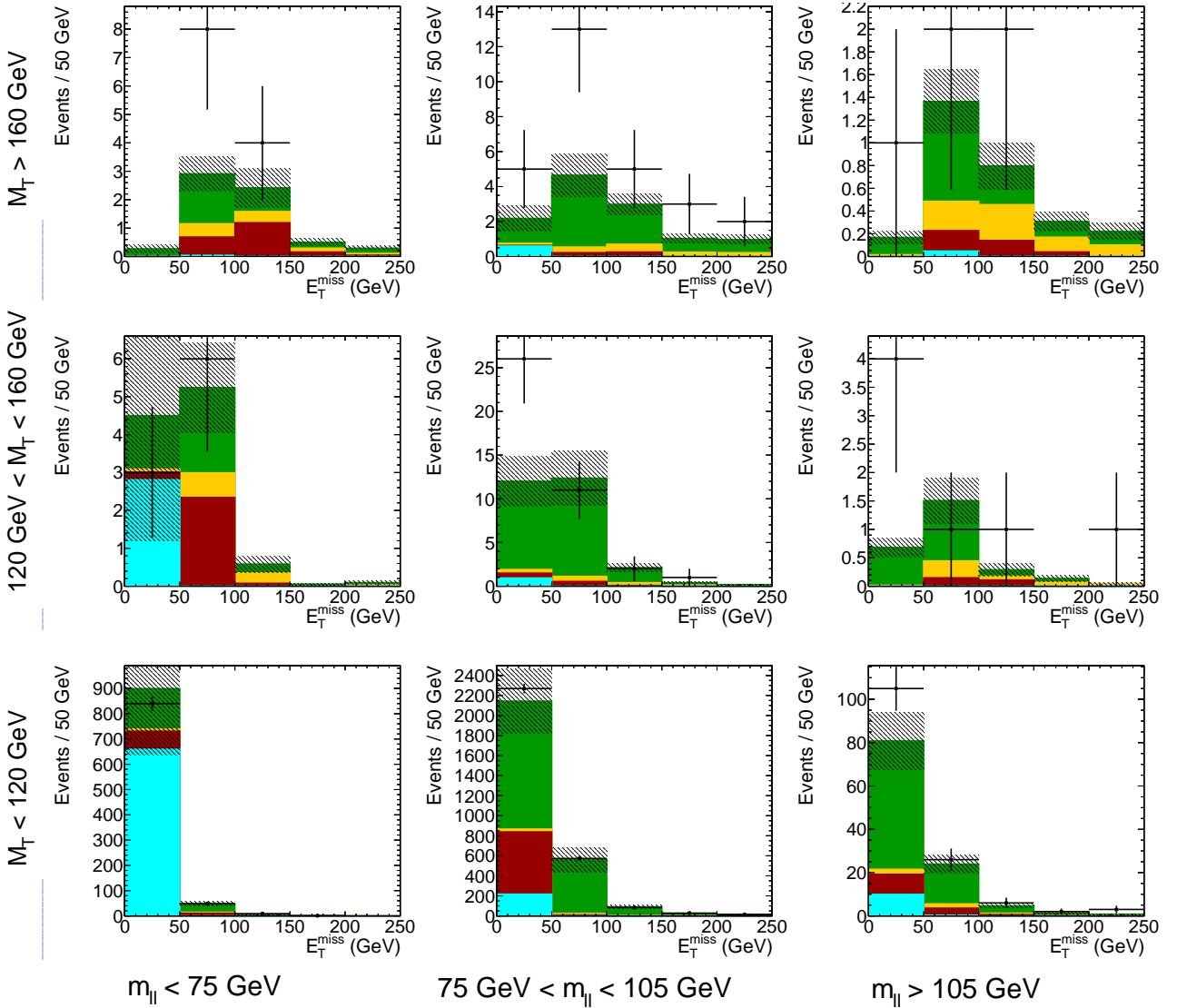
Figure 8.2.: Result for 3ℓ events with at least one opposite-sign same-flavor lepton pair and 0 taus: $(\mu^+\mu^-\mu^\pm)$, $(\mu^+\mu^-e^\pm)$, $(e^+e^-\mu^\pm)$ and $(e^+e^-e^\pm)$

flavor. Fake and rare backgrounds are also relevant. Background prediction and data agrees well.

Now coming to the 3ℓ categories containing hadronic taus. The first is the OSSF1tau category. The result of this category is presented in figure 8.4. The numbers can be found in table A.3. Backgrounds with two prompt leptons and one faked tau dominate those events. Data and background prediction agrees well in the most regions.
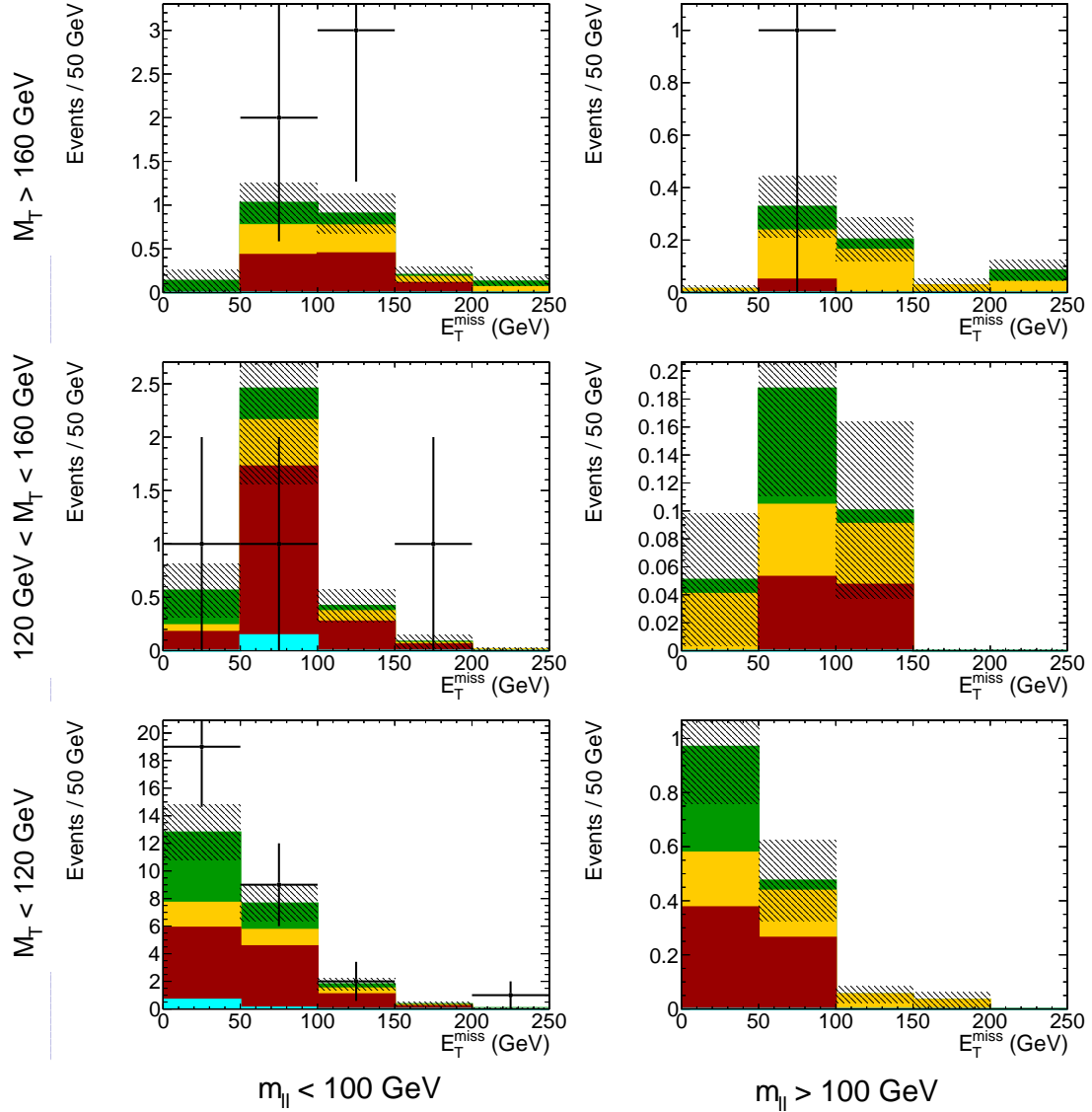
Figure 8.3.: Result for 3ℓ events with no opposite-sign same-flavor lepton pairs and 0 taus: $(\mu^+\mu^+e^-)$, $(e^+e^+\mu^-)$, $(\mu^-\mu^-e^+)$ and $(e^-e^-\mu^+)$

The SS1tau category is presented in figure 8.5 and the numbers can be found in table A.4. There the most important background are again VV events where a Z boson decays into taus. The fake background is reduced compared to the other 3ℓ final states including taus, because of the charge conservation. For this reason, the taus must coming from prompt sources. A good agreement between observation and background prediction is observed in this category.

The last category for the 3ℓ final state is the OSOF1tau. The yields are presented in figure 8.6
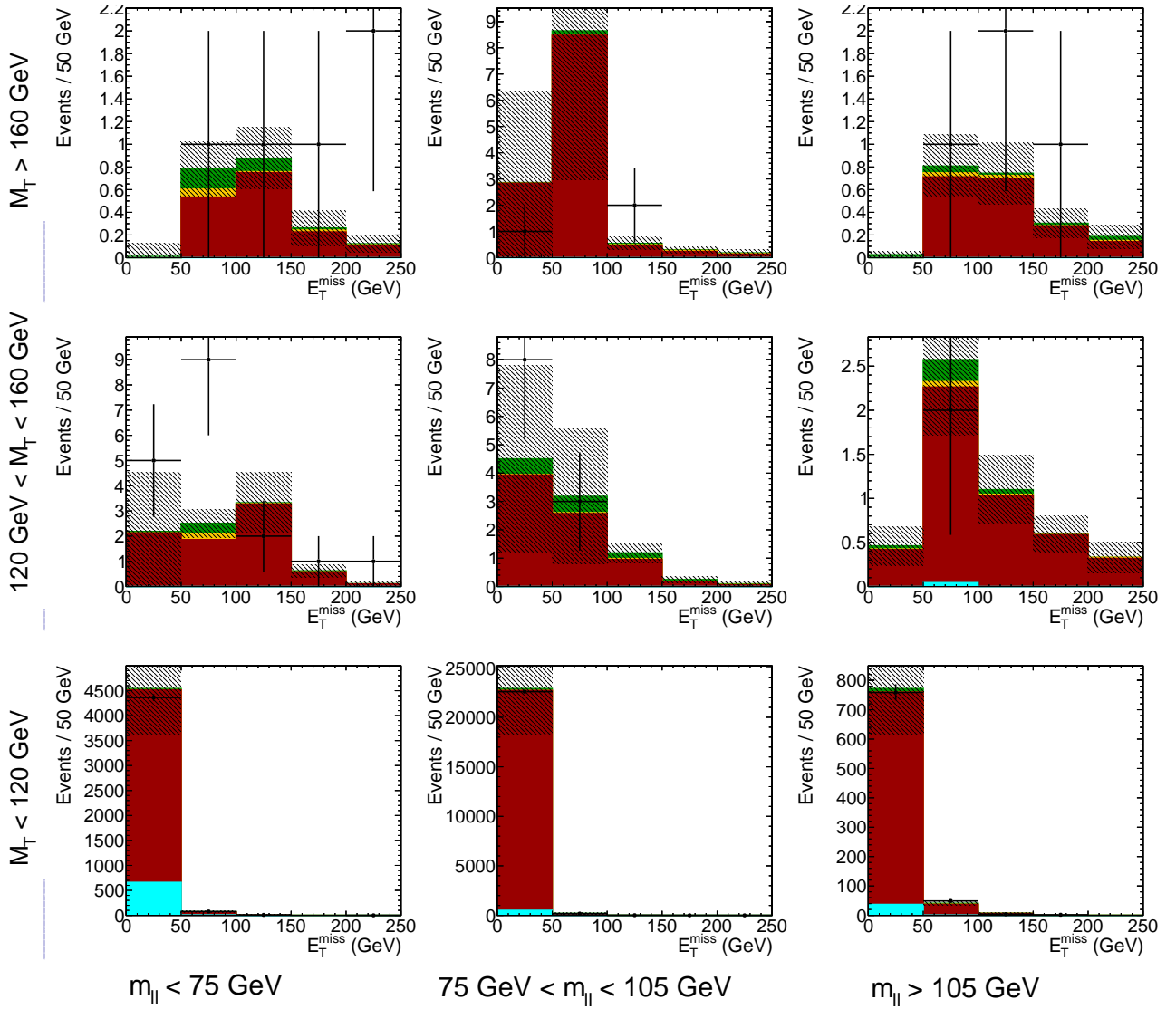
Figure 8.4.: Result for 3ℓ events with one opposite-sign same-flavor lepton pair and 1 tau: ($\mu^+\mu^-\tau^\pm$) and ($e^+e^-\tau^\pm$)

and the numbers can be found in table A.5. The dominating backgrounds consists of events including fake taus.

8.3.2. Four lepton yields

The 4ℓ final state covers all events with four leptons including hadronic taus. In order to trigger those events, two leptons have either to be electrons or muons. This selection does not consider
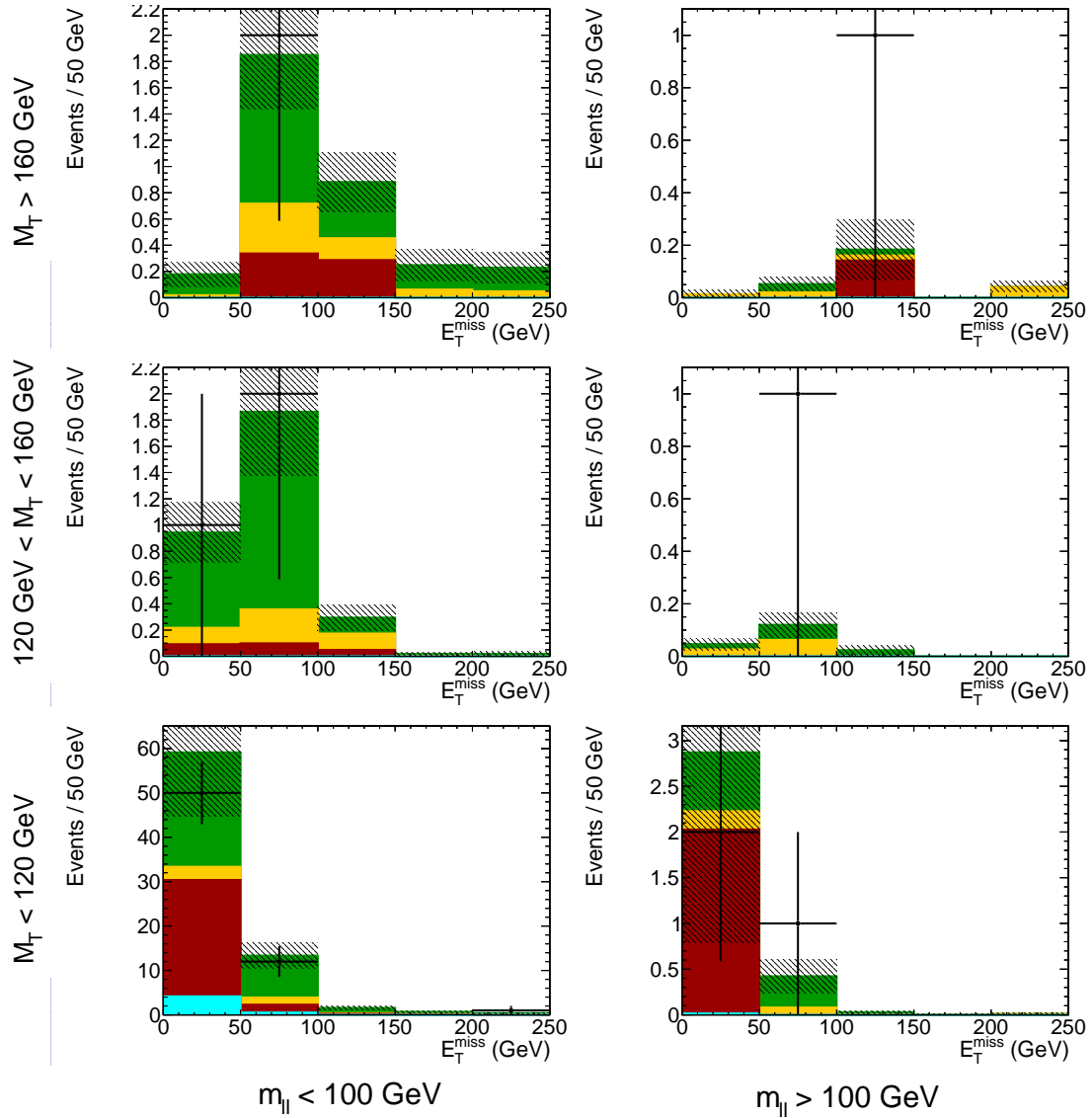
Figure 8.5.: Result for 3ℓ events with same-sign leptons and 1 taus: $(\mu^\pm\mu^\pm\tau^\mp)$, $(\mu^\pm e^\pm\tau^\mp)$ and $(e^\pm e^\pm\tau^\mp)$

events with more than four leptons. The events are categorized as described in section 8.1.2. The result are shown in figure 8.7 and the numbers are given in table A.6 in the appendix. The dominant background for the N_τ=0 and N_τ=1 region is ZZ production. In the N_τ=2 region, most of the background events stems from sources with fake leptons.
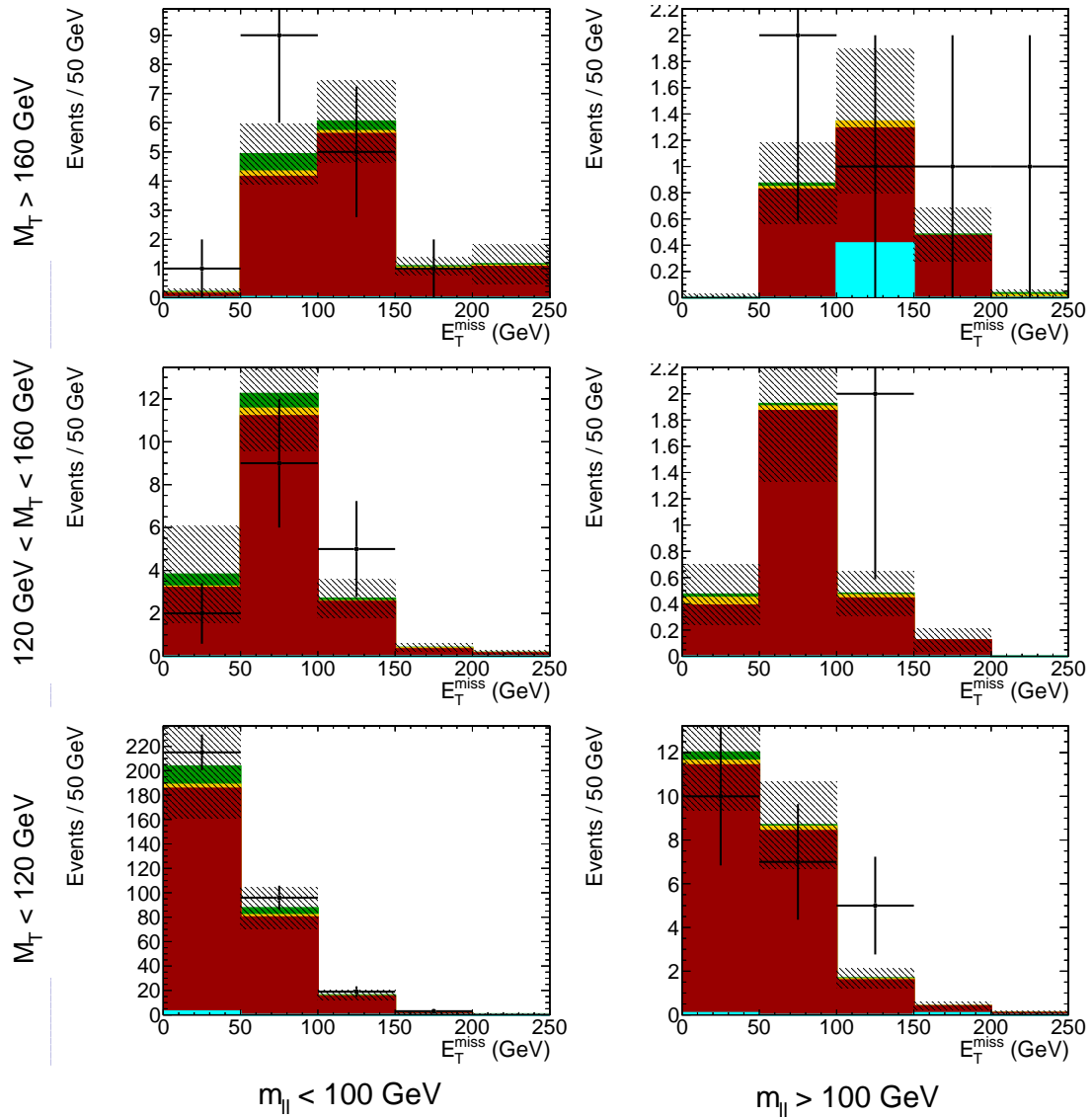
Figure 8.6.: Result for 3ℓ events with opposite-sign opposite flavor leptons and 1 taus: $(\mu^{\pm}e^{\mp}\tau^{\pm})$ and $(\mu^{\pm}e^{\mp}\tau^{\mp})$

8.3.3. Discussion of the excesses

Some presented search bins have significantly more events than predicted. In order to quantize the excesses the simplified Z_{Bi} metric as well as a fully frequentist approach (σ_{freq}) including log-normal distributed uncertainties are computed [21; 22; 39; 84–86]. The Z_{Bi} value is a good estimate of the significance of new physics signals. The Advantage of the Z_{Bi} is that it gives simple and transparent results. In the frequentist approach, all uncertainties are profiled out.
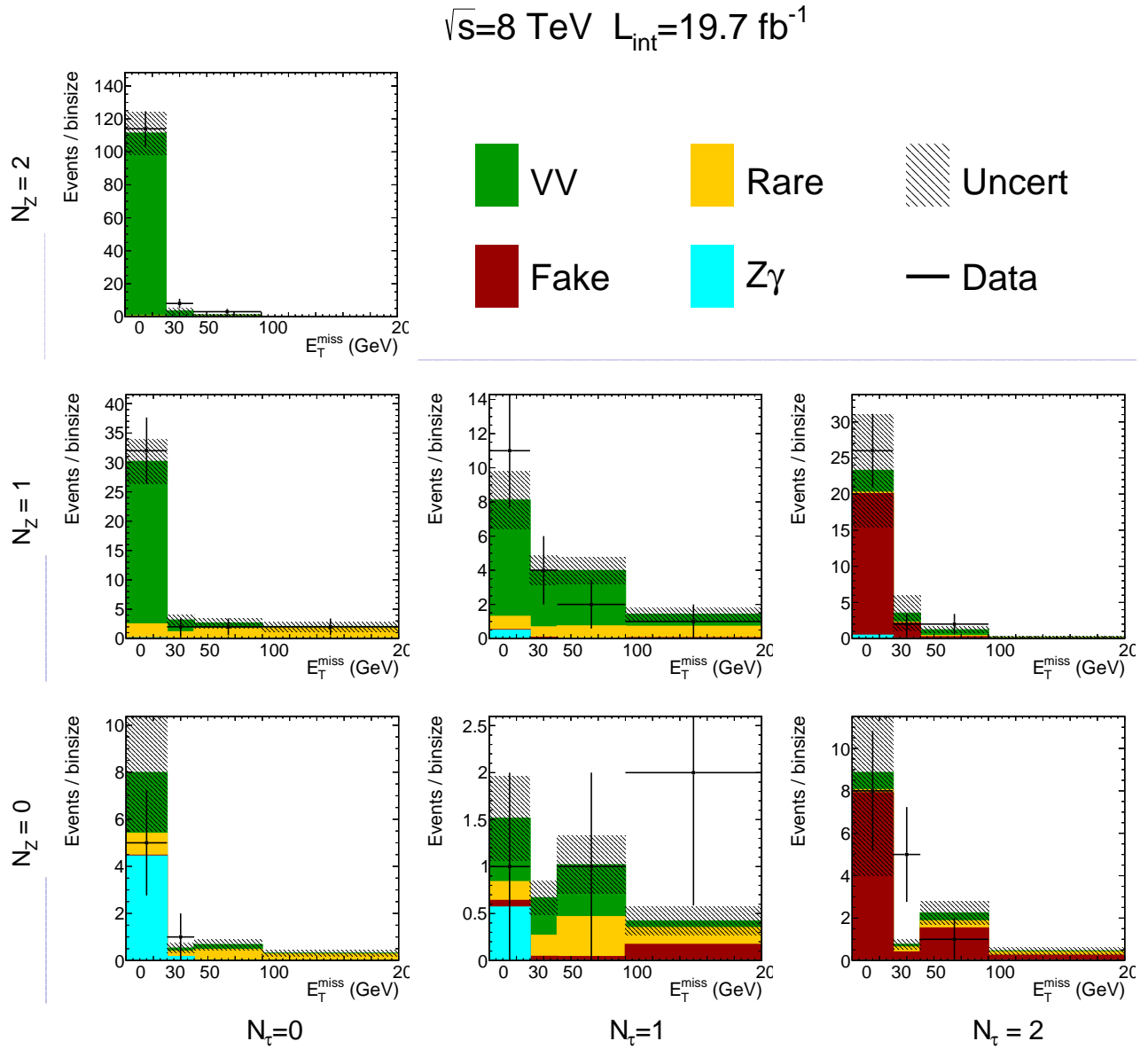
Figure 8.7.: Result for 4ℓ events.

For this reason, the numbers cannot be compared directly, and there is no claim that one of the numbers should be better. However, the qualitative outcome of both approaches is the same and therefore it is a matter of taste which number is chosen.

On the one hand, it is not unlikely to have two sigma fluctuations in over 180 search bins. However, on the contrary, this treatment is controversial since many of these bins have background predictions below one. Meaning they are not sensitive to a measurement of the background hypothesis and therefore for a statistical fluctuation of it. In table 8.2 all 3ℓ search bins that have a Z_{Bi} larger than two are summarized.

The two OSSF1tau region are dominated by backgrounds with fake taus, which have large

Table 8.2.: 3ℓ search regions with $Z_{Bi} > 2$

Selection numbers in GeV	prediction	observation	Z_{Bi}	σ_{freq}
OSSF0tau				
lowZ, $M_T > 160$, $50 < E_T^{miss} < 100$	2.911 ± 0.613	8	2.1	2.4
onZ, $120 < M_T < 160$, $E_T^{miss} < 50$	12.01 ± 2.907	26	2.4	2.8
onZ, $M_T > 160$, $50 < E_T^{miss} < 100$	4.650 ± 1.221	13	2.4	2.8
highZ, $120 < M_T < 160$, $E_T^{miss} < 50$	0.684 ± 0.175	4	2.4	2.7
OSSF1tau				
lowZ, $120 < M_T < 160$, $50 < E_T^{miss} < 100$	2.506 ± 0.577	9	2.7	2.98
lowZ, $M_T > 160$ $E_T^{miss} > 200$	0.122 ± 0.077	2	2.2	2.7

uncertainties. The statistic in the nearby bins is rather small and, therefore, these events will not discuss further and treated as a statistical fluctuation.

Four bins with an excess originate from the OSSF0tau category. This could be expected since in this region the main background is WZ. For WZ the theory prediction is 20% to low as already shown in section 7.2.1.1. This seeds about one sigma excess for all bins where WZ is dominant. Nevertheless, there are still more events than expected and therefore it is worth to take a closer look at those events. In figure 8.8 and 8.9 three lepton events where all three leptons are either muons or electrons and where the M_T is larger than 120 GeV are shown[1]. Figure 8.8 shows that the excess of events originates from events with M_T smaller than 200 GeV. A falling M_T distribution is expected but data peaks at $M_T = 170$ GeV and $M_T = 190$ GeV. The E_T^{miss} distribution shows that these extra events have E_T^{miss} lower than 140 GeV, which is small for events with M_T larger than 120 GeV. This low E_T^{miss} speaks against typical SUSY events. However, there are more exotic SUSY scenarios where the events could have low E_T^{miss}, e.g. if the two $\tilde{\chi}_1^0$ fly almost back to back. Many of these extra events include leptons from Z bosons as seen in the $m_{\ell^+\ell^-}$ distribution. Between $m_{\ell^+\ell^-} = 120$ GeV and 190 GeV an almost constant data contirbution is measured, where a falling distribution is expected. The hadronic activity for those extra events are low, but the most of these extra events have two additional jets, which are no b-jets. Figure 8.9 shows some additional lepton variables. The extra events show no difference concerning the lepton flavor. Interesting is that these events have a large charge asymmetry, meaning they originate from events produced by valence quarks[2]. This asymmetry is a hint that they come from a decay of heavy particles. The E_T^{miss} and the lepton not coming from a Z boson are almost back to back. The invariant mass of all three leptons $m_{\ell\ell\ell}$ also shows interesting features. For small $m_{\ell\ell\ell}$ values ($m_{\ell\ell\ell} < 180$ GeV) data and the background prediction agrees well. Between $m_{\ell\ell\ell} = 180$ GeV and $m_{\ell\ell\ell} = 300$ GeV and around $m_{\ell\ell\ell} = 470$ GeV two peaks are observed. The lower one is broader and on top of the WZ SM prediction,

---

[1] This means no b-veto, no $m_{\ell^+\ell^-}$ requirement and no E_T^{miss} cut are applied.
[2] Because of this the WZ production also have a charge asymmetry.

while the peak at $m_{\ell\ell}$= 470 GeV seems to be sharp. Again the distribution is almost constant between $m_{\ell\ell}$= 500 GeV and $m_{\ell\ell}$= 800 GeV.
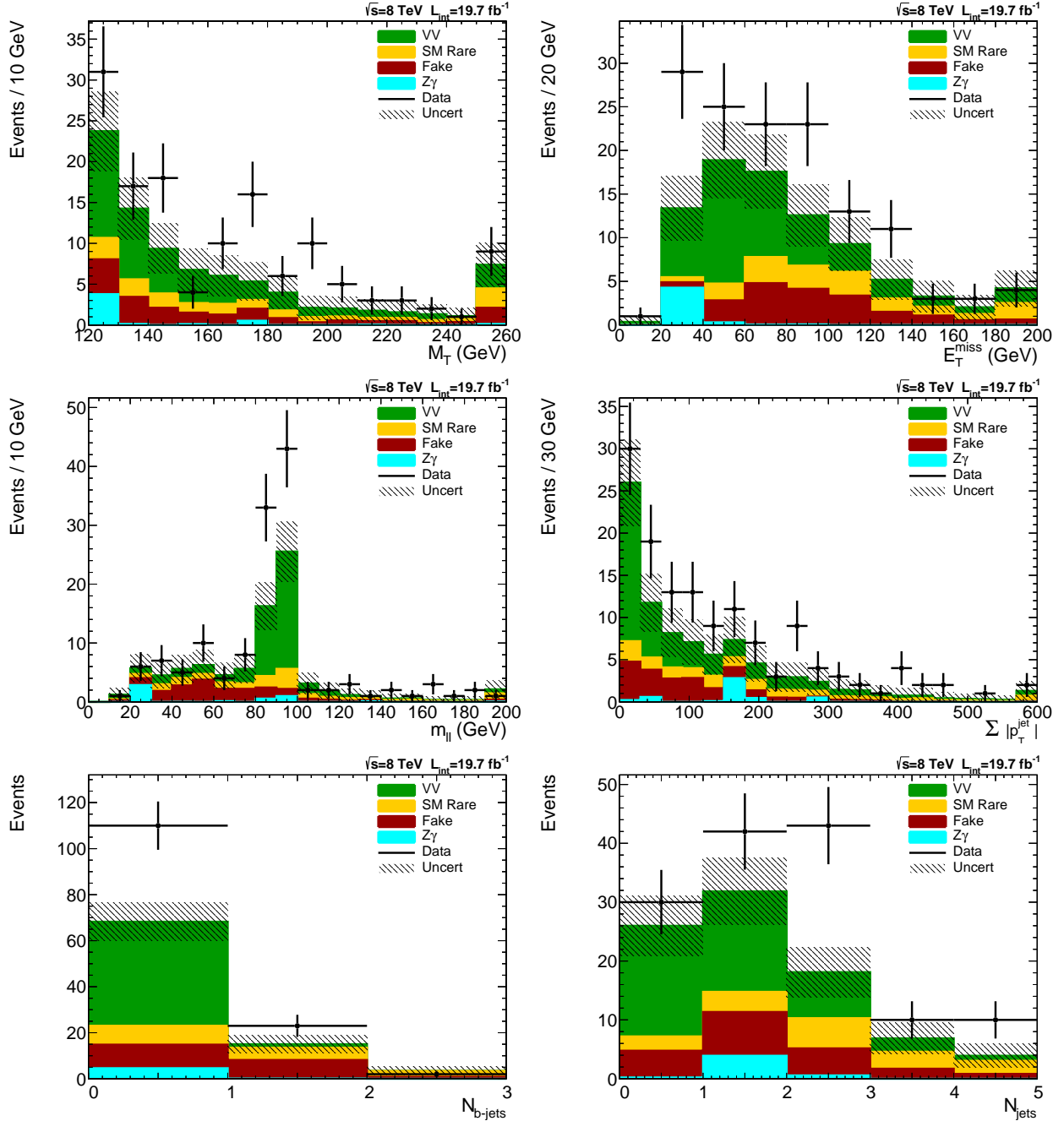
Figure 8.8.: 3ℓ events with $M_T > 120$ GeV are for data and background prediction are plotted. On the top left the M_T distribution and on the top right the E_T^{miss} distribution are shown. The middle row presents the $m_{\ell^+\ell^-}$ for the lepton pairs best matching a Z boson on the left and the right the scalar sum of all jets. On the bottom left (right) the number b-jets (jets) are shown.

A guess about the origin of these extra events is off-shell WZ-production. Since, the on-shell production already shows a discrepancy of 20%, the k-factor for the off-shell region could even be higher. We have three hypotheses where these events are coming from:
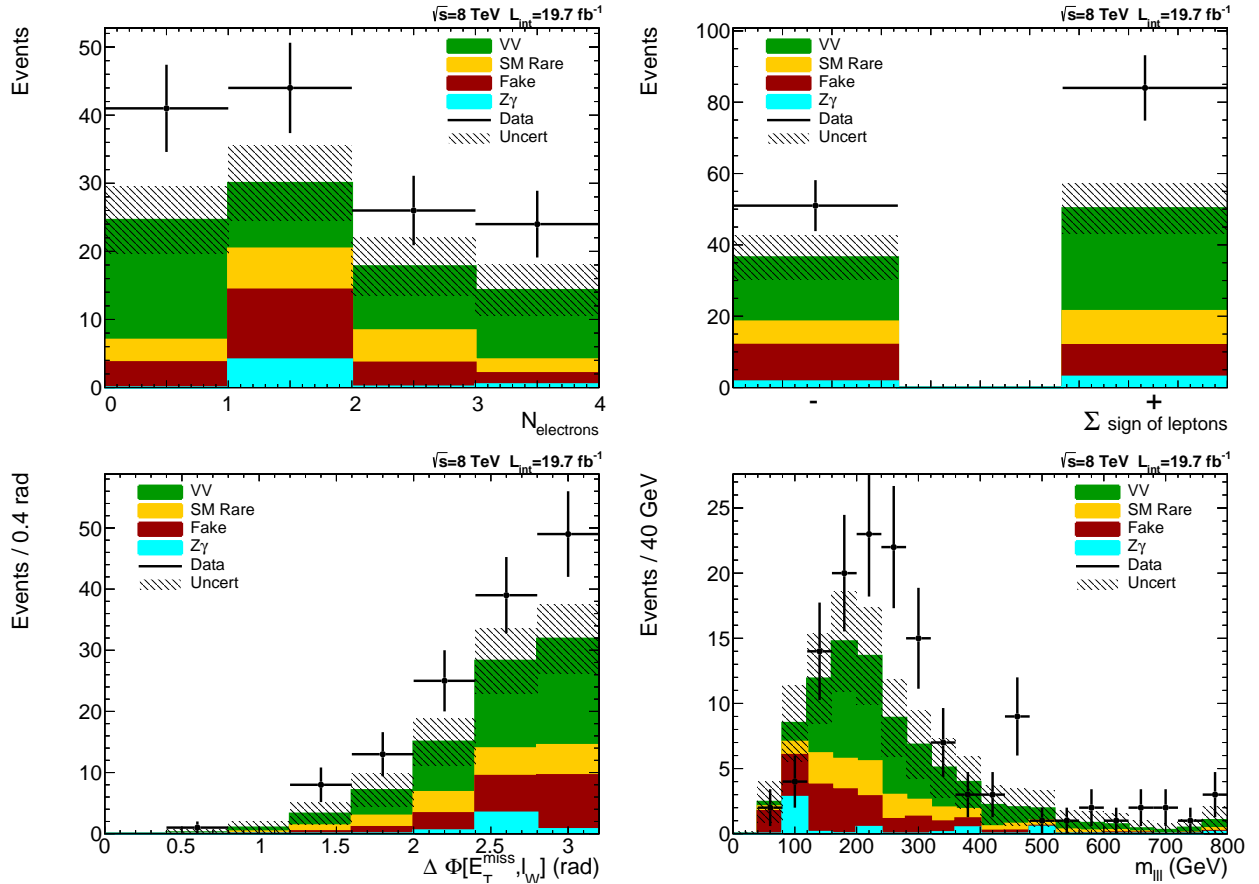
Figure 8.9.: 3ℓ events with $M_\mathrm{T} > 120$ GeV are for data and background prediction are plotted. The top left show the number of electrons. The top right plot shows the charge asymmetry. The angle between E_T^{miss} and the lepton not matching the Z boson are shown on the bottom left, and the bottom right plot show the invariant mass of all three leptons.

- Statistical fluctuation

- Underestimation of the Standard Model backgrounds (WZ)

- New physics contribution (like SUSY)

Of course, it could be a mixture of all them or something that has never been thought of. The data taking in 2015 will give the answer.

In order to bring the discussion of the excess to an end, a summary is given. In some bins we observe an excess with a statistical significance of two to three sigma. There is no simple SUSY scenario, which would fit all of these excesses at the same time. In addition, there is a bias from the Standard Model WZ-prediction, which increase these excesses.

9. Interpretation of the results

In this chapter, the results will be interpreted in scenarios with additional events from SUSY sources. So-called simplified models (SMS) are used which were introduced in chapter 6. In order to give quantitative statements about the results the CL_s statistical model is used, which has been discussed in detail in chapter 3. The general procedure is the following: first in the order of 10k to 50k events are produced for each model point. These events are passed through the analysis chain presented in the previous chapters, resulting in predictions for signal events in the individual search bins. The ten bins with the highest expected significance are chosen as signal hypothesis input for the statistical model. Additionally, some high statistic bins are added since the statistical model can fit some background uncertainties in these regions. The outcome of the statistical model is the 95% CL CL_s upper limit on the cross section, which is valid for all new physics models including this signature. In the last step, a cross section for this model point is calculated, and the result is translated into excluded parameter space.

9.1. Basics about SMS exclusions plots

The same presentation of the results using different simplified models is used in the following sections. The main features of these will be discussed below by using the left-hand side of figure 9.1. There the x-axis shows the mass of the $\tilde{\chi}_1^\pm$ $(=\tilde{\chi}_2^0$) and $\tilde{\chi}_1^0$ respectively. The sampling is done in steps of 20 GeV with the requirement $m_{\tilde{\chi}_1^0} < m_{\tilde{\chi}_2^0}$. For each of this points the observed 95% CL upper limit on the cross section is drawn on the z-axis. A three-dimensional view is chosen for illustration[1]. A lower limit on the cross section allows to exclude more parameter space. At the diagonal the limit gets worse. In this region the $\tilde{\chi}_1^\pm$ $(=\tilde{\chi}_2^0$) and $\tilde{\chi}_1^0$ have almost degenerated masses, which leads to soft decay products, so the acceptance breaks down. At large $\tilde{\chi}_1^\pm$ $(=\tilde{\chi}_2^0$) masses, the limit is in the order of 1 fb. This limit is a strong limit for a search with $\mathcal{L}_{int}$ = 19.7 fb^{-1}and implies that every new physics model producing ~20 events with this

---

[1]In the proper results the z-axis is represented via a colors code.

signature at $\sqrt{s} = 8$ TeV and $\mathcal{L}_{int} = 19.7$ fb^{-1}is excluded. This is still true if the signature would be produced in decay chains, with two exceptions: No reconstructed b-jet is present in the event due to the b-jet veto[2]. And the objects are not boosted too hard, in which case the E_T^{miss} from the $\tilde{\chi}_1^0$ cancel each other or the leptons cannot be separated.

The $\tilde{\chi}_1^\pm$ $\tilde{\chi}_2^0$ production cross section for this analysis is shown in the right plot of figure 9.1. Assuming a cross section allows us to translate the 95% CL upper limit on the cross section into exclusions of the parameter space. This procedure is done for all simplified models, and the result will be presented and discussed in the following sections. These exclusions are often interpreted in the wrong way. So this excluded parameter space depends on the assumption of cross section times branching ratio, which is highly model dependent. The chosen values are a realistic best case scenario and can be interpreted up to which masses we can test this scenario. The more robust results are the 95% CL upper limit on the cross section, which only depends on the two mass parameter.
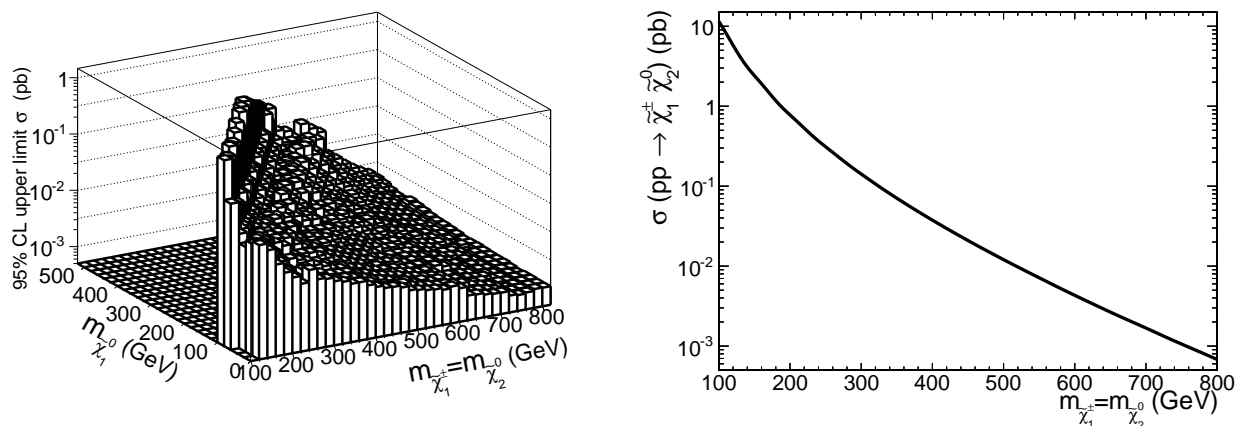
Figure 9.1.: The 95% CL upper limit on the cross section for a simplified model is shown on the left. The cross section for the process pp $\rightarrow \tilde{\chi}_1^\pm$ $\tilde{\chi}_2^0$ at a center of mass energy of $\sqrt{s}$=8 TeV is presented on the right.

9.2. Chargino Neutralino production with Slepton mediated decays

The first group of scenarios has slepton masses that are in between the $\tilde{\chi}_1^\pm$ and $\tilde{\chi}_1^0$ masses ($m_{\tilde{\chi}_1^0}< m_{\tilde{\ell}}< m_{\tilde{\chi}_1^\pm}$). As a result, $\tilde{\chi}_1^\pm$ $\tilde{\chi}_2^0$ pairs will decay via sleptons. The details of these scenarios were already introduced in section 6.1.1. The individual scenarios will be distinguished by the number of produced taus. The first scenario is the flavor democratic scenario producing all lepton flavors equally. The second scenario is called tau enriched because at least one tau is produced in this scenario. In the last scenario, all produced leptons are taus. For this reason, this scenario is called tau dominated.

---

[2]A dedicated analysis exist searching for multileptons plus b-jets [87].

9.2.1. Flavor Democratic

The result of the flavor democratic scenario is shown in figure 9.2. The important search regions are the 3ℓ OSSF0tau channels. Near the diagonal the signal events fall into the lowZ bins. The onZ bins become important if the mass difference is in the Z range. For large mass differences, all signal events go into the highZ bins, which is visible in the exclusion curves for the moderate scenario. There the expected limit slightly decreases from $m_{\tilde{\chi}_1^\pm}=450$ GeV and $m_{\tilde{\chi}_1^0}=370$ GeV to $m_{\tilde{\chi}_1^\pm}=500$ GeV and $m_{\tilde{\chi}_1^0}=350$ GeV, hence the onZ region has larger backgrounds. Then the limit increases again since the highZ region with lower backgrounds has the largest significance there. The largest differences between observed and expected limit are in the order of one sigma. This difference comes from the highZ, $M_{\mathrm{T}} > 160$ GeV, and 50 GeV $< E_{\mathrm{T}}^{miss} < 150$ GeV region. The E_{T}^{miss} of the signal increases at $m_{\tilde{\chi}_1^\pm} > 700$ GeV and, therefore, signal events having mostly $E_{\mathrm{T}}^{miss} > 150$ GeV. The smallest cross section that can be excluded in this scenario is in the order of ~ 0.7 fb. With wino-like cross section and 50% branching ratio, we can exclude $\tilde{\chi}_1^\pm$ with masses up to 700 GeV.

9.2.2. Tau Enriched

The result of the tau enriched scenario is presented in figure 9.3. Here the OSSF0tau and the OSSF1tau search regions are important. The lowZ bins dominate the sensitivity in the diagonal, and the highZ bins dominate for large mass differences, again. The one sigma difference between $m_{\tilde{\chi}_1^\pm}=400$ GeV and $m_{\tilde{\chi}_1^\pm}=650$ GeV is driven by several bins with slightly larger observation than expectation, e.g. events from the bin: OSSF0tau, highZ, $M_{\mathrm{T}} < 120$ GeV and $E_{\mathrm{T}}^{miss} > 200$ GeV, where 0.8 ± 0.2 events are expected and 3 events are observed. At higher chargino masses $m_{\tilde{\chi}_1^\pm} > 650$ GeV the majority of the signal events falling into the $M_{\mathrm{T}} > 120$ GeV and $E_{\mathrm{T}}^{miss} > 150$ GeV region. There the prediction and observation agrees, and the one sigma excess disappears. The smallest cross section that can be excluded in this scenario is around 1.3 fb. $\tilde{\chi}_1^\pm$ masses up to 700 GeV can be excluded with the assumption of wino-like cross section and a branching ratio of 100%.

9.2.3. Tau Dominated

Only the moderate stau mass is processed for the tau dominated scenario. In this scenario at least two of the produced taus have to decay leptonically. For this reason, we are only sensitive to around 0.1 of the produced events. In order to increase the sensitivity for this scenario the search regions noOSSF0tau, SS1tau and OSOF1tau were invented. All relevant decay chains are collected adding the OSSF1tau region additionally. With the combination of all these channels, the smallest cross section that can be excluded is about 60 fb. Under the assumption of wino-like cross section and a branching ratio of 100%, we can exclude $\tilde{\chi}_1^\pm$ masses up to 300 GeV.
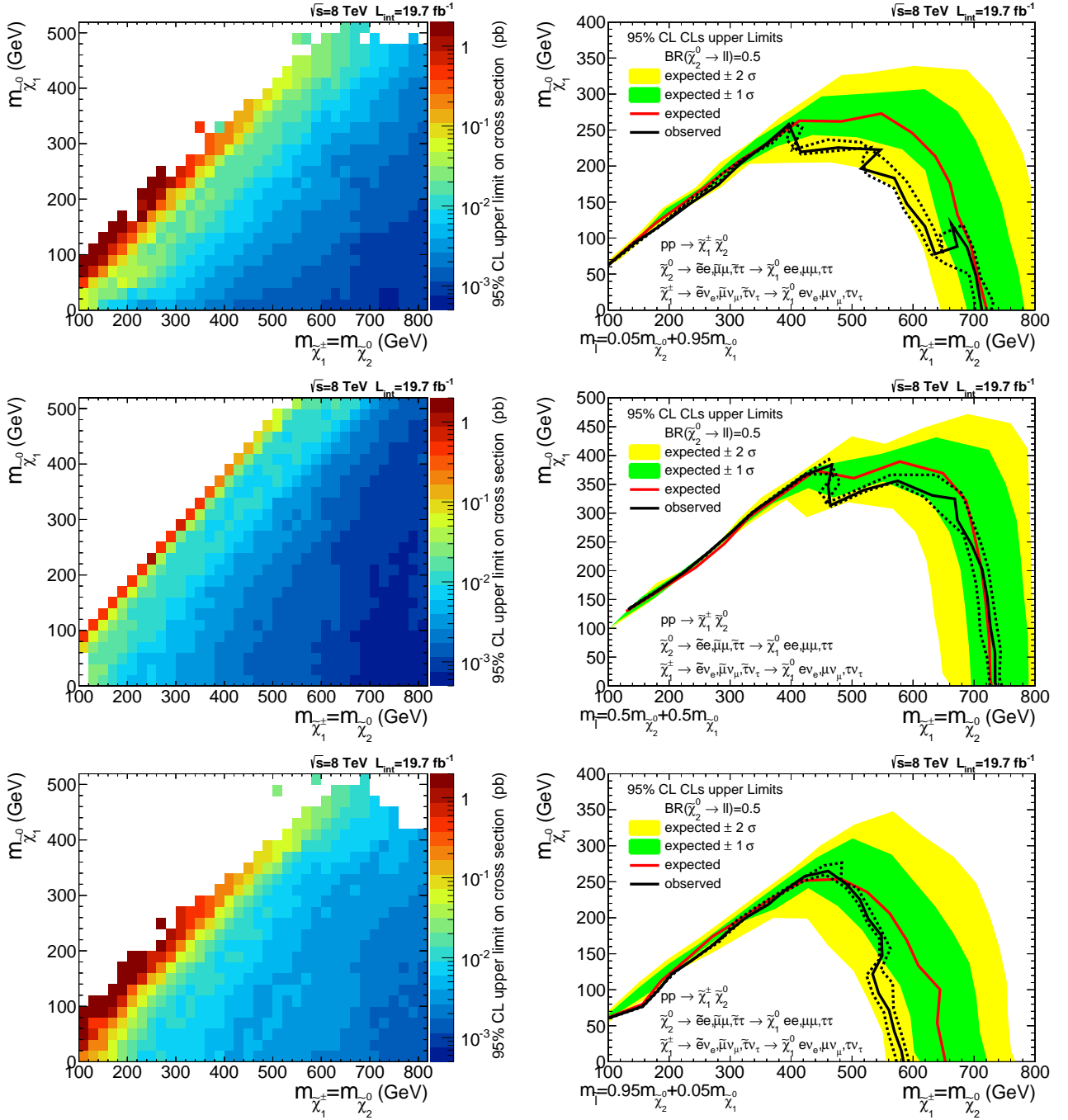
Figure 9.2.: 95% CL exclusion limits in the $m_{\tilde{\chi}_1^\pm}(=m_{\tilde{\chi}_2^0})$ $m_{\tilde{\chi}_1^0}$ plane for three different flavor democratic scenarios are presented. The light/moderate/heavy slepton scenario is shown in the top/middle/bottom. On the left-hand side the observed 95% CL exclusion limit on cross section is shown. The right-hand side shows the 95% CL excluded parameter space by assuming wino like $\tilde{\chi}_1^\pm$ $\tilde{\chi}_2^0$ production and a branching ratio of 0.5.
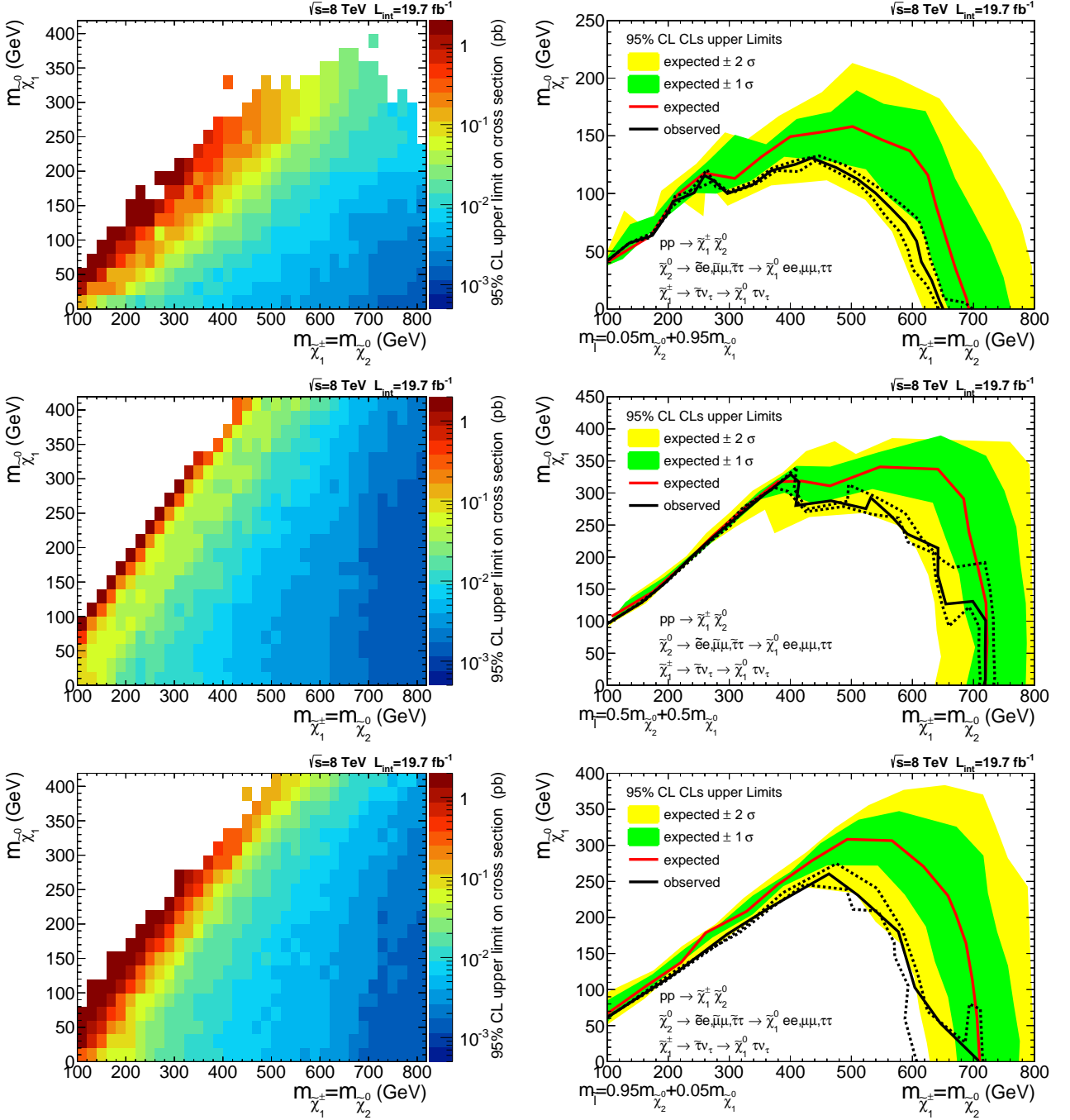
Figure 9.3.: 95% CL exclusion limits in the $m_{\tilde{\chi}_1^\pm}(=m_{\tilde{\chi}_2^0})$ $m_{\tilde{\chi}_1^0}$ plane for three different tau enriched scenarios are presented. The light/moderate/heavy slepton scenario is shown in the top/middle/bottom. On the left-hand side, the observed 95% CL exclusion limit on the cross section is shown. The right-hand side shows the 95% CL excluded parameter space by assuming wino-like $\tilde{\chi}_1^\pm$ $\tilde{\chi}_2^0$ production and a branching ratio of 1.

9.3. Chargino Neutralino production with decays into $\mathbf{WZ}\tilde{\chi}_1^0$ $\tilde{\chi}_1^0$

The chargino neutralino production is realized in the same way as for the slepton mediated decays. However, in this scenario the charginos and neutralino must decay into Standard
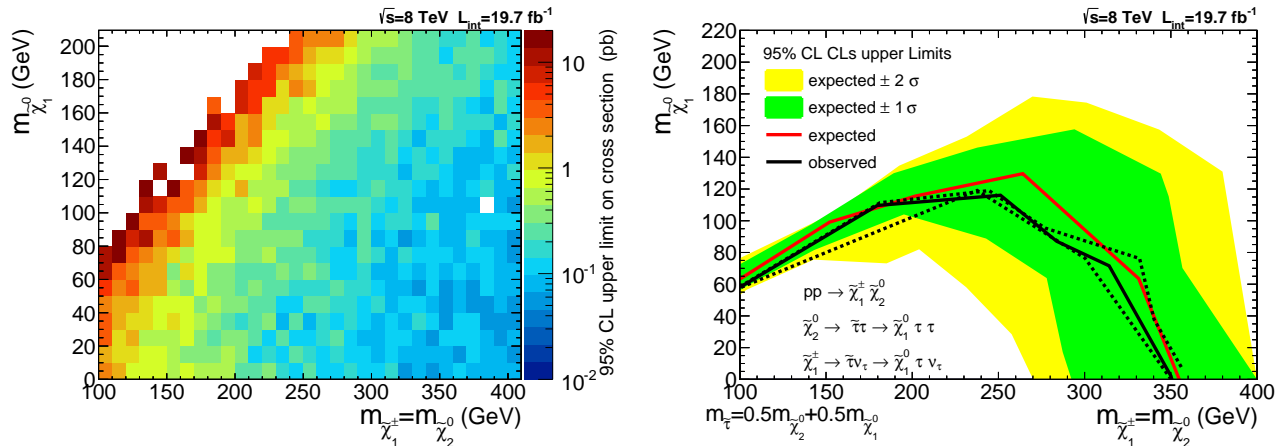
Figure 9.4.: 95% CL exclusion limits in the $m_{\tilde{\chi}_1^\pm}(=m_{\tilde{\chi}_2^0})$ $m_{\tilde{\chi}_1^0}$ plane for the tau dominated scenario. This plot corresponds to the moderate stau mass scenario. On the left-hand side, the observed 95% CL exclusion limit on the cross section is shown. The right-hand side shows the 95% CL excluded phase space by assuming wino-like $\tilde{\chi}_1^\pm$ $\tilde{\chi}_2^0$ production and a branching ratio of 1.

Model bosons since the sleptons are too heavy. The most natural decay is into final states with WZ bosons. For this reason, the signal looks similar to the Standard Model WZ production but has a larger E_T^{miss} and M_T. The result is presented in figure 9.5. If the mass differences are small also off-shell bosons are considered. The most sensitive search region is OSSF0tau, M_T > 120 GeV and onZ (or lowZ if the mass differences is below the Z mass). The lowZ region has lower backgrounds and therefore a better sensitivity. Getting closer to the diagonal of the mass plane the decay products of the bosons are getting softer, and, for this reason, the acceptance goes down. For $m_{\tilde{\chi}_2^0}=150$ GeV to $m_{\tilde{\chi}_2^0}=250$ GeV a discrepancy of two sigma is observed. The events causing this difference were already discussed in section 8.3.3. However, this signature cannot fit the full discrepancy because the excess does not exceed the two sigma level. We can exclude $\tilde{\chi}_1^\pm$ masses up to 250 GeV with the assumption of wino-like cross section and 100% branching ration into WZ final state. The smallest observed limit on the cross section for $m_{\tilde{\chi}_2^0}=$ 400 GeV is about ~ 180 fb.

9.3.1. Neutralino Neutralino production with decays into Z Boson

The gauge mediated symmetry breaking model described in section 6.2 is used to interpret the neutralino pair production. The lightest supersymmetric particle in this model is the almost massless gravitino. Therefore, the mass plane is reduced to one dimension. The result is shown in figure 9.6. The 4ℓ search region has the best sensitivity. However, the 3ℓ OSSF0tau region is also included since we gain sensitivity for events with one lepton falling our selection criteria. Data and predictions agree within two sigma, but a small excess in data is observed. This excess is driven by events coming from the 4ℓ , $N_\tau=0$, two onZ pairs and 30 GeV $< E_T^{miss} < 50$ GeV region where 3.4 ± 2.1 events are expected and 8 events are observed. This excess leads to a reduced excluded μ values of $\mu=240$ GeV compared to the expected value of $\mu=300$ GeV
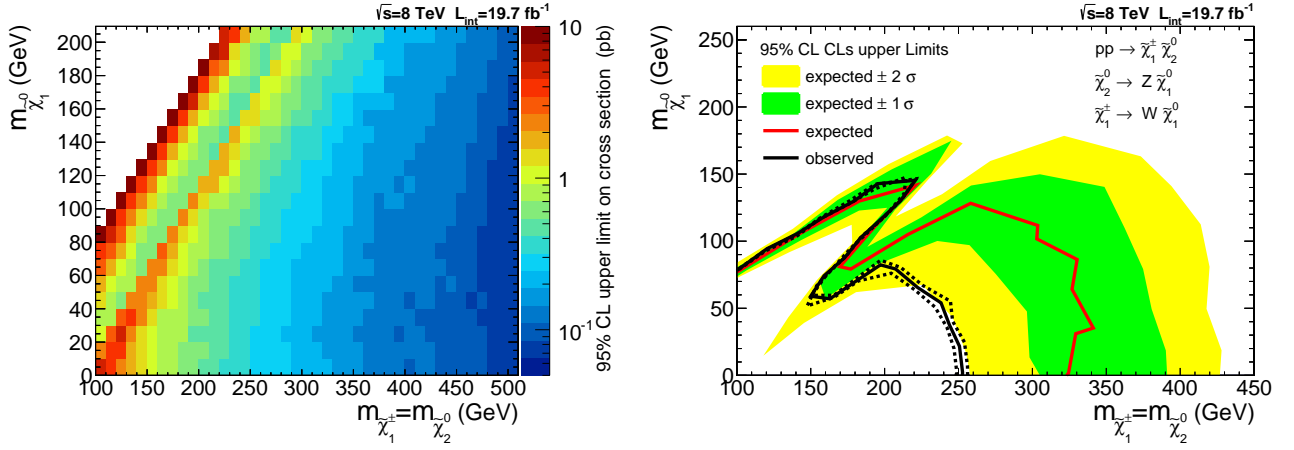
Figure 9.5.: 95% CL exclusion limits for the process pp $\rightarrow \tilde{\chi}_1^\pm$ $\tilde{\chi}_2^0 \rightarrow$ WZ$\tilde{\chi}_1^0$ $\tilde{\chi}_1^0$. On the left-hand side the observed 95% CL exclusion limit on the cross section is shown. The right-hand side shows the 95% CL excluded phase space by assuming wino like $\tilde{\chi}_1^\pm$ $\tilde{\chi}_2^0$ production.
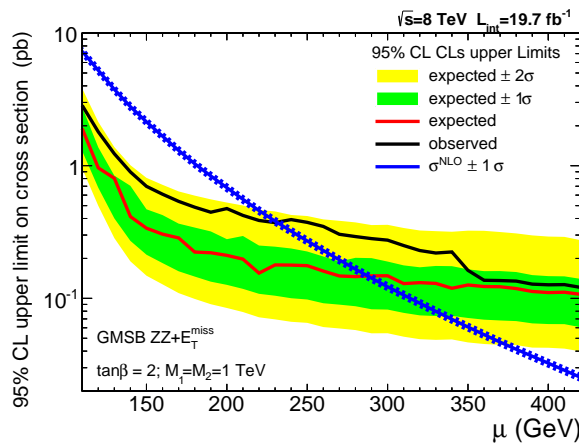
Figure 9.6.: 95% CL exclusion limits for a GMSB model described in section 6.2.

10. Summary and Outlook

In the year 2012 the LHC machine was running with a center of mass energy of $\sqrt{s} = 8$ TeV. The CMS detector was able to collect $\mathcal{L}_{int} = 19.7$ fb^{-1} during this run. This energy and the amount of data was never reached before, and the Standard Model has been tested at a new frontier. The three and four lepton final states have rather low yields from the Standard Model processes. For this reason, these final states are sensitive to a contribution from physics beyond the Standard Model. The most attractive candidate for such physics is the supersymmetric extension of the Standard Model (SUSY). The lightest supersymmetric particle (LSP) is assumed to be stable and uncharged. It does not interact with the detector and leaves an imbalance of the transverse component of the energy measurement, which is called missing transverse energy E_{T}^{miss}. The supersymmetric partners of the Standard Model W and Z boson can decay into final states with leptons and E_{T}^{miss}

The lepton efficiency has been studied in detail by data-driven methods, namely by using the SM process $Z \to \ell^+ \ell^-$, where one lepton is the tag lepton and the other lepton is the probe lepton. The uncertainty of the efficiency obtained with this data-driven method is 3%-5% for electrons and muons. Hadronically decaying tau leptons have an uncertainty on the efficiency of 6% [49]. The other objects, namely jets coming from b-quarks (b-jets) and the E_{T}^{miss}, show reliable performance in the control regions, too. There are three different types of Standard Model backgrounds that contribute to the three and four lepton final state. The first one consists of processes that produce three or four prompt leptons. These are WZ and ZZ production as well as the so-called rare backgrounds, which includes triple bosons and double boson plus t-quark production. The WZ and ZZ predictions are validated with data. For WZ, an uncertainty of 20% has to be assigned to cover the differences between simulation and data. The data agree with the predictions for ZZ having an uncertainty of 2% for on-shell production and 6% uncertainty for off-shell production. The rare processes have a tiny cross section and, for this reason, they can not be validated with this amount of data. Theory predictions with an uncertainty of 50% are used for this kind of backgrounds. The next sources are backgrounds including fake

leptons. These are leptons produced within jets or hadrons misidentified as leptons. The most important sources are processes with two prompt leptons, like Drell-Yan and $t\bar{t}$ production, which produce in addition one fake lepton from jets. In $t\bar{t}$ events which decaying di-leptonically the jet producing this fake lepton is typically a b-jet. A b-jet has a different fake rate compared to fakes from light jets because of the leptonic decay modes of B-mesons. For this reason, the fake rate in both samples has been studied separately. Corrections are applied if there are differences between data and simulation. The uncertainty for this kind of background is 20%. The last background sources are leptons from photon conversion. A real photon converts into an electron pair by interacting with the detector. Electron and muon pairs can be produced by the hard scattering, and asymmetric conversion of the photon leads to one additional lepton in the detector. The prediction and data agrees within an uncertainty of 50% for this kind of background.

The resulting yields for the three lepton final states are binned in 180 exclusive search channels. The channels are distinguished by the following variables: The number of reconstructed taus, the number of opposite-sign electron/muon pairs, the invariant mass of two opposite sign leptons, E_T^{miss} and the transverse mass M_T (lepton,E_T^{miss}). The four lepton final state consist of 28 exclusive search bins. They are distinguished by the number of taus and the invariant mass of opposite sign same flavor lepton pairs. Good agreement between data and background prediction is observed for the individual search channels. In a few channels, an excess of data in the order of 2 to 3σ is found. It is not unlikely to find such discrepancies, if one has 208 search channels, but these extra events could also originate from unknown sources.

Since no evidence for SUSY has been found an upper limit on production cross sections for the SUSY scenarios with three and four lepton final states at 95% CL limit can be set. The results are interpreted in the simplified model approach. Each simplified model considers only one supersymmetric signature. As a result, the limit on the cross section only depends on two or three parameters. The first set of simplified models consists of $\tilde{\chi}_1^{\pm}\,\tilde{\chi}_2^0$ production both decaying into sleptons. For large $\tilde{\chi}_1^{\pm}$ masses the invariant mass of the opposite-sign same-flavor lepton pair is above 105 GeV and these events fall into the highZ region. The smallest cross section, which can be excluded at 95% CL limit, is 0.7 fb, which corresponds to an exclusion of all SUSY models producing $\sim$14 events with this signature. Assuming 50%-100% branching ratios into sleptons, and a wino-like cross section allows us to exclude $\tilde{\chi}_1^{\pm}$ masses up to 700 GeV at 95% CL limit. The next simplified model under discussion is the production of $\tilde{\chi}_1^{\pm}\,\tilde{\chi}_2^0$ decaying into W and Z bosons. If one considers a wino-like cross section the observed limit on $\tilde{\chi}_1^{\pm}$ masses is only 250 GeV, since this model has many events falling in the search region with a two sigma excess of data. The last supersymmetric signature under discussion addresses the production of neutralino pairs decaying into two Z bosons and two LSPs. A gauge mediated symmetry breaking (GMSB) SUSY scenario was chosen for the interpretation of this signature. The higgsino mass parameter μ of this GMSB model could be constrained to be $\mu <$240 GeV at 95% CL.

The results presented in this thesis are an important contribution to the official CMS paper
[10].

10.1. Outlook

An interpolation of this analysis to higher energies ($\sqrt{s} = 14$ TeV) and higher luminosity ($\mathcal{L}_{int}=$
3000 fb^{-1}) has been made [88]. Such a luminosity is expected to be reached in 2033. One of the
primary motivations is to find SUSY with these data. The backgrounds, as well as the signal
processes, are computed with the Madgraph framework and passed trough the fast simulation
program Delphes, which is based on a parameterized detector response as discussed in section
4.3.2.8. This allows us to have enough statistics in all relevant regions.

The analysis is equal to the analysis presented in this thesis except for the extension of the
search region by additional E_{T}^{miss} and M_{T} bins. This extra bins leads to an increased sensitivity
for heavy $\tilde{\chi}_1^{\pm}$ $\tilde{\chi}_2^0$, which were out of reach for the 8 TeV analysis. The focus lies on the 5σ
discovery of the simplified model process pp$\to \tilde{\chi}_1^{\pm}$ $\tilde{\chi}_2^0 \to$ WZ $\tilde{\chi}_1^0$ $\tilde{\chi}_1^0$. The decay into a Z boson
is not the only possible decay chain for a $\tilde{\chi}_2^0$. It also can decay into a Higgs boson. The best
sensitivity for this decay has a search for events with a single lepton, two b-jets, and E_{T}^{miss}.
The relation BR($\tilde{\chi}_2^0 \to$ Z $\tilde{\chi}_1^0$)+BR($\tilde{\chi}_2^0 \to$ H $\tilde{\chi}_1^0$)=1 is given for many natural SUSY models
with heavy sleptons. For this reason, I have combined the result of both analyses. The result
is presented in figure 10.1 and assumes wino-like cross sections. Charginos and neutralinos can
be discovered (5σ evidence) with $\mathcal{L}_{int}=$3000 fb^{-1} at $\sqrt{s} = 14$ TeV if the wino-like $\tilde{\chi}_1^{\pm}$ masses
are below 850 GeV and the $\tilde{\chi}_1^0$ (LSP) mass is below 200 GeV.
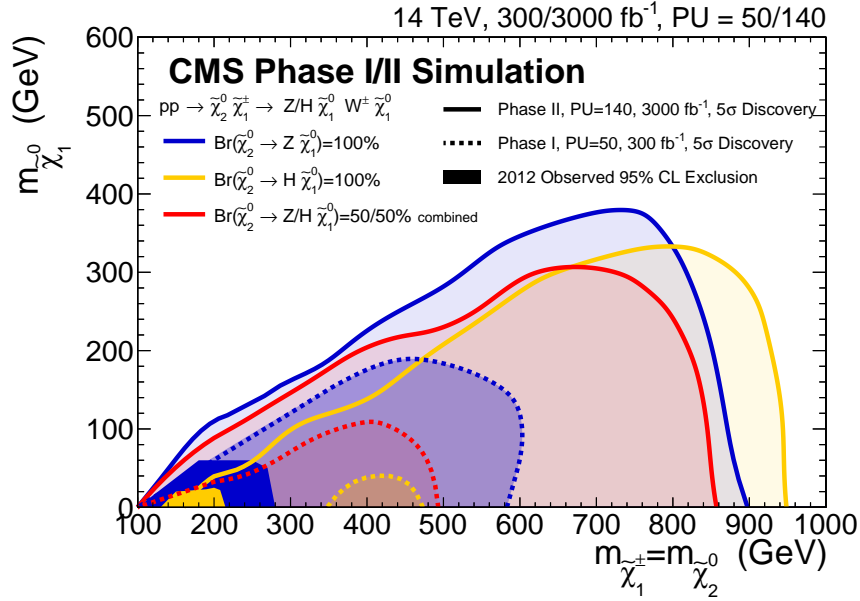
Figure 10.1.: Discovery reach for the SUSY signatures pp$\to \tilde{\chi}_1^\pm\ \tilde{\chi}_2^0 \to$ WZ/WH $\tilde{\chi}_1^0\ \tilde{\chi}_1^0$ in the $m_{\tilde{\chi}_1^\pm} m_{\tilde{\chi}_1^0}$ plane. The filled areas give the 95 % CL observed exclusion limit obtained with the data collected in 2012. The light (dark) areas corespondent to a five sigma discovery with $\mathcal{L}_{int}$=3000 (=300) fb^{-1} at $\sqrt{s} = 14$ TeV. In all scenarios the relation BR($\tilde{\chi}_2^0 \to$ Z $\tilde{\chi}_1^0$)+BR($\tilde{\chi}_2^0 \to$ H $\tilde{\chi}_1^0$)=1 is given. The BR($\tilde{\chi}_2^0 \to$ Z $\tilde{\chi}_1^0$)=1 for the blue area. In the yellow area the BR($\tilde{\chi}_2^0 \to$ H $\tilde{\chi}_1^0$)=1 and, the red area shows the combination with BR($\tilde{\chi}_2^0 \to$ Z $\tilde{\chi}_1^0$)=BR($\tilde{\chi}_2^0 \to$ H $\tilde{\chi}_1^0$)=0.5. The figure is published in [88].

Bibliography

[1] CMS Collaboration, "Observation of a new boson at a mass of 125 GeV with the CMS experiment at the LHC", *Phys.Lett.* **B716** (2012) 30–61, `arXiv:1207.7235`.

[2] ATLAS Collaboration, "Observation of a new particle in the search for the Standard Model Higgs boson with the ATLAS detector at the LHC", *Phys.Lett.* **B716** (2012) 1–29, `arXiv:1207.7214`.

[3] Planck Collaboration, "Planck 2013 results. XVI. Cosmological parameters", *Astron.Astrophys.* **571** (2014) A16, `arXiv:1303.5076`.

[4] W. de Boer, "Grand unified theories and supersymmetry in particle physics and cosmology", *Prog.Part.Nucl.Phys.* **33** (1994) 201–302, `arXiv:hep-ph/9402266`.

[5] S. P. Martin, "A Supersymmetry primer", *Adv.Ser.Direct.High Energy Phys.* **21** (2010) 1–153, `arXiv:hep-ph/9709356`.

[6] D. Kazakov, "Supersymmetry on the Run: LHC and Dark Matter", *Nucl.Phys.Proc.Suppl.* **203-204** (2010) 118–154, `arXiv:1010.5419`.

[7] D0 Collaboration, "Search for associated production of charginos and neutralinos in the trilepton final state using 2.3 fb^{-1} of data", *Phys.Lett.* **B680** (2009) 34–43, `arXiv:0901.0646`.

[8] CDF Collaboration, "Search for anomalous production of multi-lepton events in $p\bar{p}$ collisions at $\sqrt{s} = 1.96$-TeV", *Phys.Rev.Lett.* **98** (2007) 131804, `arXiv:0706.4448`.

[9] CDF Collaboration, "Search for Supersymmetry in p anti-p Collisions at s**(1/2) =1.96-TeV Using the Trilepton Signature of Chargino-Neutralino Production", `arXiv:0910.1931`.

[10] CMS Collaboration, "Searches for electroweak production of charginos, neutralinos, and sleptons decaying to leptons and W, Z, and Higgs bosons in pp collisions at 8 TeV", *Eur.Phys.J.* **C74** (2014), no. 9, 3036, `arXiv:1405.7570`.

[11] M. E. Peskin and D. V. Schroeder, "An Introduction to Quantum Field Theory; 1995 ed.". Westview, Boulder, CO, 1995. Includes exercises.

[12] O. Nachtmann, "Phänomene und Konzepte der Elementarteilchenphysik". Vieweg, 1986.

[13] E. Noether, "Invarianten beliebiger Differentialausdrücke.", *Nachr. Ges. Wiss. Göttingen, Math.-Phys. Kl.* **1918** (1918) 37–44.

[14] CMS Collaboration, S. Chatrchyan et al., "CMS Standard Model Physics Results". `https://twiki.cern.ch/twiki/bin/view/CMSPublic/PhysicsResultsSMP`, 2014.

[15] Particle Data Group Collaboration, "Review of Particle Physics", *Chin.Phys.* **C38** (2014) 090001.

[16] U. Amaldi, W. de Boer, and H. Furstenau, "Comparison of grand unified theories with electroweak and strong coupling constants measured at LEP", *Phys.Lett.* **B260** (1991) 447–455.

[17] WMAP Collaboration, "Nine-Year Wilkinson Microwave Anisotropy Probe (WMAP) Observations: Cosmological Parameter Results", *Astrophys.J.Suppl.* **208** (2013) 19, `arXiv:1212.5226`.

[18] G. Jungman, M. Kamionkowski, and K. Griest, "Supersymmetric dark matter", *Phys.Rept.* **267** (1996) 195–373, `arXiv:hep-ph/9506380`.

[19] J. Berger, "Search for the Higgs Boson Produced via Vector-Boson Fusion in the Decay Channel $H \to \tau\tau$". Dr., Karlsruhe Institute of Technology, 2014. Karlsruhe Institute of Technology, Diss., 2014.

[20] R. D. Ball, L. Del Debbio, S. Forte et al., "A first unbiased global NLO determination of parton distributions and their uncertainties", *Nucl.Phys.* **B838** (2010) 136–206, `arXiv:1002.4407`.

[21] A. L. Read, "Presentation of search results: the CL_s technique", *Journal of Physics G: Nuclear and Particle Physics* **28** (2002), no. 10, 2693.

[22] T. Junk, "Confidence level computation for combining searches with small statistics", *Nucl.Instrum.Meth.* **A434** (1999) 435–443, `arXiv:hep-ex/9902006`.

[23] F. Frensch, "Statistische Kombination verschiedener Suchen nach Supersymmetrie mit dem CMS-Detektor am LHC". Master., KIT, 2012. KIT, Diploma thesis., 2012.

[24] The CMS Statistics Committee Collaboration, B. Cousins, "Probability Density Functions for Positive Nuisance Parameters", technical report, UCLA, Geneva, May, 2010.

[25] ATLAS Statistics Forum Collaboration, G. Cowan, "The CLs method: information for conference speakers", technical report, Sydney, Geneva, July, 2011.

[26] ATLAS Collaboration, "The ATLAS Experiment at the CERN Large Hadron Collider", *JINST* **3** (2008) S08003.

[27] ALICE Collaboration, "The ALICE experiment at the CERN LHC", *JINST* **3** (2008) S08002.

[28] CMS Collaboration, "The CMS experiment at the CERN LHC", *JINST* **3** (2008) S08004.

[29] LHCb Collaboration, "The LHCb Detector at the LHC", *JINST* **3** (2008) S08005.

[30] J. Goodson, "Search for Supersymmetry in States with Large Missing Transverse Momentum and Three Leptons including a Z-Boson". PhD thesis, Stony Brook University, May, 2012. Presented 17 Apr 2012.

[31] CMS Collaboration, S. Chatrchyan et al., "CMS Physics: Technical Design Report Volume 1: Detector Performance and Software". Technical Design Report CMS. CERN, Geneva, 2006. There is an error on cover due to a technical problem for some items.

[32] CERN, "BIG SCIENCE The LHC in pictures". http://bigscience.web.cern.ch/bigscience/en/cms/cms2.html, 2008.

[33] CMS Collaboration, "Alignment of the CMS Muon System with Cosmic-Ray and Beam-Halo Muons", *JINST* **5** (2010) T03020, arXiv:0911.4022.

[34] CMS Collaboration, "The CMS high level trigger", *The European Physical Journal C - Particles and Fields* **46** (2006), no. 3, 605–667.

[35] T. Virdee, A. Petrilli, and A. Ball, "CMS High Level Trigger", Technical Report LHCC-G-134. CERN-LHCC-2007-021, CERN, Geneva, Jun, 2007. revised version submitted on 2007-10-19 16:57:09.

[36] CMS Collaboration, G. Bayatyan, L. Della, M. Negra et al., "CMS computing: Technical Design Report". Technical Design Report CMS. CERN, Geneva, 2005. Submitted on 31 May 2005.

[37] I. Antcheva, M. Ballintijn, B. Bellenot et al., "ROOT: A C++ framework for petabyte data storage, statistical analysis and visualization", *Comput.Phys.Commun.* **180** (2009) 2499–2512.

[38] A. Hoecker, P. Speckmayer, J. Stelzer et al., "TMVA: Toolkit for Multivariate Data Analysis", *PoS* **ACAT** (2007) 040, arXiv:physics/0703039.

[39] The ATLAS Collaboration, The CMS Collaboration, The LHC Higgs Combination Group Collaboration, T. L. H. C. G. The ATLAS Collaboration, The CMS Collaboration, "Procedure for the LHC Higgs boson search combination in Summer 2011", Technical Report CMS-NOTE-2011-005. ATL-PHYS-PUB-2011-11, CERN, Geneva, Aug, 2011.

[40] Alwall, Johan and Herquet, Michel and Maltoni, Fabio and Mattelaer, Olivier and Stelzer, Tim, "MadGraph 5: going beyond", *Journal of High Energy Physics* **2011** (2011), no. 6,.

[41] C. Oleari, "The POWHEG-BOX", *Nucl.Phys.Proc.Suppl.* **205-206** (2010) 36–41, `arXiv:1007.3893`.

[42] T. Sjostrand, S. Mrenna, and P. Z. Skands, "PYTHIA 6.4 Physics and Manual", *JHEP* **0605** (2006) 026, `arXiv:hep-ph/0603175`.

[43] V. Lefébure, S. Banerjee, and I. González, "CMS Simulation Software Using Geant4",.

[44] J. de Favereau, C. Delaere, P. Demin et al., "DELPHES 3, A modular framework for fast simulation of a generic collider experiment", `arXiv:1307.6346`.

[45] CMS Collaboration, S. Chatrchyan et al., "Electron reconstruction and identification at sqrt(s) = 7 TeV", Technical Report CMS-PAS-EGM-10-004, CERN, Geneva, 2010.

[46] CMS Collaboration, S. Chatrchyan et al., "Performance of muon identification in pp collisions at s**0.5 = 7 TeV", Technical Report CMS-PAS-MUO-10-002, CERN, 2010. Geneva, 2010.

[47] M. Cacciari and G. P. Salam, "Pileup subtraction using jet areas", *Phys.Lett.* **B659** (2008) 119–126, `arXiv:0707.1378`.

[48] CMS Collaboration, S. Chatrchyan et al., "Search for Higgs Bosons Decaying to Tau Pairs in pp Collisions at $\sqrt{s}$=7 TeV", CMS Physics Analysis Summary CMS AN-2011-153-v22, CERN, 2011.

[49] CMS Collaboration, "Performance of τ-lepton reconstruction and identification in CMS", *Journal of Instrumentation* **7** (2012), no. 01, P01001.

[50] CMS Collaboration, S. Chatrchyan et al., "Particle-Flow Event Reconstruction in CMS and Performance for Jets, Taus, and MET", Technical Report CMS-PAS-PFT-09-001, CERN, 2009. Geneva, Apr, 2009.

[51] M. Cacciari, G. P. Salam, and G. Soyez, "The anti- k t jet clustering algorithm", *Journal of High Energy Physics* **2008** (2008), no. 04, 063.

[52] CMS Collaboration, "Identification of b-quark jets with the CMS experiment", *Journal of Instrumentation* **8** (2013), no. 04, P04013.

[53] CMS Collaboration, S. Chatrchyan et al., "Performance of b tagging at sqrt(s)=8 TeV in multijet, ttbar and boosted topology events", Technical Report CMS-PAS-BTV-13-001, CERN, Geneva, 2013.

[54] CMS Collaboration, "Performance of the missing transverse energy reconstruction by the CMS experiment in sqrt(s) = 8 TeV pp data", `arXiv:1411.0511`.

[55] CMS Collaboration, "Missing transverse energy performance of the CMS detector", *J. Instrum.* **6** (Jun, 2011) P09001. 56 p.

[56] CMS Collaboration, S. Chatrchyan et al., "MET performance in 8 TeV data", Technical Report CMS-PAS-JME-12-002, CERN, Geneva, 2013.

[57] CMS Collaboration, "Determination of jet energy calibration and transverse momentum resolution in CMS", *Journal of Instrumentation* **6** (November, 2011) 11002, arXiv:1107.4277.

[58] The CMS Collaboration, "Phenomenological MSSM interpretation of the CMS 7 and 8 TeV results",.

[59] B. Fuks, M. Klasen, D. R. Lamprea et al., "Precision predictions for electroweak superpartner production at hadron colliders with Resummino", *Eur.Phys.J.* **C73** (2013) 2480, arXiv:1304.0790.

[60] B. Fuks, M. Klasen, D. R. Lamprea et al., "Gaugino production in proton-proton collisions at a center-of-mass energy of 8 TeV", *JHEP* **1210** (2012) 081, arXiv:1207.2159.

[61] B. Fuks, M. Klasen, D. R. Lamprea et al., "Revisiting slepton pair production at the Large Hadron Collider", *JHEP* **1401** (2014) 168, arXiv:1310.2621.

[62] J. T. Ruderman and D. Shih, "General Neutralino NLSPs at the Early LHC", *JHEP* **1208** (2012) 159, arXiv:1103.6083.

[63] P. Meade, M. Reece, and D. Shih, "Prompt Decays of General Neutralino NLSPs at the Tevatron", *JHEP* **1005** (2010) 105, arXiv:0911.4130.

[64] K. T. Matchev and S. D. Thomas, "Higgs and Z boson signatures of supersymmetry", *Phys.Rev.* **D62** (2000) 077702, arXiv:hep-ph/9908482.

[65] CMS Collaboration, H. Y.-S. Tong and S.-S. Yu, "Determination of the uncertainties on the MCFM cross sections for the diboson and ttbar productions", CMS Physics Analysis Summary CMS AN-2014-062-v2, CERN, 2014.

[66] Q. Cao, "Single top quark production and decay in hadron collision at next-to-leading order",.

[67] U. Baur, T. Han, and J. Ohnemus, "QCD corrections to hadronic $W\gamma$ production with nonstandard $WW\gamma$ couplings", *Phys.Rev.* **D48** (1993) 5140–5161, arXiv:hep-ph/9305314.

[68] J. Ohnemus, "Order $\alpha^- s$ calculations of hadronic $W^{\pm}\gamma$ and $Z\gamma$ production", *Phys.Rev.* **D47** (1993) 940–955.

[69] CMS Collaboration Collaboration, "Measurements of differential and double-differential Drell-Yan cross sections in proton-proton collisions at $\sqrt{s} = 8$ TeV", arXiv:1412.1115.

[70] J. M. Campbell and R. Ellis, "MCFM for the Tevatron and the LHC", *Nucl.Phys.Proc.Suppl.* **205-206** (2010) 10–15, `arXiv:1007.3492`.

[71] J. M. Campbell and R. K. Ellis, "An Update on vector boson pair production at hadron colliders", *Phys.Rev.* **D60** (1999) 113006, `arXiv:hep-ph/9905386`.

[72] J. M. Campbell, R. K. Ellis, and C. Williams, "Vector boson pair production at the LHC", *JHEP* **1107** (2011) 018, `arXiv:1105.0020`.

[73] CMS Collaboration Collaboration, "Measurement of the $pp \to ZZ$ production cross section and constraints on anomalous triple gauge couplings in four-lepton final states at $\sqrt{s} =$8 TeV", *Phys.Lett.* **B740** (2014) 250–272, `arXiv:1406.0113`.

[74] CMS Collaboration Collaboration, "Measurement of W+W- and ZZ production cross sections in pp collisions at sqrt(s) = 8 TeV", *Phys.Lett.* **B721** (2013) 190–211, `arXiv:1301.4698`.

[75] CMS Collaboration, S. Chatrchyan et al., "Measurement of WZ production rate", Technical Report CMS-PAS-SMP-12-006, CERN, Geneva, 2013.

[76] K. Arnold, J. Bellm, G. Bozzi et al., "VBFNLO: A Parton Level Monte Carlo for Processes with Electroweak Bosons – Manual for Version 2.5.0", `arXiv:1107.4038`.

[77] F. Campanario, V. Hankele, C. Oleari et al., "QCD corrections to charged triple vector boson production with leptonic decay", *Phys.Rev.* **D78** (2008) 094012, `arXiv:0809.0790`.

[78] M. Garzelli, A. Kardos, C. Papadopoulos et al., "Z0 - boson production in association with a top anti-top pair at NLO accuracy with parton shower effects", *Phys.Rev.* **D85** (2012) 074022, `arXiv:1111.1444`.

[79] A. Kardos, Z. Trocsanyi, and C. Papadopoulos, "Top quark pair production in association with a Z-boson at NLO accuracy", *Phys.Rev.* **D85** (2012) 054015, `arXiv:1111.0610`.

[80] J. M. Campbell and R. K. Ellis, "$t\bar{t}W^{+-}$ production and decay at NLO", *JHEP* **1207** (2012) 052, `arXiv:1204.5678`.

[81] D. Troendle, "SEARCH FOR SUPERSYMMETRY USING MULTILEPTONIC SIGNATURES IN PROTON-PROTON COLLISIONS WITH THE CMS DETECTOR AT THE LHC". Dr., KIT, 2013. KIT, Diss., 2013.

[82] (CMS Collaboration) Collaboration, "Measurement of the properties of a Higgs boson in the four-lepton final state", *Phys. Rev. D* **89** (May, 2014) 092007.

[83] CMS Collaboration, S. Chatrchyan et al., "CMS Luminosity Based on Pixel Cluster Counting - Summer 2013 Update", Technical Report CMS-PAS-LUM-13-001, CERN, Geneva, 2013.

[84] R. D. Cousins, J. T. Linnemann, and J. Tucker, "Evaluation of three methods for calculating statistical significance when incorporating a systematic uncertainty into a test of the background-only hypothesis for a Poisson process", *Nuclear Instruments and Methods in Physics Research A* **595** (October, 2008) 480–501, `arXiv:physics/0702156`.

[85] K. Cranmer, "Statistical Challenges for Searches for New Physics at the LHC", in *Statistical Problems in Particle Physics, Astrophysics and Cosmology*, L. Lyons and M. Karagöz Ünel, eds., p. 112. 2006. `arXiv:physics/0511028`.

[86] J. Linnemann, "Measures of Significance in HEP and Astrophysics", in *Statistical Problems in Particle Physics, Astrophysics, and Cosmology*, L. Lyons, R. Mount, and R. Reitmeyer, eds., p. 35. 2003. `arXiv:physics/0312059`.

[87] CMS Collaboration Collaboration, "Search for anomalous production of events with three or more leptons in pp collisions at $\sqrt{(s)} = 8$ TeV", *Phys.Rev.* **D90** (2014), no. 3, 032006, `arXiv:1404.5801`.

[88] CMS Collaboration, S. Chatrchyan et al., "Supersymmetry discovery potential in future LHC and HL-LHC running with the CMS detector", Technical Report CMS-PAS-SUS-14-012, CERN, Geneva, 2015.

Appendix

A. Detailed result Tables

Table A.1.: Result table for the OSSF0Tau events

Selection: $m_{\ell^+\ell^-} < 75$ GeV and $M_T < 120$ GeV						
E_T^{miss} (GeV)	VV	Fake	Zgamma	Rare	Bkg full	Data
< 50	631.7 ± 264.8	71.38 ± 20.22	187.7 ± 44.22	8.817 ± 0.938	899.6 ± 285.1	840
50-100	34.26 ± 7.622	10.49 ± 3.867	0.019 ± 0.021	3.822 ± 0.525	48.59 ± 9.146	48
100-150	4.158 ± 0.969	1.386 ± 0.483	0 ± 0	0.687 ± 0.183	6.231 ± 1.256	9
150-200	1.108 ± 0.269	0.326 ± 0.144	0 ± 0	0.114 ± 0.040	1.548 ± 0.322	1
> 200	0.492 ± 0.138	0.107 ± 0.068	0 ± 0	0.115 ± 0.050	0.715 ± 0.169	0
Selection: $m_{\ell^+\ell^-} < 75$ GeV and 120 GeV $< M_T < 160$ GeV						
E_T^{miss} (GeV)	VV	Fake	Zgamma	Rare	Bkg full	Data
< 50	1.406 ± 0.339	0.198 ± 0.118	2.812 ± 3.200	0.085 ± 0.026	4.500 ± 3.309	3
50-100	2.249 ± 0.552	2.344 ± 0.973	0 ± 0	0.649 ± 0.145	5.242 ± 1.212	6
100-150	0.231 ± 0.079	0.077 ± 0.109	0 ± 0	0.277 ± 0.125	0.584 ± 0.217	0
150-200	0.040 ± 0.025	0.006 ± 0.006	0 ± 0	0.009 ± 0.008	0.056 ± 0.027	0
> 200	0.061 ± 0.029	0 ± 0	0 ± 0	0.034 ± 0.028	0.095 ± 0.041	0
Selection: $m_{\ell^+\ell^-} < 75$ GeV and $M_T > 160$ GeV						
E_T^{miss} (GeV)	VV	Fake	Zgamma	Rare	Bkg full	Data
< 50	0.271 ± 0.142	0 ± 0	0 ± 0	<0.001 ± 0.003	0.272 ± 0.143	0
50-100	1.758 ± 0.467	0.642 ± 0.237	0.043 ± 0.049	0.467 ± 0.117	2.911 ± 0.613	8
100-150	0.837 ± 0.212	1.189 ± 0.606	0 ± 0	0.394 ± 0.110	2.420 ± 0.688	4
150-200	0.209 ± 0.067	0.160 ± 0.088	0 ± 0	0.134 ± 0.055	0.503 ± 0.132	0
> 200	0.184 ± 0.061	0.047 ± 0.037	0 ± 0	0.061 ± 0.024	0.292 ± 0.078	0
Selection: 75 GeV $< m_{\ell^+\ell^-} < 105$ GeV and $M_T < 120$ GeV						
E_T^{miss} (GeV)	VV	Fake	Zgamma	Rare	Bkg full	Data
< 50	1368 ± 296.6	621.7 ± 143.1	125.6 ± 47.24	28.2 ± 4.447	2144 ± 384.1	2269
50-100	534.5 ± 117.3	9.072 ± 3.440	1.765 ± 1.453	14.23 ± 3.662	559.6 ± 119	573
100-150	85.54 ± 18.91	0.690 ± 0.254	0 ± 0	4.141 ± 1.296	90.37 ± 19.17	84
150-200	23.16 ± 5.072	0.404 ± 0.172	0 ± 0	1.484 ± 0.543	25.05 ± 5.179	28
> 200	14.32 ± 3.178	0.061 ± 0.050	0 ± 0	1.106 ± 0.453	15.49 ± 3.263	14
Selection: 75 GeV $< m_{\ell^+\ell^-} < 105$ GeV and 120 GeV $< M_T < 160$ GeV						
E_T^{miss} (GeV)	VV	Fake	Zgamma	Rare	Bkg full	Data
< 50	10.1 ± 2.367	0.555 ± 0.387	0.942 ± 0.944	0.414 ± 0.147	12.01 ± 2.907	26
50-100	11.23 ± 3.017	0.543 ± 0.208	0 ± 0.013	0.581 ± 0.212	12.36 ± 3.115	11
100-150	1.730 ± 0.408	0.097 ± 0.073	0 ± 0	0.304 ± 0.124	2.131 ± 0.453	2
150-200	0.265 ± 0.086	0 ± 0	0 ± 0	0.140 ± 0.089	0.405 ± 0.134	1
> 200	0.168 ± 0.057	0 ± 0	0 ± 0	0.028 ± 0.018	0.196 ± 0.061	0
Selection: 75 GeV $< m_{\ell^+\ell^-} < 105$ GeV and $M_T > 160$ GeV						
E_T^{miss} (GeV)	VV	Fake	Zgamma	Rare	Bkg full	Data
< 50	1.429 ± 0.349	0.039 ± 0.040	0.597 ± 0.609	0.118 ± 0.057	2.183 ± 0.738	5
50-100	4.106 ± 1.170	0.222 ± 0.118	0 ± 0	0.322 ± 0.132	4.650 ± 1.221	13
100-150	2.287 ± 0.522	0.259 ± 0.125	0 ± 0	0.444 ± 0.179	2.989 ± 0.594	5
150-200	0.786 ± 0.213	0.009 ± 0.009	0 ± 0	0.240 ± 0.109	1.035 ± 0.251	3
> 200	0.747 ± 0.301	0 ± 0	0 ± 0	0.220 ± 0.108	0.967 ± 0.325	2
Selection: $m_{\ell^+\ell^-} > 105$ GeV and $M_T < 120$ GeV						
E_T^{miss} (GeV)	VV	Fake	Zgamma	Rare	Bkg full	Data
< 50	59.66 ± 13.31	9.276 ± 4.046	9.617 ± 4.606	2.265 ± 0.510	80.82 ± 16.91	105
50-100	18.41 ± 3.997	3.265 ± 0.827	0.327 ± 0.292	1.958 ± 0.425	23.96 ± 4.367	26
100-150	3.420 ± 0.791	0.644 ± 0.249	0 ± 0	0.582 ± 0.153	4.646 ± 0.914	6
150-200	0.925 ± 0.228	0.167 ± 0.109	0 ± 0	0.193 ± 0.063	1.285 ± 0.272	2
> 200	0.705 ± 0.208	0 ± 0	0 ± 0	0.092 ± 0.044	0.797 ± 0.216	3
Selection: $m_{\ell^+\ell^-} > 105$ GeV and 120 GeV $< M_T < 160$ GeV						
E_T^{miss} (GeV)	VV	Fake	Zgamma	Rare	Bkg full	Data
< 50	0.668 ± 0.170	0 ± 0.012	0 ± 0	0.016 ± 0.011	0.684 ± 0.175	4
50-100	1.061 ± 0.360	0.149 ± 0.100	0 ± 0	0.296 ± 0.094	1.506 ± 0.418	1
100-150	0.114 ± 0.044	0.110 ± 0.090	0 ± 0	0.066 ± 0.037	0.290 ± 0.111	1
150-200	0.065 ± 0.034	0 ± 0	0 ± 0	0.072 ± 0.048	0.137 ± 0.060	0
> 200	0 ± 0	0 ± 0	0 ± 0	0.037 ± 0.032	0.037 ± 0.032	1
Selection: $m_{\ell^+\ell^-} > 105$ GeV and $M_T > 160$ GeV						
E_T^{miss} (GeV)	VV	Fake	Zgamma	Rare	Bkg full	Data
< 50	0.152 ± 0.051	0 ± 0	0 ± 0	0.016 ± 0.010	0.168 ± 0.053	1
50-100	0.879 ± 0.218	0.180 ± 0.092	0.048 ± 0.059	0.258 ± 0.111	1.364 ± 0.292	2
100-150	0.341 ± 0.099	0.141 ± 0.094	0 ± 0.024	0.315 ± 0.127	0.797 ± 0.207	2
150-200	0.139 ± 0.049	0.041 ± 0.041	0 ± 0	0.129 ± 0.054	0.309 ± 0.087	0
> 200	0.121 ± 0.046	0 ± 0	0 ± 0	0.101 ± 0.054	0.222 ± 0.072	0

Table A.2.: Result table for the noOSSF0Tau events

Selection: $m_{\ell^+\ell^-}$ < 100 GeV and M_T < 120 GeV						
E_T^{miss} (GeV)	VV	Fake	Zgamma	Rare	Bkg full	Data
< 50	5.714 ± 1.264	5.220 ± 1.317	0.048 ± 0.054	1.808 ± 0.312	12.79 ± 2.119	19
50-100	1.913 ± 0.439	4.446 ± 1.091	0.101 ± 0.113	1.186 ± 0.260	7.646 ± 1.329	9
100-150	0.309 ± 0.095	1.067 ± 0.369	0 ± 0	0.419 ± 0.112	1.796 ± 0.436	2
150-200	0.067 ± 0.029	0.212 ± 0.119	0 ± 0	0.070 ± 0.044	0.350 ± 0.135	0
> 200	0.042 ± 0.022	0 ± 0	0 ± 0	0.024 ± 0.014	0.067 ± 0.026	1
Selection: $m_{\ell^+\ell^-}$ < 100 GeV and 120 GeV < M_T < 160 GeV						
E_T^{miss} (GeV)	VV	Fake	Zgamma	Rare	Bkg full	Data
< 50	0.325 ± 0.178	0.176 ± 0.108	0 ± 0	0.063 ± 0.053	0.564 ± 0.256	1
50-100	0.296 ± 0.124	1.580 ± 0.825	0.145 ± 0.146	0.433 ± 0.135	2.455 ± 0.897	1
100-150	0.050 ± 0.025	0.274 ± 0.131	0 ± 0.011	0.097 ± 0.050	0.421 ± 0.153	0
150-200	0.011 ± 0.011	0.060 ± 0.061	0 ± 0	0.014 ± 0.012	0.085 ± 0.064	1
> 200	0 ± 0	0 ± 0	0 ± 0	0.014 ± 0.011	0.014 ± 0.011	0
Selection: $m_{\ell^+\ell^-}$ < 100 GeV and M_T > 160 GeV						
E_T^{miss} (GeV)	VV	Fake	Zgamma	Rare	Bkg full	Data
< 50	0.134 ± 0.134	0 ± 0	0 ± 0	0 ± 0.004	0.134 ± 0.136	0
50-100	0.256 ± 0.078	0.431 ± 0.179	0 ± 0	0.340 ± 0.089	1.027 ± 0.235	2
100-150	0.135 ± 0.049	0.449 ± 0.188	0 ± 0	0.320 ± 0.109	0.904 ± 0.232	3
150-200	0.023 ± 0.016	0.111 ± 0.082	0 ± 0	0.068 ± 0.030	0.202 ± 0.090	0
> 200	0.064 ± 0.032	0 ± 0	0 ± 0	0.063 ± 0.039	0.127 ± 0.052	0
Selection: $m_{\ell^+\ell^-}$ > 100 GeV and M_T < 120 GeV						
E_T^{miss} (GeV)	VV	Fake	Zgamma	Rare	Bkg full	Data
< 50	0.391 ± 0.111	0.376 ± 0.160	0 ± 0	0.202 ± 0.063	0.970 ± 0.217	0
50-100	0.038 ± 0.022	0.263 ± 0.132	0 ± 0	0.174 ± 0.065	0.475 ± 0.153	0
100-150	0 ± 0	0 ± 0	0 ± 0	0.054 ± 0.031	0.054 ± 0.031	0
150-200	0 ± 0	0 ± 0	0 ± 0	0.034 ± 0.030	0.034 ± 0.030	0
> 200	0 ± 0	0 ± 0	0 ± 0	$<0.001 \pm <0.001$	$<0.001 \pm <0.001$	0
Selection: $m_{\ell^+\ell^-}$ > 100 GeV and 120 GeV < M_T < 160 GeV						
E_T^{miss} (GeV)	VV	Fake	Zgamma	Rare	Bkg full	Data
< 50	0.010 ± 0.016	0 ± 0	0 ± 0	0.041 ± 0.039	0.051 ± 0.047	0
50-100	0.083 ± 0.035	0.053 ± 0.059	0 ± 0	0.052 ± 0.022	0.188 ± 0.078	0
100-150	0.010 ± 0.010	0.047 ± 0.054	0 ± 0	0.044 ± 0.029	0.100 ± 0.064	0
150-200	0 ± 0	0 ± 0	0 ± 0	$<0.001 \pm <0.001$	$<0.001 \pm <0.001$	0
> 200	0 ± 0	0 ± 0	0 ± 0	$<0.001 \pm <0.001$	$<0.001 \pm <0.001$	0
Selection: $m_{\ell^+\ell^-}$ > 100 GeV and M_T > 160 GeV						
E_T^{miss} (GeV)	VV	Fake	Zgamma	Rare	Bkg full	Data
< 50	0 ± 0.005	0 ± 0	0 ± 0	0.014 ± 0.010	0.014 ± 0.012	0
50-100	0.091 ± 0.038	0.049 ± 0.051	0 ± 0	0.187 ± 0.094	0.327 ± 0.116	1
100-150	0.040 ± 0.024	0 ± 0	0 ± 0	0.163 ± 0.078	0.203 ± 0.082	0
150-200	0 ± 0.006	0.002 ± 0.002	0 ± 0	0.026 ± 0.024	0.028 ± 0.026	0
> 200	0.043 ± 0.024	0 ± 0	0 ± 0	0.041 ± 0.030	0.084 ± 0.040	0

Table A.3.: Result table for the OSSF1Tau events

Selection: $m_{\ell^+\ell^-} < 75$ GeV and $M_T < 120$ GeV					
E_T^{miss} (GeV)	VV	Fake	Zgamma	Rare	Bkg full	Data
< 50	35.13 ± 8.571	3853 ± 835.5	651 ± 149.4	2.641 ± 0.317	4542 ± 960.4	4363
50-100	6.268 ± 1.533	56.6 ± 15.06	8.658 ± 5.048	1.114 ± 0.185	72.64 ± 19.07	77
100-150	1.035 ± 0.283	7.386 ± 1.911	0.335 ± 0.376	0.271 ± 0.108	9.028 ± 2.078	9
150-200	0.210 ± 0.071	1.037 ± 0.333	0 ± 0	0.089 ± 0.051	1.336 ± 0.352	0
> 200	0.116 ± 0.043	0.085 ± 0.087	0 ± 0	0.016 ± 0.010	0.217 ± 0.099	1

Selection: $m_{\ell^+\ell^-} < 75$ GeV and 120 GeV $< M_T < 160$ GeV					
E_T^{miss} (GeV)	VV	Fake	Zgamma	Rare	Bkg full	Data
< 50	0.060 ± 0.034	2.126 ± 2.348	0 ± 0	<0.001 ± <0.001	2.186 ± 2.358	5
50-100	0.427 ± 0.142	1.862 ± 0.525	0 ± 0	0.217 ± 0.068	2.506 ± 0.577	9
100-150	0.037 ± 0.023	3.270 ± 1.206	0 ± 0	0.016 ± 0.016	3.323 ± 1.210	2
150-200	0.043 ± 0.027	0.578 ± 0.241	0 ± 0	0 ± <0.001	0.621 ± 0.248	1
> 200	0.009 ± 0.010	0.101 ± 0.073	0 ± 0	0 ± 0	0.110 ± 0.073	1

Selection: $m_{\ell^+\ell^-} < 75$ GeV and $M_T > 160$ GeV					
E_T^{miss} (GeV)	VV	Fake	Zgamma	Rare	Bkg full	Data
< 50	0.011 ± 0.015	0 ± 0	0 ± 0.110	0 ± 0	0.011 ± 0.120	0
50-100	0.180 ± 0.063	0.534 ± 0.221	0 ± 0	0.070 ± 0.033	0.784 ± 0.240	1
100-150	0.119 ± 0.051	0.749 ± 0.264	0 ± 0	0.009 ± 0.011	0.877 ± 0.275	1
150-200	0.018 ± 0.018	0.227 ± 0.146	0 ± 0	0.017 ± 0.013	0.262 ± 0.156	1
> 200	0.009 ± 0.009	0.106 ± 0.076	0 ± 0	0.008 ± 0.008	0.122 ± 0.077	2

Selection: 75 GeV $< m_{\ell^+\ell^-} < 105$ GeV and $M_T < 120$ GeV					
E_T^{miss} (GeV)	VV	Fake	Zgamma	Rare	Bkg full	Data
< 50	190.3 ± 29.16	22200 ± 4779	506.4 ± 213	4.651 ± 0.770	22900 ± 4822	22590
50-100	54.87 ± 12	135.7 ± 66.67	5.204 ± 3.375	2.397 ± 0.487	198.1 ± 73.74	175
100-150	13.22 ± 3.133	3.341 ± 0.951	0 ± 0.014	0.660 ± 0.214	17.22 ± 3.603	16
150-200	3.876 ± 1.019	0.475 ± 0.186	0 ± 0	0.260 ± 0.102	4.611 ± 1.082	6
> 200	2.136 ± 0.551	0.048 ± 0.062	0 ± 0	0.173 ± 0.064	2.357 ± 0.590	2

Selection: 75 GeV $< m_{\ell^+\ell^-} < 105$ GeV and 120 GeV $< M_T < 160$ GeV					
E_T^{miss} (GeV)	VV	Fake	Zgamma	Rare	Bkg full	Data
< 50	0.552 ± 0.232	3.931 ± 3.004	0 ± 0.445	0.021 ± 0.015	4.504 ± 3.295	8
50-100	0.576 ± 0.179	2.573 ± 2.261	0 ± 0.025	0.031 ± 0.018	3.180 ± 2.376	3
100-150	0.199 ± 0.068	0.954 ± 0.336	0 ± 0	0.032 ± 0.016	1.185 ± 0.354	0
150-200	0.061 ± 0.030	0.184 ± 0.116	0 ± 0	<0.001 ± <0.001	0.245 ± 0.124	0
> 200	0.025 ± 0.020	0.060 ± 0.061	0 ± 0	0.008 ± 0.006	0.093 ± 0.065	0

Selection: 75 GeV $< m_{\ell^+\ell^-} < 105$ GeV and $M_T > 160$ GeV					
E_T^{miss} (GeV)	VV	Fake	Zgamma	Rare	Bkg full	Data
< 50	0.024 ± 0.027	2.836 ± 3.449	0 ± 0	0 ± 0.002	2.860 ± 3.468	1
50-100	0.145 ± 0.056	8.476 ± 5.635	0 ± 0	0.023 ± 0.016	8.644 ± 5.658	0
100-150	0.049 ± 0.029	0.461 ± 0.229	0 ± 0	0.034 ± 0.025	0.544 ± 0.243	2
150-200	0.022 ± 0.018	0.237 ± 0.123	0 ± 0	0.040 ± 0.037	0.299 ± 0.132	0
> 200	0.029 ± 0.019	0.134 ± 0.102	0 ± 0	0.019 ± 0.021	0.182 ± 0.117	0

Selection: $m_{\ell^+\ell^-} > 105$ GeV and $M_T < 120$ GeV					
E_T^{miss} (GeV)	VV	Fake	Zgamma	Rare	Bkg full	Data
< 50	11.51 ± 2.043	722.6 ± 159.6	37.21 ± 14.45	0.610 ± 0.107	771.9 ± 163.9	759
50-100	3.434 ± 0.848	36.15 ± 7.837	1.030 ± 0.815	0.528 ± 0.130	41.14 ± 8.144	49
100-150	0.825 ± 0.204	5.863 ± 1.703	0.434 ± 0.487	0.166 ± 0.071	7.288 ± 1.856	4
150-200	0.176 ± 0.080	0.538 ± 0.195	0 ± 0	0.046 ± 0.025	0.761 ± 0.229	2
> 200	0.185 ± 0.062	0.364 ± 0.171	0 ± 0	0.050 ± 0.032	0.599 ± 0.191	0

Selection: $m_{\ell^+\ell^-} > 105$ GeV and 120 GeV $< M_T < 160$ GeV					
E_T^{miss} (GeV)	VV	Fake	Zgamma	Rare	Bkg full	Data
< 50	0.036 ± 0.033	0.419 ± 0.211	0 ± 0	0.007 ± 0.007	0.461 ± 0.222	0
50-100	0.249 ± 0.091	2.219 ± 0.842	0.044 ± 0.049	0.063 ± 0.025	2.574 ± 0.861	2
100-150	0.053 ± 0.027	1.035 ± 0.372	0 ± 0.022	0.012 ± 0.009	1.099 ± 0.389	0
150-200	0.004 ± 0.004	0.587 ± 0.216	0 ± 0	0.002 ± 0.004	0.593 ± 0.217	0
> 200	0 ± 0	0.319 ± 0.176	0 ± 0	0.012 ± 0.012	0.331 ± 0.177	0

Selection: $m_{\ell^+\ell^-} > 105$ GeV and $M_T > 160$ GeV					
E_T^{miss} (GeV)	VV	Fake	Zgamma	Rare	Bkg full	Data
< 50	0.026 ± 0.027	0 ± 0	0 ± 0	0 ± 0.003	0.026 ± 0.028	0
50-100	0.060 ± 0.036	0.712 ± 0.264	0 ± 0	0.036 ± 0.018	0.808 ± 0.276	1
100-150	0.019 ± 0.013	0.695 ± 0.267	0 ± 0	0.030 ± 0.016	0.744 ± 0.270	2
150-200	0.021 ± 0.016	0.280 ± 0.124	0 ± 0	0.002 ± 0.005	0.303 ± 0.126	1
> 200	0.035 ± 0.027	0.141 ± 0.096	0 ± 0	0.010 ± 0.007	0.186 ± 0.104	0

Table A.4.: Result table for the SS1Tau events

Selection: $m_{\ell^+\ell^-} < 100$ GeV and $M_T < 120$ GeV						
E_T^{miss} (GeV)	VV	Fake	Zgamma	Rare	Bkg full	Data
< 50	27.57 ± 6.208	26.21 ± 11.33	2.377 ± 1.941	2.983 ± 0.442	59.13 ± 14.8	50
50-100	9.440 ± 2.474	1.763 ± 0.523	0.532 ± 0.598	1.613 ± 0.310	13.35 ± 2.888	12
100-150	1.169 ± 0.316	0.233 ± 0.133	0 ± 0	0.170 ± 0.075	1.572 ± 0.391	0
150-200	0.471 ± 0.129	0.138 ± 0.111	0 ± 0	0.080 ± 0.056	0.688 ± 0.186	0
> 200	0.307 ± 0.105	0 ± 0	0.035 ± 0.040	0.044 ± 0.021	0.387 ± 0.118	1
Selection: $m_{\ell^+\ell^-} < 100$ GeV and 120 GeV $< M_T < 160$ GeV						
E_T^{miss} (GeV)	VV	Fake	Zgamma	Rare	Bkg full	Data
< 50	0.727 ± 0.208	0.092 ± 0.068	0 ± 0	0.125 ± 0.036	0.944 ± 0.232	1
50-100	1.506 ± 0.415	0.099 ± 0.114	0 ± 0	0.258 ± 0.063	1.863 ± 0.493	2
100-150	0.121 ± 0.045	0.049 ± 0.055	0 ± 0	0.125 ± 0.060	0.295 ± 0.101	0
150-200	0.014 ± 0.014	0 ± 0	0 ± 0	0.005 ± 0.003	0.018 ± 0.015	0
> 200	0.019 ± 0.017	0 ± 0	0 ± 0	$<0.001 \pm <0.001$	0.019 ± 0.017	0
Selection: $m_{\ell^+\ell^-} < 100$ GeV and $M_T > 160$ GeV						
E_T^{miss} (GeV)	VV	Fake	Zgamma	Rare	Bkg full	Data
< 50	0.160 ± 0.100	0 ± 0	0 ± 0	0.019 ± 0.012	0.179 ± 0.102	0
50-100	1.133 ± 0.330	0.337 ± 0.165	0 ± 0	0.380 ± 0.082	1.850 ± 0.421	2
100-150	0.428 ± 0.132	0.287 ± 0.150	0 ± 0	0.166 ± 0.054	0.882 ± 0.227	0
150-200	0.186 ± 0.064	0 ± 0.053	0 ± 0	0.062 ± 0.047	0.248 ± 0.118	0
> 200	0.180 ± 0.122	0 ± 0	0 ± 0	0.049 ± 0.023	0.229 ± 0.125	0
Selection: $m_{\ell^+\ell^-} > 100$ GeV and $M_T < 120$ GeV						
E_T^{miss} (GeV)	VV	Fake	Zgamma	Rare	Bkg full	Data
< 50	0.659 ± 0.222	2.011 ± 2.058	0 ± 0	0.202 ± 0.078	2.871 ± 2.084	2
50-100	0.342 ± 0.191	0 ± 0	0 ± 0	0.080 ± 0.035	0.423 ± 0.203	1
100-150	0.027 ± 0.019	0 ± 0	0 ± 0	0.003 ± 0.003	0.029 ± 0.019	0
150-200	0 ± 0	0 ± 0	0 ± 0	0.004 ± 0.003	0.004 ± 0.003	0
> 200	0 ± 0	0 ± 0	0 ± 0	0.011 ± 0.011	0.011 ± 0.011	0
Selection: $m_{\ell^+\ell^-} > 100$ GeV and 120 GeV $< M_T < 160$ GeV						
E_T^{miss} (GeV)	VV	Fake	Zgamma	Rare	Bkg full	Data
< 50	0.020 ± 0.015	0 ± 0	0 ± 0	0.027 ± 0.017	0.047 ± 0.023	0
50-100	0.058 ± 0.031	0 ± 0	0 ± 0	0.062 ± 0.034	0.120 ± 0.047	1
100-150	0.023 ± 0.018	0 ± 0	0 ± 0	$<0.001 \pm <0.001$	0.023 ± 0.018	0
150-200	0 ± 0	0 ± 0	0 ± 0	0 ± 0	0 ± 0	0
> 200	0 ± 0	0 ± 0	0 ± 0	0 ± 0	0 ± 0	0
Selection: $m_{\ell^+\ell^-} > 100$ GeV and $M_T > 160$ GeV						
E_T^{miss} (GeV)	VV	Fake	Zgamma	Rare	Bkg full	Data
< 50	0 ± 0	0 ± 0	0 ± 0	0.013 ± 0.015	0.013 ± 0.015	0
50-100	0.032 ± 0.022	0 ± 0	0 ± 0	0.021 ± 0.013	0.052 ± 0.026	0
100-150	0.022 ± 0.016	0.142 ± 0.113	0 ± 0	0.020 ± 0.015	0.184 ± 0.115	1
150-200	0 ± 0	0 ± 0	0 ± 0	$<0.001 \pm <0.001$	$<0.001 \pm <0.001$	0
> 200	0 ± 0	0 ± 0	0 ± 0	0.042 ± 0.021	0.042 ± 0.021	0

Table A.5.: Result table for the OSOF1Tau events

Selection: $m_{\ell^+\ell^-} < 100$ GeV and $M_T < 120$ GeV					
E_T^{miss} (GeV)	VV	Fake	Zgamma	Rare	Bkg full	Data
< 50	16.72 ± 3.884	182.5 ± 42.36	1.217 ± 0.879	3.173 ± 0.444	203.6 ± 43.43	215
50-100	5.728 ± 1.599	79.94 ± 17.21	0.006 ± 0.007	1.853 ± 0.352	87.52 ± 17.76	96
100-150	0.833 ± 0.218	15.06 ± 4.210	0.041 ± 0.047	0.183 ± 0.069	16.12 ± 4.271	19
150-200	0.236 ± 0.074	1.159 ± 0.389	0 ± 0	0.087 ± 0.049	1.482 ± 0.411	3
> 200	0.180 ± 0.062	0.346 ± 0.156	0 ± 0	0.032 ± 0.018	0.558 ± 0.177	0

Selection: $m_{\ell^+\ell^-} < 100$ GeV and 120 GeV $< M_T < 160$ GeV					
E_T^{miss} (GeV)	VV	Fake	Zgamma	Rare	Bkg full	Data
< 50	0.567 ± 0.173	3.196 ± 2.217	0 ± 0	0.056 ± 0.022	3.819 ± 2.253	2
50-100	0.687 ± 0.210	11.2 ± 2.590	0 ± 0.014	0.350 ± 0.106	12.23 ± 2.667	9
100-150	0.123 ± 0.056	2.546 ± 0.875	0 ± 0	0.029 ± 0.017	2.697 ± 0.906	5
150-200	0.024 ± 0.027	0.338 ± 0.165	0 ± 0	0.046 ± 0.044	0.407 ± 0.177	0
> 200	0.011 ± 0.011	0.152 ± 0.103	0 ± 0	0.014 ± 0.012	0.177 ± 0.107	0

Selection: $m_{\ell^+\ell^-} < 100$ GeV and $M_T > 160$ GeV					
E_T^{miss} (GeV)	VV	Fake	Zgamma	Rare	Bkg full	Data
< 50	0.031 ± 0.020	0.144 ± 0.104	0 ± 0	0.026 ± 0.028	0.201 ± 0.117	1
50-100	0.592 ± 0.159	4.122 ± 1.023	0.027 ± 0.032	0.184 ± 0.054	4.926 ± 1.067	9
100-150	0.329 ± 0.102	5.608 ± 1.386	0.010 ± 0.013	0.100 ± 0.046	6.046 ± 1.415	5
150-200	0.050 ± 0.029	0.958 ± 0.294	0 ± 0	0.078 ± 0.037	1.085 ± 0.304	1
> 200	0.055 ± 0.028	1.063 ± 0.684	0 ± 0	0.039 ± 0.019	1.156 ± 0.687	0

Selection: $m_{\ell^+\ell^-} > 100$ GeV and $M_T < 120$ GeV					
E_T^{miss} (GeV)	VV	Fake	Zgamma	Rare	Bkg full	Data
< 50	0.380 ± 0.229	11.34 ± 2.612	0.087 ± 0.076	0.208 ± 0.080	12.01 ± 2.658	10
50-100	0.074 ± 0.034	8.419 ± 1.978	0 ± 0	0.198 ± 0.080	8.691 ± 1.992	7
100-150	0.042 ± 0.025	1.591 ± 0.455	0 ± 0	0.049 ± 0.030	1.682 ± 0.464	5
150-200	0 ± 0	0.313 ± 0.171	0.086 ± 0.096	0.010 ± 0.011	0.408 ± 0.200	0
> 200	0.009 ± 0.010	0.092 ± 0.069	0 ± 0	0.003 ± 0.002	0.104 ± 0.070	0

Selection: $m_{\ell^+\ell^-} > 100$ GeV and 120 GeV $< M_T < 160$ GeV					
E_T^{miss} (GeV)	VV	Fake	Zgamma	Rare	Bkg full	Data
< 50	0.025 ± 0.021	0.388 ± 0.206	0 ± 0	0.058 ± 0.051	0.472 ± 0.227	0
50-100	0.019 ± 0.015	1.869 ± 0.579	0 ± 0	0.036 ± 0.035	1.924 ± 0.589	0
100-150	0.012 ± 0.014	0.442 ± 0.170	0 ± 0	0.025 ± 0.018	0.479 ± 0.174	2
150-200	0 ± 0.006	0.123 ± 0.084	0 ± 0	$<0.001 \pm <0.001$	0.123 ± 0.087	0
> 200	0 ± 0	0 ± 0	0 ± 0	$<0.001 \pm <0.001$	$<0.001 \pm <0.001$	0

Selection: $m_{\ell^+\ell^-} > 100$ GeV and $M_T > 160$ GeV					
E_T^{miss} (GeV)	VV	Fake	Zgamma	Rare	Bkg full	Data
< 50	0 ± 0	0 ± 0.028	0 ± 0	0.002 ± 0.002	0.002 ± 0.029	0
50-100	0.027 ± 0.018	0.825 ± 0.304	0 ± 0	0.018 ± 0.013	0.871 ± 0.309	2
100-150	$<0.001 \pm 0.006$	0.876 ± 0.276	0.416 ± 0.466	0.052 ± 0.047	1.344 ± 0.552	1
150-200	0.011 ± 0.013	0.471 ± 0.200	0 ± 0	$<0.001 \pm 0.001$	0.482 ± 0.204	1
> 200	0.015 ± 0.016	0 ± 0	0 ± 0	0.021 ± 0.015	0.036 ± 0.022	1

Table A.6.: Result table for the 4ℓ events

Selection: N_Z=2 and N_τ=0						
E_T^{miss} (GeV)	VV	Fake	Zgamma	Rare	Bkg full	Data
< 30	110.9 ± 14.11	0 ± 0	0 ± 0	0.418 ± 0.173	111.3 ± 14.15	114
30-50	3.204 ± 2.034	0 ± 0	0 ± 0	0.157 ± 0.078	3.361 ± 2.056	8
50-100	0.615 ± 0.268	0 ± 0	0 ± 0	0.343 ± 0.177	0.958 ± 0.333	3
> 200	0 ± 0	0 ± 0	0 ± 0	0.168 ± 0.097	0.168 ± 0.097	0
Selection: N_Z=1 and N_τ=0						
E_T^{miss} (GeV)	VV	Fake	Zgamma	Rare	Bkg full	Data
< 30	27.78 ± 3.818	0 ± 0	0 ± 0	2.375 ± 0.346	30.16 ± 4.034	32
30-50	1.988 ± 0.733	0.014 ± 0.014	0 ± 0	1.127 ± 0.351	3.128 ± 0.878	2
50-100	0.876 ± 0.291	0 ± 0	0 ± 0	1.766 ± 0.756	2.642 ± 0.832	2
> 200	0.201 ± 0.125	0 ± 0	0 ± 0	1.841 ± 0.827	2.042 ± 0.842	2
Selection: N_Z=0 and N_τ=0						
E_T^{miss} (GeV)	VV	Fake	Zgamma	Rare	Bkg full	Data
< 30	7.019 ± 1.211	0.034 ± 0.035	0 ± 0	0.928 ± 0.129	7.982 ± 1.286	5
30-50	0.294 ± 0.165	0 ± 0	0 ± 0	0.232 ± 0.088	0.526 ± 0.193	1
50-100	0.205 ± 0.132	0 ± 0	0 ± 0	0.468 ± 0.173	0.674 ± 0.225	0
> 200	0.038 ± 0.051	0 ± 0	0 ± 0	0.271 ± 0.114	0.309 ± 0.131	0
Selection: N_Z=1 and N_τ=1						
E_T^{miss} (GeV)	VV	Fake	Zgamma	Rare	Bkg full	Data
< 30	6.810 ± 1.352	0.041 ± 0.042	0.480 ± 0.589	0.775 ± 0.206	8.106 ± 1.690	11
30-50	3.311 ± 0.685	0.070 ± 0.071	0 ± 0.240	0.608 ± 0.167	3.989 ± 0.863	4
50-100	3.240 ± 0.726	0 ± 0.024	0 ± 0	0.735 ± 0.224	3.975 ± 0.811	2
> 200	0.708 ± 0.202	0.049 ± 0.055	0 ± 0	0.665 ± 0.265	1.421 ± 0.366	1
Selection: N_Z=0 and N_τ=1						
E_T^{miss} (GeV)	VV	Fake	Zgamma	Rare	Bkg full	Data
< 30	1.183 ± 0.302	0.070 ± 0.075	0.061 ± 0.068	0.200 ± 0.069	1.514 ± 0.354	1
30-50	0.400 ± 0.147	0.043 ± 0.045	0 ± 0	0.224 ± 0.085	0.667 ± 0.184	0
50-100	0.553 ± 0.217	0.041 ± 0.038	0 ± 0	0.425 ± 0.177	1.019 ± 0.308	1
> 200	0.070 ± 0.050	0.171 ± 0.122	0 ± 0	0.179 ± 0.065	0.420 ± 0.151	2
Selection: N_Z=1 and N_τ=2						
E_T^{miss} (GeV)	VV	Fake	Zgamma	Rare	Bkg full	Data
< 30	3.002 ± 0.746	19.59 ± 7.668	0.450 ± 0.396	0.214 ± 0.067	23.26 ± 7.813	26
30-50	1.241 ± 0.374	2.113 ± 2.337	0.027 ± 0.033	0.124 ± 0.037	3.506 ± 2.430	2
50-100	0.800 ± 0.348	0.222 ± 0.187	0.016 ± 0.022	0.156 ± 0.048	1.194 ± 0.431	2
> 200	0.087 ± 0.079	0.051 ± 0.052	0 ± 0	0.055 ± 0.031	0.193 ± 0.117	0
Selection: N_Z=0 and N_τ=2						
E_T^{miss} (GeV)	VV	Fake	Zgamma	Rare	Bkg full	Data
< 30	0.807 ± 0.272	7.909 ± 4.869	0 ± 0	0.144 ± 0.057	8.859 ± 4.889	8
30-50	0.127 ± 0.052	0.398 ± 0.175	0 ± 0	0.237 ± 0.093	0.762 ± 0.222	5
50-100	0.372 ± 0.191	1.529 ± 0.484	0 ± 0	0.337 ± 0.109	2.238 ± 0.556	1
> 200	0.038 ± 0.029	0.245 ± 0.123	0 ± 0	0.163 ± 0.077	0.447 ± 0.156	0

B. Validation of ZZ private production

There should be no differences between the central and private produced $ZZ \to 4\,\ell$ sample if all four leptons are reconstructed. This is because of the rejection of events with $m_{\ell\ell} < 12$ GeV. Figure B.1 shows that the private produced sample and the centrally produced samples agrees within the uncertainties.
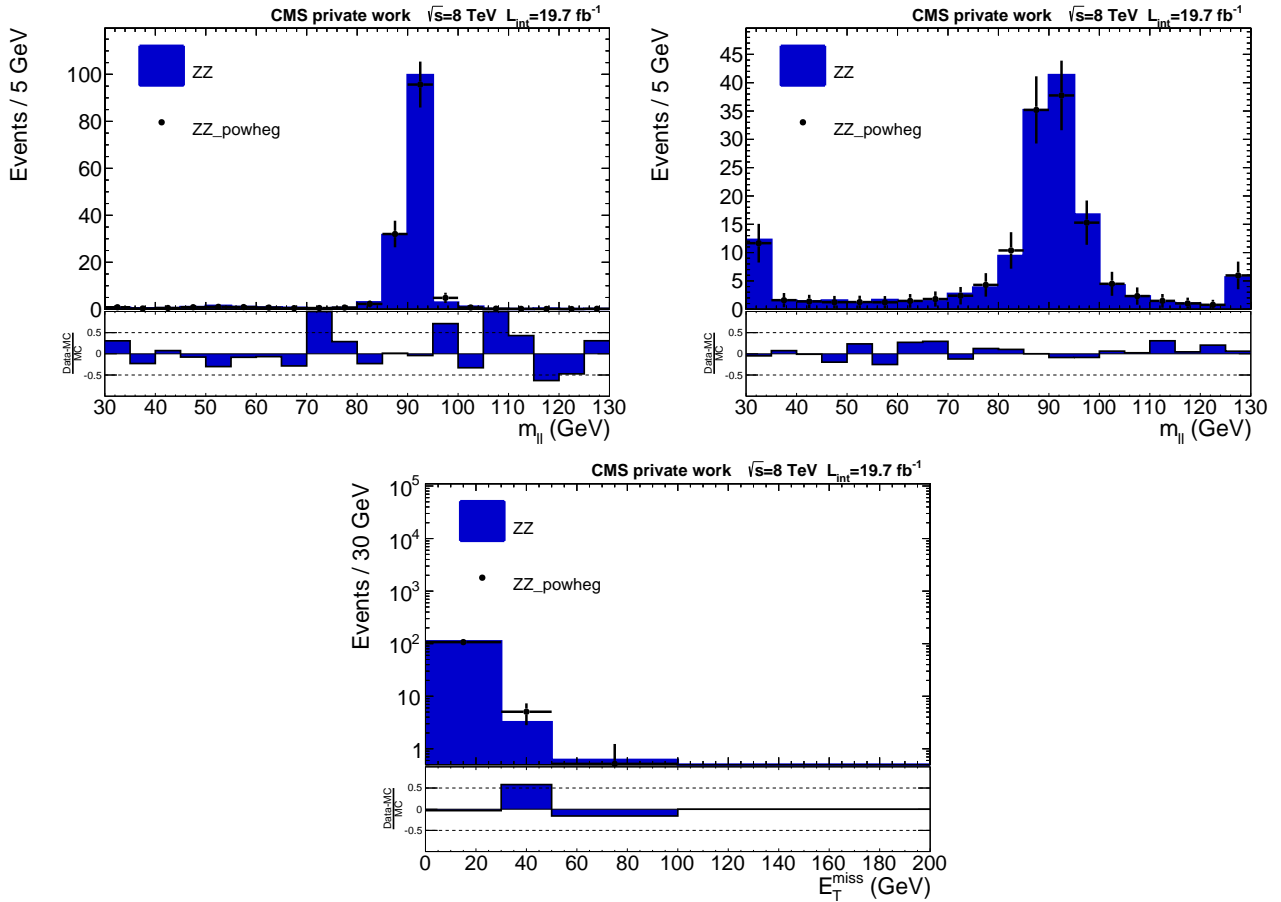

Figure B.1.: Validation of the private produced ZZ sample. The blue area correspond to the private sample whereas the black points are from the centrally produced sample. On the top left the invariant mass of the opposite sign same flavor lepton pair closest to the Z mass is shown. On the top right the invariant mass of the second pair. The bottom shows the E_{T}^{miss} distribution. The two samples agrees within the statistical uncertainty.